AD-767 270

AN INVESTIGATION OF METALLURGICAL FACTORS WHICH AFFECT FRACTURE TOUGHNESS OF ULTRA-HIGH STRENGTH STEELS

William E. Wood, et al

California University

Prepared for:

Army Materials and Mechanics Research Center
Atomic Energy Commission

May 1973

DISTRIBUTED BY:

NTIS
National Technical Information Service
U. S. DEPARTMENT OF COMMERCE
5285 Port Royal Road, Springfield Va. 22151

Best
Available
Copy

AD

AD767270

AMMRC CTR 73-24

AN INVESTIGATION OF METALLURGICAL FACTORS WHICH AFFECT FRACTURE TOUGHNESS OF ULTRA-HIGH STRENGTH STEELS

May 1973

WILLIAM E. WOOD, EARL R. PARKER,
and VICTOR F. ZACKAY

Lawrence Berkeley Laboratory
University of California
Berkeley, California 94720

D D C
RECEIVED
OCT 5 1973
B

Final Report Contract Number DAAG46-72-C-0220
LBL-1474

Approved for public release; distribution unlimited.

Prepared for

ARMY MATERIALS AND MECHANICS RESEARCH CENTER
Watertown, Massachusetts 02172

Reproduced by
NATIONAL TECHNICAL
INFORMATION SERVICE
US Department of Commerce
Springfield, VA. 22151

ACCESSION for
NTIS White Section ☑
DDC Buff Section ☐
UNANNOUNCED ☐
JUSTIFICATION.....
BY.....
DISTRIBUTION/AVAILABILITY CODES
Dist. AVAIL. and/or SPECIAL
A

The findings in this report are not to be construed as an official Department of the Army position, unless so designated by other authorized documents.

Mention of any trade names or manufacturers in this report shall not be construed as advertising nor as an official indorsement or approval of such products or companies by the United States Government.

DISPOSITION INSTRUCTIONS

Destroy this report when it is no longer needed. Do not return it to the originator.

UNCLASSIFIED
Security Classification

DOCUMENT CONTROL DATA - R & D

(Security classification of title, body of abstract and indexing annotation must be entered when the overall report is classified)

1. ORIGINATING ACTIVITY *(Corporate author)* Lawrence Berkeley Laboratory University of California Berkeley, California 94720	2a. REPORT SECURITY CLASSIFICATION Unclassified 2b. GROUP

3. REPORT TITLE

AN INVESTIGATION OF METALLURGICAL FACTORS WHICH AFFECT FRACTURE TOUGHNESS OF ULTRA HIGH STRENGTH STEELS

4. DESCRIPTIVE NOTES *(Type of report and inclusive dates)*

5. AUTHOR(S) *(First name, middle initial, last name)*

William E. Wood, Earl R. Parker, and Victor F. Zackay

6. REPORT DATE May 1973	7a. TOTAL NO. OF PAGES ~~207~~ 213	7b. NO. OF REFS 89
8a. CONTRACT OR GRANT NO. DAAG46-72-C-0220 b. PROJECT NO. D/A 1T061101A91A c. AMCMS Code 611101.11.844 d. Agency Accession No. DA OD4801	9a. ORIGINATOR'S REPORT NUMBER(S) AMMRC CTR 73-24 9b. OTHER REPORT NO(S) *(Any other numbers that may be assigned this report)* LBL-1474	

10. DISTRIBUTION STATEMENT

Approved for public release; distribution unlimited.

11. SUPPLEMENTARY NOTES Details of illustrations in this document may be better studied on microfiche	12. SPONSORING MILITARY ACTIVITY Army Materials and Mechanics Research Center Watertown, Massachusetts 02172

13. ABSTRACT

The relationship between microstructure, heat treatment and room temperature fracture toughness has been determined for the low alloy ultra-high strength steels 4130, 4330, 4340, 4140 and 300-M. Optical metallography, microprobe analysis, and scanning electron microscopy were used to characterize the structure and morphology, while both Charpy V-notch impact tests and plane strain fracture toughness tests were used to determine the fracture properties. The normal commercial heat treatment resulted in the formation of some bainite in all the alloys. MnS inclusions on prior austenite grain boundaries were found to initiate cracks during loading. By increasing the austenitizing temperature to 1200°C, the fracture toughness could be increased by at least 60%. For some alloys increasing the severity of the quench in conjunction with the higher austenitizing temperatures resulted in further increases in the fracture toughness, and the elimination of any observable upper bainite. There was no correlation between the Charpy impact test results and the fracture toughness results. The alloys 4130, 4140, 4340 all showed a severe intergranular embrittlement when austenitized at high temperatures and tempered above 200°C, while the alloys 4330 and 300-M exhibited no drop in toughness for the same heat treatment conditions. The as-quenched tensile specimens had a very low "micro" yield strength which rapidly increased to the level of the "macro" yield strength when tempered. (Authors)

DD FORM 1 NOV 65 1473 REPLACES DD FORM 1473, 1 JAN 64, WHICH IS OBSOLETE FOR ARMY USE.

UNCLASSIFIED

UNCLASSIFIED
Security Classification

14 KEY WORDS	LINK A ROLE	LINK A WT	LINK B ROLE	LINK B WT	LINK C ROLE	LINK C WT
Fracture properties						
Toughness						
High strength steels						
Heat treatment						
Martensite						

UNCLASSIFIED
Security Classification

AMMRC CTR 73-24

AN INVESTIGATION OF METALLURGICAL FACTORS WHICH AFFECT FRACTURE TOUGHNESS OF ULTRA–HIGH STRENGTH STEELS

Technical Report by

WILLIAM E. WOOD, EARL R. PARKER, and VICTOR F. ZACKAY

Lawrence Berkeley Laboratory
University of California
Berkeley, California 94720

May 1973

Final Report
LBL-1474

Contract Number DAAG46-72-C-0220

D/A Project 1T061101A91A
AMCMS Code 611101.11.844
In-House Laboratory Initiated R&D
Agency Accession Number DA OD4801

Approved for public release; distribution unlimited.

Prepared for

ARMY MATERIALS AND MECHANICS RESEARCH CENTER
Watertown, Massachusetts 02172

FOREWORD

This report covers the work done in the period June 26 to December 26, 1972, under the general title *Untempered Ultra-High Strength Steels of High Fracture Toughness*. The work was sponsored by the Army Materials and Mechanics Research Center on Contract No. DAAG46-72-C-0220. It was funded under ILIR category, Accession No. 4801, Program Element 61101A, Project No. 1T0611091A. Dr. L. A. Shepard acted as Contract Officer Representative.

A portion of the work was sponsored under AEC Contract No. W-7405-eng-48.

AN INVESTIGATION OF METALLURGICAL FACTORS WHICH AFFECT THE FRACTURE TOUGHNESS OF ULTRA HIGH STRENGTH STEELS

Contents

Abstract v

I. Introduction 1

II. Experimental Procedure 3

A. Material Preparation 3

B. Heat Treatment 3

C. Mechanical Testing 5

1. Impact Tests 5

2. Tensile Tests 6

3. Fracture Toughness Tests 7

D. Microscopy 8

1. Optical Metallography 8

2. Scanning Electron Microscopy 9

III. Results 10

A. Heat Flow Profiles 10

B. Mechanical Tests 11

1. Fracture Toughness Tests 11

2. Impact Tests 18

3. Tensile Testing Results 19

C. Microscopy 21

1. Metallography 21

2. Fractography 29

IV. Discussion 38

V. Summary and Conclusions 59

Acknowledgements 61

References 62

Tables 69

Figure Captions 100

Figures 111

AN INVESTIGATION OF METALLURGICAL FACTORS WHICH AFFECT THE FRACTURE TOUGHNESS OF ULTRA HIGH STRENGTH STEELS

William E. Wood,* Earl R. Parker and Victor F. Zackay

Inorganic Materials Research Division, Lawrence Berkeley Laboratory and Department of Materials Science and Engineering, College of Engineering; University of California, Berkeley, California

ABSTRACT

The relationship between microstructure, heat treatment and room temperature fracture toughness has been determined for the low alloy ultra-high strength steels 4130, 4330, 4340, 4140 and 300-M. Optical metallography, microprobe analysis, and scanning electron microscopy were used to characterize the structure and morphology, while both Charpy V-notch impact tests and plane strain fracture toughness tests were used to determine the fracture properties. The normal commercial heat treatment resulted in the formation of some bainite in all the alloys. MnS inclusions on prior austenite grain boundaries were found to initiate cracks during loading. By increasing the austenitizing temperature to 1200°C, the fracture toughness could be increased by at least 60%. For some alloys increasing the severity of the quench in conjunction with the higher austenitizing temperatures resulted in further increases in the fracture toughness, and the elimination of any observable upper bainite. There was no correlation between the Charpy impact test results and the fracture toughness results. The alloys 4130, 4140, 4340 all showed a severe intergranular embrittlement when austenitized at high temperatures and tempered above 200°C, while the alloys 4330 and 300-M exhibited no drop in toughness for the same heat treatment conditions.

---

*Submitted to the University of California Graduate Division in partial fulfillment for the degree of Doctor of Engineering.

The as-quenched tensile specimens had a very low "micro" yield strength which rapidly increased to the level of the "macro" yield strength when tempered.

I. INTRODUCTION

Low alloy ultra-high strength steels such as 4340 have been available commercially for over forty years.[1] However, they are seldom used above 200,000 psi because their toughness is very low at these high strength levels. There are some instances where these alloys are heat treated to achieve the maximum strength level, where strength in relation to size and weight is the dominating factor. These situations are exactly the ones where the toughness is the worst, and where better toughness is desperately needed.

The alloys studied in this investigation were 4130, 4330, 4140, 4340, and 300-M. In addition, a limited amount of work has been done on alloys 3140 and 4350. These alloys allowed varying the carbon content while keeping the other elements the same. Also, it allowed the alloy contents to be changed without changing the amount of carbon present. Thus both the effect of varying the carbon (and hence strength) and the effect of varying the alloying elements could be studied as a function of the austenitizing temperature, quenching rate, and tempering temperature.

All of these steels are conventionally put in a class called tempered martensitic, which implies that they are capable of being quenched to form a martensitic structure for the section sizes in which they are used.

The purpose of this investigation was to determine the microstructure-toughness relationship of several commercially heat treated low alloy ultra high strength steels that are widely used today. Once this relationship is known, then the toughness can be optimized by altering

the heat treatment schedule to produce a microstructure more resistant to fracture.

The resistance to fracture was measured using both Charpy V-notch impact tests and the concepts of linear elastic fracture mechanics to establish the plane strain fracture toughness of the alloys under a variety of heat treatment conditions. A knowledge of the fracture toughness of these materials and the way in which it depends on their heat treatment is essential for the safe design of structures utilizing high strength steels in which very small flaws can lead to catastrophic failure.

It is difficult, if not impossible, to design reliable structures which meet todays demands by using alloys that were developed over forty years ago utilizing concepts and standards, which since then have proven to be inadequate. However, it is equally difficult to design new alloys for todays needs without first understanding not only the limitations of alloys currently in use, but also what fundamental aspect of the material is responsible for these limitations. In a sense then, this investigation seeks to first define the limitations of several low alloy steels which commercially used, then to determine what causes these limitations, and then finally to improve the mechanical properties as much as possible without changing the basic alloy itself. Thus, this represents an intermediate stage, which hopefully will lead to the development of new alloys.

II. EXPERIMENTAL PROCEDURE

A. Material Preparation

The low alloy ultra high strength steels used in this investigation were all commercial aircraft quality steels received in the fully annealed condition. Table I lists these alloys and the chemical analysis of each. Several alloys were received in two or more lengths and a chemical analysis was then done for each length. Thus, in Table I the letter A, B or C following a particular alloy (i.e., 4340-A or 4340-B) refers to a particular piece of that alloy. The carbon level of the alloys was checked at least twice because of the sensitive way in which the mechanical properties depend on the amount of carbon present.

B. Heat Treatment

The austenitizing treatment was done in a vertical tube type furnace shown in Fig. 1. The furnace was sealed at both the top and bottom and austenitizing was carried out in an argon atmosphere for 1 hour. The material being austenitized was then quenched by removing the bottom and dropping it through the bottom and directly into the agitated quench bath below. The tempered specimens were held in a salt bath for 1 hour.

For this investigation the austenitizing temperature, the quench medium, and the tempering temperatures were varied, although not all possible combinations were used for any one alloy. Austenitization was done for 1 hour at either 870°C, 1100°C, 1200°C or at 1200°C for 1 hour followed by cooling to 870°C and holding for a total of 30 minutes and then quenching. This austenitizing schedule will be referred to as a step quench treatment. There were three basic quenches used:

1) room temperature oil quench, 2) room temperature water quench, and 3) ice brine quench followed immediately by refrigeration in liquid nitrogen. In a few cases an oil quench was followed by liquid nitrogen refrigeration.

In order to obtain a quantitative measurement of the differences in the severity of the quenches used and to determine how much time was required to bring specimens to the temperature of the furnace, cooling and heating rates were measured for the fracture toughness specimen. Two platinum-platinum 10% rhodium thermocouples were placed as shown in Fig. 2. Both thermocouples were placed at the midsection thickness and alloy steel set screws were placed in the side of the specimen to insure that the junction of the thermocouples would be held firmly in place. Finally, a silica cement was used to seal the point where the ceramic tubing entered the specimen and to also provide support. In order to prevent the ceramic tubing from cracking when immersed in the quench, and the wires from shorting, a second ceramic sleeve was fitted over the thermocouple tubing. This outer sleeve could either be replaced or major cracks cemented with the silica paste. This enabled one thermocouple and specimen to be used several times.

With the thermocouple firmly in place and sealed, the entire setup could be positioned in the furnace and the temperature recorded on two strip chart recorders. As soon as the specimen had reached the furnace temperature the entire setup was pulled from the vertical tube furnace and dropped into the appropriate quenching medium. This arrangement allowed the internal temperature of the fracture toughness specimen to be continuously monitored and recorded throughout the

entire heat treatment using two independent thermocouples, each acting as a check on the other.

All fracture toughness specimens, Fig. 3, were heat treated individually. However, an attempt was made to duplicate the cooling rates in the fracture toughness specimens as closely as possible in the Charpy V-notch specimens too. To do this, Charpy blanks were cut 5/8 in. × 5/8 in. × 2 1/4 in. and wired together in groups of four (Fig. 4) to form one block 2 1/4 in. × 2 1/2 in. × 5/8 in. These blocks were then austenitized and quenched individually. Similarly, the tensile specimens (Fig. 5) were first cut as blanks, each 5/8 in. × 5/8 in. × 3 3/4 in. These were wired together in groups of three in the same manner as the Charpy specimen blanks.

C. Mechanical Testing

1. Impact Tests

The room temperature longitudinal impact properties were determined using the standard ASTM Charpy V-notch specimen as shown in Fig. 6. The tests were done on a pendulum type impact testing machine adjusted to a 60 ft-lb capacity.

The austenitized and quenched Charpy blanks were first tempered and then ground equally on all four sides to final dimensions, and a notch machined on the sides as shown in Fig. 7. Duplicate tests were done for all heat treatments. In order to check whether there was an effect on the Charpy values due to position in the prior heat treated block (i.e., position 1, 2, 3 or 4 in Fig. 4) specimens to be tempered duplicately were always taken from the first and third positions or second and fourth positions in the block.

2. Tensile Tests

The room temperature longitudinal tensile properties were determined using a 1.4 in. gage length, 0.357 in. diameter ASTM specified round specimen shown in Fig. 8. These specimens were ground from the blanks that had been previously austenitized, quenched and tempered. Duplicate tests were performed on all the specimens in the as-quenched and 280°C tempered condition.

A 300,000 lb capacity MTS machine was used to test the specimens at a loading rate of 0.04 in./min. The yield strength was determined on both a "macro" and micro yield strength level.

The "macro" 0.2% offset yield strength was determined from the load vs total stroke or crosshead displacement curve and the measured elongation. The total crosshead movement was divided into the total amount of elongation from which the amount of stroke movement corresponding to 0.002 strain can be determined. The "micro" yield strength on the other hand was determined by using two linear variable displacement transducers (LVDT) mounted on opposite sides of the tensile specimen in a configuration shown in Fig. 9.

By using two transducers mounter on opposite sides, any error due to specimen buckling or non-uniform loading is automatically cancelled. Also extraneous strain from the specimen grips, threads, etc is eliminated. The signal from each LVDT was fed into a Daytronic model 300D Transducer amplifier which added the signals from both transducers. Calibration of the output of the transducers, Daytronic amplifier and X-Y recorder setup was done using a special micrometer calibration unit shown in Fig. 10. By switching the amplifier from the single output modes to

the add modes, it was possible to calibrate the output of either one or both of the transducers simultaneously. The micrometer attached to the calibration unit had a 1.0 in. barrel movement with a 100 to 1 reduction sleeve inside. Thus, the micrometer had a total range of 0.01 in. This provided a method of calibrating the output of the entire setup down to a least reading of 10^{-5} in. of displacement. Hence it is possible to measure strain very accurately and to observe any microyielding, which is not evident, if only the total crosshead movement is measured.

3. Fracture Toughness Tests

The room temperature longitudinal plane strain fracture toughness was determined using the ASTM specified[2] compact tension testing specimen, Fig. 3. All specimens were machined from 5/8 in. thick bar stock to final dimensions except for the thickness and 0.008 in. slot. After heat treating 0.010 in. was ground off each side and an 0.008 in. thick slot was machined in order to act as a notch for introducing a fatigue crack. A 300,000 lb capacity MTS machine was used to fatigue-precrack the specimens at 6 cycles/sec. All fatigue cracks were fatigued at least 0.10 in. and fatigue loads were kept within ASTM recommendations.[3]

The stress intensity for the compact tension specimen has been determined by Srawley and Gross, and can be expressed as a function of specimen geometry and loading to result in the following equation

$$K = \frac{P}{BW^{1/2}} f\left(\frac{a}{W}\right) \tag{1}$$

$$f\left(\frac{a}{W}\right) = 29.6\left(\frac{a}{W}\right)^{1/2} - 185.5\left(\frac{a}{W}\right)^{3/2} + 655.7\left(\frac{a}{W}\right)^{5/2} - 1017\left(\frac{a}{W}\right)^{7/2} + 638.9\left(\frac{a}{W}\right)^{9/2}$$

where K is the stress intensity, P the load, B the thickness, W the specimen width and a the crack length.

The fracture toughness specimens were tested on a 5000 kg. Instron at a crosshead movement rate of 0.04 in./min which resulted in a loading rate within ASTM recommendations.[9] A crack-opening-displacement (COD) gage was used to follow the crack length during each test. With the use of a crack-opening-displacement vs crack length calibration curve, Fig. 11, for this particular specimen geometry, the crack length during each test could be determined from the crack-opening-displacement (ν) measured with the COD gage. Hence the stress intensities K_{Ic} and K_Q could be determined using Eq. (1) in accordance with the ASTM standards.[3]

D. Microscopy

1. Optical Metallography

Sections to be used for metallography were cut from the midthickness of the fracture toughness specimens. They were mounted in Koldmount and ground on successively finer papers to 600 grit and then polished to a 1μ finish using a diamond paste. All specimens were etched in a 4% picral, 1% nital solution. Metallography was done using bright field, polarized light and/or interference contrast methods.

2. Scanning Electron Microscopy

A Jeolco JSM-U3 scanning electron microscope (SEM) with a secondary emission at 25 kV was used to examine the fracture surfaces. While the specimens were being sectioned in order to fit in the SEM, the fracture surface was protected with acetate tape. Afterwards the tape was stripped and the specimen ultrasonically cleaned.

III. RESULTS

A. Heat Flow Profiles

Heating and cooling curves corresponding to the temperature profiles in the center of a fracture toughness specimen were determined for the different heat treatment schedules used in this investigation. Table II shows the temperature profile during heating from room temperature in an argon atmosphere. The temperature profile was monitored two times and appears in Table II as run 1 and run 2. Also shown in Table II is data corresponding to furnace cooling from about 1200°C to 870°C. Figure 12 shows these results graphically.

Tables III and IV give the results of the ice brine, water and oil quenches from either 870°C or 1200°C. These results, plotted in Figs. 13 and 14, show the differences in the severity of the different quenches. The oil quench is markedly slower than the other two quenches. Cooling rates at selected temperatures were determined by drawing a tangent line to the curves. These rates, Table V, were determined at 150, 300, 500, 700 and 900°C for each of the cooling curves. The results show that the ice brine quench results in a faster cooling rate than a water quench at temperatures above 300°C, but that at 300°C and 150°C the cooling rates are essentially the same. The oil cooling rates are, however, much slower, as expected.

B. Mechanical Tests

1. Fracture Toughness Tests

The room temperature longitudinal plane strain fracture toughness results for the alloys investigated are given in Tables VI through XII. In these tables the ratio $\frac{P_m}{P_q}$ is determined from the load vs crack opening displacement curve generated during the test. This is shown schematically in Fig. 15. These ratios are included in the tables since they are a new restriction placed on the determination of the validity of K_{Ic}. The ASTM now specifies[3] that this ratio must be less than or equal to 1.10. However, this requirement is believed to have been added because of discrepancies in the fracture toughness of titanium alloys. As can be seen in Tables VI through XII, the values of this ratio varied, both above and below the value of 1.10, within duplicate tests. This did not result in any significant differences in the calculated fracture toughness however, and for this investigation the fracture toughness values are reported as valid plain strane fracture toughness tests as long as the other requirements are met.

The plane strain fracture toughness, K_{Ic}, is calculated using the load P_Q and the associated crack opening displacement (Fig. 15). The value calculated is the valid plane strain fracture toughness if the following two conditions are met:

1. $\frac{P_m}{P_Q} < 1.10$

2. $B > 2.5 \frac{K_Q}{\sigma_{ys}}$

The critical stress intensity, K_{crit}, is calculated at the point of the maximum load, P_{max}.

a. Alloy 4130

The fracture toughness results for all conditions tested are given in Table VI, and some of these are plotted in Fig. 16. For this alloy the normal commercial heat treatment is to austenitize at 870°C followed by oil quenching, (870, Oil). This results in a fracture toughness of 57 ksi-in.$^{1/2}$ for the as-quenched condition. If the specimen is ice brine quenched and refrigerated in liquid nitrogen (L.N.) after austenitizing at 870°C, (870, IBQLN) there is no increase in toughness. However, by raising the austenitizing temperature from 870°C to 1200°C, followed by oil quenching, the toughness abruptly increases to 85 ksi-in.$^{1/2}$ in the as-quench condition. From Fig. 16, it is seen that the maximum toughness is obtained by austenitizing at 1200°C followed by an ice brine quench and L.N. refrigeration (1200, IBQLN). If the austenitizing temperature is lowered to 1100°C, the toughness again drops from 99 ksi-in.$^{1/2}$ to 69 ksi-in.$^{1/2}$. The response to tempering for the commercial heat treatment (870, Oil) and the best heat treatment (1200, IBQLN) are exactly opposite. The (870, Oil) heat treatment shows no response until tempered at a high enough level to cause a drop in strength and hence an increase in toughness. On the other hand, the (1200, IBQLN) treatment does exhibit a response to a low 200°C temper but then drops catastrophically at higher temperatures down to the level of the commercial heat treatment. This is a common phenomenon in high strength steels and is referred to as "500°F embrittlement". Finally, the value of the fracture toughness

achieved for any heat treatment condition is very sensitive to the amount of carbon. Figure 16 illustrates how changing the carbon content from 0.30 to 0.33 shifts the fracture toughness of both the commercial heat treatment and the (1200, IBQLN) heat treatment lower. Summarizing then, in order to obtain the best possible fracture toughness, both a 1200°C austenitizing temperature and a very severe quench are required.

b. Alloy 4140

The longitudinal fracture toughness results for all the conditions investigated are given in Table VII. This alloy is similar to alloy 4130 except for the higher carbon and slightly higher manganese content. The as-quenched (870, Oil) commercial heat treatment has a very low fracture toughness of 27 ksi-in.$^{1/2}$. By increasing the austenitizing temperature to 1100°C, the fracture toughness is only raised to 33 ksi-in.$^{1/2}$. However, austenitizing at 1200°C and oil quenching results in a much larger increase in toughness to about 51 ksi-in.$^{1/2}$. In addition, if the (1200, Oil) heat treatment is followed by liquid nitrogen refrigeration, the fracture toughness remains unchanged from that of the (1200, Oil) heat treatment without L.N. refrigeration. Finally, from Table VII, it can be seen that a step quench (1200→870, Oil) heat treatment results in only a very small increase in fracture toughness over that of a commercial (870, Oil) heat treatment.

Ice brine liquid nitrogen (IBQLN) quenches were used after both a 1200°C and a 1200→870°C austenization treatment. The (1200→870, IBQLN) treatment resulted in little, if any increase over that of a (1200→870, Oil) heat treatment, and the (1200, IBQLN) heat treatment actually showed a drop in toughness as compared to a (1200, Oil) heat treatment.

The response of the fracture toughness to tempering for three heat treatments is shown in Fig. 17. It can be seen that the increase in fracture toughness associated with an increasing austenitizing temperature is maintained during tempering until the "500°F embrittlement" range is reached. Then both the higher austenitizing heat treatments have an abrupt drop in toughness similar to that of alloy 4130. Also, as in the case of the alloy 4130, the higher the maximum toughness achieved, the greater the loss in toughness when tempered in the 280 to 350°C range. As in the alloy 4130, when the drop in toughness occurs, it reduces the toughness to that of the commercial heat treatment at the tempering temperature of 350°C.

c. Alloy 4330

Table VIII lists the fracture toughness results for all the test conditions used in this investigation for alloy 4330. The normal commercial heat treatment is again to austenitize at 870°C and oil quench. The fracture toughness results and response to tempering after an (870, Oil) and a (1200, IBQLN) heat treatment are shown in Fig. 18. Unlike alloy 4130, this alloy responds to tempering after being given an (870, Oil) heat treatment. Most significantly though, is the fact that this alloy does not exhibit a severe drop in toughness when tempered above 200°C. There are two other significant results. Referring to Table VIII, it can be seen that a (1200, Oil) heat treatment results in a fracture toughness intermediate between the commercial (870, Oil) and the high temperature, severe quench (1200, IBQLN) heat treatment. This result parallels that of 4130, in that both the high

austenitizing temperature and the extreme quench are necessary in order to obtain the best results. Secondly, the step quench heat treatment (that is 1 hour at 1200°C followed by 30 minutes at 870°C and then quenching) with either an ice brine quench with L.N. refrigeration, or an oil quench does not result in as high a fracture toughness as a direct quench from 1200°C into either an IBQLN or oil quench.

d. Alloy 4340

This alloy was the most thoroughly investigated in so far as thirteen different austenitizing and quenching combinations were examined in the as-quenched condition. Of these combinations, three were selected to further investigate the tempering response. Table IX lists the results obtained for all the tests that were done using the alloy 4340. The most obvious result is that four of the heat treatments resulted in quench cracks radiating outwardly from the notch in the fracture toughness specimen. On the one hand, an oil quench after either 870°C, 1200°C or 1200→870°C austenitization did not produce any quench cracks. On the other hand, either an ice brine quench with L.N. refrigeration (IBQLN) or a water quench resulted in a quench crack, if the specimen was first austenitized at either 870°C or 1200°C. However, neither the IBQLN quench nor the water quench resulted in quench cracks following a step quench (1200→870) austenitization sequence. It should be noted that a complete test was obtained in one case for a (1200, IBQLN) heat treatment. However, this specimen was probably internally cracked which would explain the low value of K_{Ic} and K_{crit} obtained. It should also be noted that all quench cracks followed prior austenite grain boundaries and that cracking occurred during the quench itself.

In an attempt to determine whether any retained austenite might be affecting the fracture toughness a (1200→870, Oil) and a (870, Oil) heat treatment were followed by immediately refrigerating into liquid nitrogen. The fracture toughness results did not indicate any significant effect due to the refrigeration.

For alloy 4340, it is evident from Table IX that there is no advantage to quenching in a medium faster than oil, and in fact there is no advantage in quenching directly from 1200°C as opposed to a step quench. As with alloys 4130 and 4140, 4340 exhibits a drop in toughness if either a direct quench from 1100°C or a (1100→870) treatment is used rather than the equivalent heat treatment from 1200°C. Figure 19 shows graphically the increase in fracture toughness that can be achieved over that of a commercial (870, Oil) heat treatment. The (870, Oil) heat treatment has an extremely low as-quenched fracture toughness, but climbs rapidly with tempering, except in the "500°F embrittlement" range. The step quenched treatment shows its best toughness tempered at 200°C, but then exhibits a sharp drop in toughness similar to that of alloys 4130 and 4140.

e. Alloy 300-M

The chemical composition of alloy 300-M (Table I) is very similar to that of 4340 except that alloy 300-M has silicon and a small amount of vanadium added. The longitudinal plane strain fracture toughness results for all conditions investigated for 300-M are given in Table X. Three of the specimens were double tempered at 245°C. Double tempering consisted of tempering for 1 hour at 245°C followed by quenching to room temperature in water and then re-tempered for one additional hour

at 245°C. However, none of these treatments result in a significantly higher fracture toughness than did the single temper treatment at 245°C. This alloy does have a significantly different response to both a step quench and to tempering than does alloy 4340. Alloy 4340 showed no difference in toughness when given a (1200, Oil) or (1200→870, Oil) heat treatment. However, Figure 20 shows that alloy 300-M develops a response similar to the other alloys investigated, in that the step quench does not result in as high a fracture toughness as does the direct quench from 1200°C. Also alloy 300-M does not exhibit a sharp drop in toughness when tempered above 200°C, as do all the other alloys, except alloy 4330. 300-M does seem to be affected by liquid nitrogen refrigeration after an oil quench. A (1200, Oil) heat treatment in the as-quenched condition results in a fracture toughness of about 46 ksi-in.$^{1/2}$; whereas, the same heat treatment followed by an immediate refrigeration in liquid nitrogen results in a fracture toughness of only 35 ksi-in.$^{1/2}$. However, additional tests are required to determine if there is a real difference or just scatter in the data.

f. Alloy 4350

A preliminary investigation has been done on alloy 4350 to determine whether a high austenization and a step quench treatment would result in an increase in fracture toughness over that of the commercial (870, Oil) heat treatment for a relatively high carbon low alloy steel. The results in Table XI indicate that the beneficial increase in toughness is obtained, even though the fracture toughness is low compared to the lower carbon alloys.

g. Alloy 3140

A limited amount of data has been obtained for alloy 3140 and is given in Table XII. The fracture toughness for both the (1200, Oil) and (870, Oil) heat treatments are graphed as a function of tempering temperature in Fig. 21. While the information is not complete, the results in Table XII and Fig. 21 show that this alloy does respond significantly to the (1200, Oil) heat treatment and that as for several other alloys the step quench heat treatment does not result in as high a fracture toughness as the direct (1200, Oil) heat treatment. Finally, this alloy does show an abrupt drop in toughness when the direct (1200, Oil) heat treatment is tempered above 200°C.

2. Impact Tests

The room temperature Charpy V-notch impact properties were determined for alloys 4130, 4330, 4340, 300-M and D6-AC as a function of tempering temperature for different austenitizing temperatures and quenches. Table XIII gives the results obtained for all the tests. These results are also shown graphically in Figs. 22 through 25. The graphs were plotted by using the average value of the two Charpy tests done each heat treatment.

The results show that there is very little difference, if any, in the general shape or values of the Charpy V-notch data regardless of the austenitizing temperature or quench used. There is no correlation between these results and those obtained using fracture toughness specimens.

3. Tensile Testing Results

The room temperature longitudinal tensile properties of alloys 4130, 4330, 4140, 4340, 300-M and D6-AC were determined using the parallel linear transducer arrangement described previously. The results are listed in Tables XIV through XIX and shown graphically in Figs. 26 through 31. There are several important points which will be discussed further: (1) the presence of quench cracks, (2) micro vs macro yield strengths, and (3) the effect of specimen size on strength.

The problem of quench cracks occurred in the specimens with a large grain size and quenched in an IBQLN and sometimes a water quench. The immediate effect is that the elongation and reduction of area are very low. The specimens that had visible quench cracks are marked by an asterisk in Tables XIV through XIX. However, the lack of a visible quench crack does not mean that failure did not originate from a surface flaw or machining mark. The high strength and large grain size makes these materials very sensitive to surface finish. By carefully polishing the reduced section of the specimens it is quite easy to drastically increase the reduction of area achieved during a test.

The second point, that of micro vs macro yield strength, is also very important. The shaded region (Figs. 26 through 31) represents the difference in the measured 0.2% offset yield strength. For every alloy this difference is a maximum for the as-quenched specimens and upon tempering gradually shrinks to a point where there is no difference between the two measurements. In an attempt to measure the error introduced in the macro yield strength measurement due to loading in

the grips and the threads, a "zero" gage length "specimen" was machined. This "specimen" consisted of a 2 in. long 5/8 in. diameter completely threaded section, heat treated to approximately a 210,000 psi yield strength. This "specimen" was then threaded into the tensile grips until the grips were touching each other, and a load then applied up to 35,000 pounds, which corresponded to the maximum load reached in the actual tensile tests. The amount of crosshead displacement can then be measured for any load up to 35,000 pounds. These results were then subtracted from actual tensile tests for alloy 4340, and the corrected macro yield stress, designated "macro", included in Table XVII. This did reduce the difference between the micro and macro yield by about half for the low tempered specimens, and at the same time did not change the results for the specimens tempered at 280 or 350°C. This latter result is probably due to the definite yield point that occurs for the 280 and 350°C tempered specimens, since when a definite inflection point occurs, it is automatically taken as the yield point. Subtracting the displacement due to the grips and threads does not alter the load at which this point occurs.

The general shape of the tensile curves obtained using the extensometers is shown in Fig. 32A as a function of tempering temperature for alloy 4130 given a (870, Oil) heat treatment, while Fig. 32B shows the macro stress strain curves for the same two tensile specimens. The as-quenched specimen has almost no linear region as measured by the extensometer arrangement, and has an essentially parabolic shape. On the other hand, the "macro" curves are both linear. The general shape of these curves is the same for all alloys, both large and small grain sizes

and for all heat treatments.

All the tensile data shown in the tables and figures was obtained using 0.357 in. diameter tensile specimen heat treated in blocks of three as described previously. However, some initial work was done using 0.250 in. round specimens ground slightly over sized, and then heat treated. This resulted in a macro yield strength for alloy 4340 of about 255,000 psi or about 25-30,000 psi higher. On the other hand, the same test procedure did not result in a macro yield stress that was any higher for alloys 4130 and 4330.

C. Microscopy

1. Metallography

Optical metallography was done to determine the as-quenched structure of alloys 4130, 4330, 4140, 4340 and 300-M. The metallography was done in all cases on sections cut from actual fracture toughness specimens. The results show that there is a mixed microstructure present in probably all of the specimens examined. These microstructures ranged from that of blocky ferrite, bainite and martensite, to almost entirely martensite with just a trace of decomposition product along prior austenite grain boundaries. All of the specimens austenitized at 870°C have a fine grain size, while those austenitized at 1200°C have a very large coarse grain size with grain diameters averaging about 0.15 mm as compared with a grain diameter of approximately 0.015 mm for the fine grain material. The fine grain size made it difficult to resolve the microstructural constituents either in the grains or along grain boundaries, since at a magnification of 1000× a grain would only be about 1 cm in diameter. Thus for all the fine

grained specimens, micrographs were taken at magnifications ranging from 1000× to 2500× using an oil immersion lense. These negatives were then enlarged approximately 2× for final printing.

By using EPI-Nomarski differential interference microscopy, it is possible to achieve a much greater contrast and surface relief effect than by using just reflected light methods. The interference technique, abbreviated as I.C., generates contrast optically by interference of light waves traversing slightly different optical paths. This differential interference produces an optically "shadow cast" image, creating a 3 dimensional effect and bringing any surface differences into high relief. In effect, it can be used to view the surface topography within the limits of resolution of the microscope. This technique is used in conjunction with cross polarized light and a green filter. Thus when working at magnification of 1000× and above, the amount of light reaching the specimen is very small. Therefore, long exposure times were required even when using very high speed film, ASA 800. The combination of high magnification and long exposures made the problem of vibration very difficult, to the point where even the shutter being released caused enough vibrations to sometimes blur the photomicrograph. The microstructure of the alloys studied has been characterized in the following sections. For all the samples examined, a detailed and extensive examination was made of many areas of these samples at least three times. Thus it is felt that the micrographs shown in the following sections are representative of the microstructure of the fracture toughness specimens tested.

Reproduced from best available copy.

a. Alloy 4340 (0.027 in. Thick Sheet)

The as-quenched microstructure for a (1200°C, IBQLN) heat treated section of 4340, 0.027 in. thick is shown in Fig. 33. This structure is fully martensitic without any trace of a decomposition product visible.

b. Alloy 4130

The as-quenched microstructure after austenitizing at 1200°C and ice brine quenching followed by liquid nitrogen refrigeration is shown in Figs. 34, 35 and 36. The large grain size of the specimens austenitized at 1200°C is revealed in these figures. The microstructure is comprised of martensite and bainite which has nucleated along prior austenite grain boundaries (Fig. 35). Figure 36 clearly shows how these plates grow out from the grain boundaries. Small particles can be seen in Fig. 35 and are about 1 micron in diameter. These have been identified as MnS particles by a microprobe analysis.

If an oil quench is used from 1200°C rather than an ice brine quench, then a significant change occurs in the resulting microstructure. The (1200, Oil) heat treatment results in extensive formation of upper bainite through nucleation along prior austenite grain boundaries, Figs. 37 through 42 (bainite is indicated by arrows in Fig. 37, 38 and 39). The alternating parallel sheaths of ferrite and iron carbide are clearly visible and characteristic of upper bainite.[4,5]

Using a step quench into oil, (1200→870, Oil) does not produce a change in the microstructure. Upper bainite is visible again originating from grain boundaries (Figs. 43 and 44).

The first microstructure so far with a fine grain size is shown in Fig. 45. This sample was cut from a fracture toughness specimen that had been given a (870, IBQLN) heat treatment. At first glance there is nothing particularly distinctive about this micrograph, except that the structure is much finer than for the large grained material. However, a closer examination reveals that the microstructure consists of thin plates or in some cases several plates parallel to each other (see arrows in Fig. 45). Figure 46A is another micrograph taken at the same magnification as Fig. 45 and again these dark etching plates are visible. A higher magnification micrograph taken from the same area as Fig. 46a is shown in Fig. 46B. Now the nature of these dark plates can be more clearly identified. Figure 47, taken at twice the magnification of Fig. 46B, clearly shows the parallel arrangement of the upper bainite laths, which have nucleated along the grain boundaries. The lengths of the bainite laths and also of any martensite laths is limited by the size of the prior austenite grain size. Thus an ice brine quench is still not fast enough to avoid the formation of upper bainite in the fine grained material. Finally, a micrograph of the same material but utilizing interference contrast techniques is shown in Fig. 48. This clearly shows the bainitic nature[4,5,6] of the microstructure which resulted from a (870, IBQLN) heat treatment.

The microstructure which results from the commercial 870°C austenitization followed by an oil quench is shown in Figs. 49 and 50. Figure 50 reveals that this heat treatment results in the formation of ferrite and very coarse upper bainite in which the ferrite laths

are very wide. Figure 49 represents an area very near to the surface of the specimen where the material underwent a more rapid rate of cooling. The structure is still bainite although on the finer scale than in the middle of the specimen. The structure near the surface of the oil quenched specimen (Fig. 49) is very similar to the appearance of the specimen cut from the center of the (870, IBQLN) specimens.

c. Alloy 4330

The microstructure of the (1200, IBQLN) heat treated fracture toughness specimen is very similar to that of alloy 4130. The general appearance of the microstructure of this alloy for this heat treatment is shown in Fig. 51. It is difficult to identify without transmission electron microscopy whether this heat treatment results in a fully martensitic or mixed martensitic and bainitic structure. However, a decomposition product can be seen along the sites of prior austenite grain boundaries. For the (1200, Oil) heat treatment though, there are small regions of upper bainite found occasionally along prior austenite grain boundaries. An interference contrast micrograph (Fig. 52) in which the dark etching region, marked by arrows, can actually be seen to consist of many very finely spaced parallel plates originating from the grain boundary. The long dark etching plates radiating outward from the grain boundaries in the (1200, Oil) heat treatment (Fig. 53) are actually made up of several parallel units characteristic of bainite. Finally, a very fine film of ferrite outlines the grain boundary in Fig. 54 for the (1200, Oil) heat treatment. All the features identified in Figs. 52 through 54 for the (1200, Oil) heat treatment can also be found in the specimen given a (1200 -870, Oil) heat treatment (Fig. 55).

The microstructure of the fine grained material given a (870, Oil) heat treatment is shown in Fig. 56. This microstructure is very similar to that of alloy 4130 in that the structure consists of both martensite and bainite with upper bainite visible throughout the microstructure and marked by the arrow in Fig. 56.

d. Alloy 4140

The microstructure of this alloy is shown in Figs. 56 through 62. As with the previously examined alloys, the (870, Oil) heat treatment resulted in the formation of extensive amounts of upper bainite (Figs. 57A and 57B). The large grained (1200, Oil) heat treatment eliminated almost all of the coarse upper bainite features found in the fine grained material. Occasionally a finger like or feathery type of decomposition product was observed. Examples of this are marked by arrows in Figs. 58 and 59, and also in Fig. 60, an interference contrast micrograph.

While there is not an extensive amount of dark etching constituent with a resolvable feathery type of morphology, there is a rather extensive network of black etching plate-like decomposition produce visible in Figs. 61 and 62. Figure 61, a bright field micrograph, shows this network very clearly and also shows some very long needle like dark etching constituents running completely across the grain. The surface relief effect of the same area using the interference contrast technique is shown in Fig. 62. In this figure, the two areas marked by the arrows are heavily etched and mottled due to the etching of the carbide by the nital and picral etch. Also, a close examination reveals that the area marked by the lower arrow actually has spikes growing

out from it, while the area marked by the upper arrow has several steps or ledges associated with it. Both these features are characteristic of the bainite reaction.[4,5,6] The beginnings of the long needle like rods that extend all the way across the grain are visible at the top of Fig. 62. These too have a feathery type of appearance which can just barely be resolved.

e. Alloy 4340

Both the step quenched (1200→870, Oil) and the (8/0, Oil) heat treatment in the as-quenched condition were examined extensively. As in the alloy 4140, a dark etching constituent is present along many of the grain boundaries of the large grained step quenched specimen (Fig. 63). Figures 64 and 65 are higher magnification micrographs in which the feathery type appearance is very clearly indicated by the arrows. Finally, Fig. 66 is a very high magnification micrograph with three important features visible. First, a ferrite film is visible along the prior austenite grain boundary. Second, a distinctly feathery type morphology is clearly distinguishable and characteristic of all the dark etching plates, the most pronounced of which is marked by the arrow at the top of the figure. Third, a large inclusion is present in the grain boundary and is marked by an arrow.

The effect of the added contrast due to the differential interference contrast techniques is brought out in Figs. 67 and 68 for the (1200→870, Oil) heat treatment. Both Figs. 67 and 68 were taken of the same exact area, with Fig. 67 using only normal bright field microscopy and Fig. 68 taken with I.C. technique. Note that the I.C. setup was adjusted for maximum contrast and not to show the surface relief effect

as was done in Fig. 62. Three areas are marked with arrows in Fig. 67, and the same three areas again marked in Fig. 68. The I.C. technique clearly shows the multiple parallel relief effect that exists within each dark etching plate in Fig. 67.

Finally, Fig. 69 was taken from a section cut parallel to the rolling direction for the (870, Oil) heat treated fracture toughness specimen. Again, bainitic plates are distinguishable throughout the microstructure and are marked by arrows. Also, and most noticeable, are the two rod-like stringers running nearly the entire length of the micrograph.

f. Alloy 300-M

Two micrographs are shown for this alloy. Just as in alloy 4140 and 4340, a dark etching constituent is found along many prior austenite grain boundaries of the large grained specimens (Figs. 70 and 71 after a (1200, Oil) heat treatment). The bright field micrograph in Fig. 70 does not reveal very clearly, if at all, the very finely spaced parallel lath type of arrangement growing out from the grain boundary, which is indicative of upper bainite,[4,5,6] and the individual subunits growing out from the end of two plates, characteristic of lower bainite. This fine detail is, however, very clearly revealed in Fig. 71 by the use of I.C. techniques.

g. Fracture Path Characteristics

The effect of upper bainite along grain boundaries is shown in Fig. 72. The fracture surface was nickel plated to protect it while a vertical section was cut through the fracture surface. Fracture has occurred intergranularly in a very brittle manner along a prior austenite

grain boundary from which upper bainite has nucleated (Fig. 72B). There is no plastic deformation visible along the bainite interface and thus very little energy was absorbed as the crack front advanced. This is in contrast to Fig. 72A in which plastic deformation is evident and in which the advancing crack front had to change directions many times in the absence of any upper bainite.

2. Fractography

An effort was made to determine whether an alloy that is 100% martensite and in which little or no autotempering occurred, is ductile or brittle. Strips of both alloys 4140 and 4340 were cut 3 in. by 3/4 in. and ground flat to a final thickness of 0.027 in. One piece of each alloy was given the commercial heat treatment consisting of (870, Oil) while a second piece of each alloy was given a (1200, IBQLN) heat treatment. Immediately after quenching each piece was clamped in a vise and hit with a hammer. The results are shown in Fig. 73 for alloy 4340. Alloy 4140 behaved in exactly the same manner as alloy 4340. The (870, Oil) heat treatment bent a full 90° without cracking, while the (1200, IBQLN) heat treated pieces broke in a completely brittle intergranular manner without any bending at all. Each half of the brittle specimen was perfectly flat.

A careful study of the fracture surface of the fracture toughness specimens has been done with the use of a scanning electron microscope. The fracture morphology of five alloys was examined as a function of heat treatment. Nearly all of the specimens examined showed a mixed fracture mode morphology, which ranged form intergranular failures to quasi-cleavage, to ductile rupture. In some instances the fracture

occurred by nearly either 100% ductile rupture or 100% intergranular facets. Also the presence of particles on the fracture surface was common to all specimens. By a microprobe analysis and also by the use of a combined scanning electron microscope-microprobe system, these particles were uniquely identified as manganese sulphide (MnS) stringers or inclusions. These inclusions can be identified as crack initiation sites and as such are detrimental to fracture toughness.

All the specimens that had been austenitized at 870°C had very fine scaled macro fracture surface appearance, while those austenitized at 1200°C had a very coarse macro fracture surface appearance. In general, all the specimens austenitized at the higher temperature exhibited a combined semi-transgranular and semi-intergranular fracture appearance. However, both quasi-cleavage and ductile rupture were found on both transgranular and intergranular fracture surfaces.

In every case where tempering led to a abrupt loss in fracture toughness, the fracture morphology was found to be intergranular. These types of intergranular faceted fracture modes could easily be identified on a macro scale, due to the way in which the smooth facets result in a bright shiny appearance. The specimens in Fig. 74 are representative of the three general types of macro fracture appearance exhibited in alloy 4130. The specimen at the bottom of Fig. 74 was austenitized at 870°C, (to give a fine grain size) quenched in oil and tempered at 200°C resulting in a fracture toughness of 53 ksi-in.$^{1/2}$. The middle specimen was austenitized at 1200°C, (to give a large grain size) quenched in an ice brine quench with L.N. refrigeration and also tempered at 200°C. This resulted in the maximum fracture toughness

for this alloy of 110 ksi-in.$^{1/2}$. The top specimen was given the same heat treatment as the one in the middle except for the fact that it was tempered at 350°C. This resulted in an abrupt drop in toughness to a level of 67 ksi-in.$^{1/2}$. The lower specimen is typical of a commercial fine grain plane strain fracture toughness surface appearance, that has very fine details and a very flat fracture surface. The middle specimen with the large grains has much more rough features, while the top specimen has the same rough features but has a shiny faceted appearance. These three specimens are typical of the macro fracture surface appearances of the commercial heat treatment, the high austenitizing treatment tempered to optimum toughness, and the high austenitizing heat treatment followed by tempering in an embrittling range.

a. Morphology of alloy 4130

Typical fracture surface appearances for alloy 4130 are shown in Figs. 75 through 80. A (1200, IBQLN) heat treatment tested in the as-quenched condition (Fig. 75) resulted in a mixed mode of fracture consisting of large roughly intergranular failure, regions of quasi-cleavage, and also dimpled rupture. Figure 75A shows a region with both an intergranular and ductile rupture, while Figs. 75B and 75C are almost entirely ductile rupture. While these photomicrographs show several particles on the fracture surface, particles were observed with this treatment at the same frequency as with the other heat treatments. Thus, the particles shown in Fig. 76 for the (1200, Oil) heat treatment tested in the as-quenched condition, were also observed in the (1200, IBQLN) treatment. The shape of the MnS particles are shown in Fig. 76C and 76D. Figure 76B shows a ductile region with the end of

MnS particles located in the center of cup-cone type features characteristic of ductile rupture. Figs. 76C, D and E on the other hand show a MnS particle protruding from an intergranular region. These particles are clearly cylindrical rods or stringers which run parallel to the rolling direction. With this type of an intergranular fracture interface, it can be seen that the material has pulled away from the particle. This then results in a small crack forming ahead of the main crack front.

The fracture morphology of the specimen with the commercial (870, Oil) heat treatment tested in the as-quenched condition is shown in Fig. 77. This specimen has a fine grain size and also has fine fracture features relative to the large grain size material. Figure 77A shows a region containing primarily quasi-cleavage, but with small areas of ductile rupture. On the other hand, Fig. 77B shows a region consisting almost entirely of ductile rupture. Figures 77C and 77D again show MnS particles present. An (870, Oil) heat treatment followed by tempering at 350°C does not change the fracture appearance (Fig. 78B) over that of the as-quenched specimen. However, there is evidence that the MnS particle-matrix interface undergoes much more plastic deformation. This results in cup-cone type dimples forming around the inclusions (Fig. 78B).

This ability of the matrix to plastically deform around the inclusion is also evident in the specimens heat treated to achieve maximum toughness, [(1200, IBQLN) followed by tempering at 200°C]. Figure 79 shows this type of feature. The ability of the matrix to flow plastically before reaching the fracture stress prevents small microcracks from forming ahead of the advancing crack front and at the

same time provides a method of absorbing strain energy in the plastically deformed region rather than dissipating this energy through the formation of microcracks.

Accompanying the loss in toughness when alloy 4130 is heat treated by (1200, IBQLN) and tempered at either 280°C or 350°C, is a dramatic change in fracture morphology (Fig. 80). Tempering at 280°C results in a pronounced intergranular type of failure combining both a very smooth surface appearance on the facets with regions of ductile rupture also on adjacent grain boundary facets. Tempering at 350°C results in an almost total smooth grain boundary type of failure. Again MnS particles are present in both cases.

b. Morphology of Alloy 4330

The morphology of alloy 4330 is characteristically different than that of alloy 4130. For both the commercial (870, Oil) heat treatment and the (1200, IBQLN) heat treatment for all temper conditions, the fracture occurred by 100% ductile rupture. However, there is a difference in the ductile rupture in each case. Figure 81 shows a typical region of the fracture surface resulting from a (1200, IBQLN) heat treatment in the as-quenched condition, while Fig. 82 represents the fracture surface of a specimen given a (870, Oil) heat treatment and also tested in the as-quenched condition. Figure 82 represents almost a borderline situation between quasi-cleavage and dimpled rupture. The dimples are very shallow representative of a minimum amount of energy being absorbed through plastic deformation. On the other hand, Fig. 81 shows that there is extensive plastic flow associated with each dimple and each dimple is much larger. MnS

particles are again present in both cases. Tempering for this alloy does not lead to a loss in toughness and correspondingly does not result in a change in fracture mode. The (870, Oil) heat treatment tempered at 350°C (Fig. 83C) now has a fracture morphology consisting of many more elongated dimples similar to the (1200, IBQLN) heat treatment shown in Figs. 83A and B. The increased capability for plastic flow can be seen by observing the deep cup-cone type of ductile failure around a MnS particle in Fig. 83C.

c. Morphology of Alloy 4340

As described earlier, alloy 4340 is subject to quench cracking under certain conditions. Figure 84 shows the intergranular type of failure along prior austenite grain boundaries which is characteristic of all the quench cracks found in this investigation. Some specimens of 4340 showed a more than typical amount of MnS particles present on the fracture surface. This type of heavy inclusion density is shown in Fig. 85 for a specimen step quenched (1200→870, Oil) and tempered at 200°C. This heat treatment resulted in a substantial increase in fracture toughness over that of the commercially used heat treatment, even though there seemed to be many particles present. From Fig. 85A it is evident that this heat treatment resulted in a mixed fracture mode consisting of rough intergranular facets, a small amount of ductile rupture, and extensive quasi-cleavage. The normal commercial heat treatment (870, Oil) tested in the as-quenched condition is fine grained and thus does not exhibit coarse intergranular fracture features (Fig. 86). It is almost entirely quasi-cleavage with pockets of ductile rupture present. Each of the cleavage regions

visible in Fig. 86A is approximately the size of the prior austenite grain . When the (1200→870, Oil) heat treatment is tempered at 200°C it reaches a maximum in toughness and its fracture morphology undergoes a subtle change (Fig. 87). It still exhibits all the features of the as-quenched specimen, that is, coarse intergranular shapes with both quasi-cleavage and ductile rupture present. However, these regions of ductile rupture make up a greater portion of the fracture surface and also are more ductile (Fig. 87B) than in the as-quenched specimen. That is, the dimples are deeper and indicate a greater capacity for plastic flow.

A grain boundary crack can be seen in Fig. 87B. One end of this crack is enlarged in Fig. 87C to show in detail the end of the crack where it joins with another grain boundary orientated approximately at right angles to it. It is interesting to note that the adjacent grain boundary is delineated in Fig. 87C by a finely spaced row of pock marks which are the result of particles pulling away from the matrix or breaking during loading. These markings form a sort of parabola around the grain boundary and could easily have led to the initiation of microcracks around the grain which in turn led to a transgranular quasi-cleavage fracture mode across the grain.

Ductile regions of the fracture surface are shown in Figs. 87D and 87E. As mentioned before, tempering at 200°C results in a greater amount of deformation accompanying ductile rupture and this increased ductility leads to a greater amount of plastic deformation around each MnS particle.

The embrittlement that accompanies the step-quenched specimens when tempered at 280°C is again characterized by a completely intergranular type of fracture morphology (Fig. 88). The role of MnS inclusions becomes even more crucial in this case since the grain boundaries are capable of very little plastic flow. Thus the brittle inclusions in the grain boundaries act as crack initiation sites along a brittle interface. These boundaries then are not capable of absorbing much strain energy and hence provide a path of least resistance for the advancing crack front to follow.

d. Morphology of Alloy 4140

Figures 89 and 90 show the fracture morphology of alloy 4140 for both the (1200, Oil) and the commercial (870, Oil) heat treatments tested in both the as-quenched and tempered conditions. Both the (870, Oil) (Fig. 89A) and (1200, Oil) (Figs. 89B-D) heat treatments tested in the as-quenched condition appear to be almost entirely quasi-cleavage with the large grained specimen again showing rough intergranular features. The fracture morphology of the fine grained material also reveals its grain size, not due to its intergranular type of failure, but rather due to the regions of transgranular cleavage, visible in Fig. 89A, which extends across individual grains. Also, it can be seen that grain boundaries have pulled away from each other in the plane perpendicular to the fracture surface. However, upon tempering at 200°C there does not seem to be any change in fracture morphology even though the toughness increases. Tempering the (870, Oil) specimens at 280°C and 390°C results in progressively larger amounts of ductile rupture (Figs. 90A and B). MnS particles

are present in this alloy also and Fig. 90C shows a particle which has broken. However, the (1200, Oil) heat treatment responds in just the opposite way to higher tempering temperatures. As with alloy 4130 and 4340 this alloy also undergoes an abrupt morphological change to a 100% intergranular type of failure (Fig. 90D).

e. Morphology of Alloy 300-M

This alloy provided the most clear difference in fracture morphologies between the (870, Oil) (Fig. 91A) and the (1200, Oil) (Fig. 91B) heat treatments tested in the as-quenched condition. The (870, Oil) treatment results in an entirely quasi-cleavage mode of fracture, while the (1200, Oil) treatment is almost entirely ductile rupture. Furthermore, upon tempering the (1200, Oil) treatment at 325°C (Fig. 91C) no sign of intergranular type of fracture morphology was observed. This agrees with the fact that there is no loss in fracture toughness when the material is tempered at 325°C.

IV. DISCUSSION

The heat treatment of steel and its effects on the resulting microstructure and mechanical properties is an extremely complex phenomenon. The various processes, mechanisms and effects have been studied, argued and debated for hundreds of years.[7] Today, still, the debate continues[6] in nearly every aspect of metallurgy. Each step in the heat treatment used in this investigation, the austenitization temperature and time, the quench medium, and the tempering temperature affects the final microstructure of the steels studied. The microstructure in turn controls all the properties that a particular alloy exhibits. The purpose of this investigation was not to study the effects of any one particular phenomenon or process on the properties of these alloys. For the last fifty years people have been doing experiments in an attempt to prove, disprove, explain or explore individual phenomenon that occur in steels. This has led to an incredible amount of literature dealing with nearly every aspect of the characteristics of steel. The object of this investigation was then to utilize this information in an attempt to develop a heat treatment and hence microstructure that would result in an improvement in the fracture characteristics of several commercial low alloy steels. Due to the complex response of steel to heat treatment, it is difficult to discuss and interpret the results in a general way and also difficult to discuss individual observations and phenomenon due to their interconnectedness with other processes. At the same time that it is impossible to review all the theories, explanations and contradictions that exist for each area involved in this study, it is necessary to spend some time to explain

the possible effects of each stage of heat treatment on the microstructure and the variations within the microstructure itself. Then the fracture toughness of the various alloys that results from different heat treatments can be discussed in terms of particular microstructures.

The first stage in the heat treatment of these steels is austenitization. The austenitizing temperature affects indirectly the final microstructure by controlling several parameters which play key parts in the subsequent phase transformation during cooling. For example, a high enough austenitizing temperature can result in a very large grain size. During subsequent cooling the grain size can play an important role in controlling the distribution, amount and the temperature of decomposition products[8,9] that are nucleated from the prior austenite grain boundaries. For example, Barford and Owen[8] have shown that the time to any chosen percentage reaction of bainite less than 25% is directly proportional to the mean austenite grain diameter and that the rate of upper bainite transformation is first retarded as the austenitizing temperature is increased from 900°C and then at high enough temperatures, actually accelerated.

In addition to increasing the austenite grain size, a higher austenitization temperature will influence the chemical homogenity of the austenite as well as the defect structure. Higher austenitizing temperatures tend to reduce the segregation and partitioning of impurity and alloy elements especially that of carbon. This reduces lean zones that tend to transform earlier and to different structures than the more highly alloyed zones. With regard to the Ms temperature and the "reaction rate" (the amount of martensite formed per degree

of cooling), Sastri and West[10] found that an increasing austenitization temperature raised the Ms somewhat and decreased the reaction rate while very short austenitization times lowered the Ms and increased the reaction rate. They concluded that the dominant factor was the defect structure of the austenite and not the grain size.

The austenitizing temperature also effects the size, shape and distribution of residual carbides.[11-14] Contractor et al.[10] found that for an ultra high strength secondary hardening steel, the weight of extracted carbides decreased steadily as the austenitizing temperature is increased from 900°C to 1150°C. Banerjee[15] found $M_{23}C_6$ type carbides present in 4340 steel quenched after austenitizing at 850°C. Above 1150°C there is little change in the weight percent of undissolved carbides. While vanadium has a notorious reputation for being very stable and difficult to dissolve, Contractor, et al.[11] showed 95% solution of vanadium after austenitizing at 1065°C. Aaron, et al.[14] made a detailed theoretical study of the dissolution of vanadium carbide and found that vanadium carbide was quite easily dissolved while complex alloy sulphides, silicates and oxides persisted with little dissociation. Both Aaron, et al.[14] and Wada, et al.,[13] who studied the Fe-V-C system, refute previously published reports on the Fe-V-C phase diagram. The amount of undissolved carbides can have a pronounced effect on the amount of martensite formed at any temperature.[12]

The second part of the heat treatment is the quench or cooling medium. Again, there has been an incredibly large amount of work done

on the microstructure that results during both continuous cooling and isothermal transformation curves for many alloys.[16-21] The rate at which many steels are cooled, combined with the prior history and chemical composition, determines whether the basic microstructure contains ferrite, pearlite, bainite, martensite to a combination of any or all of these constituents. Entire books have been written[4,5] on the subject of phase transformation that occurs during quenching of steel. Short of writing another book, it is impossible to discuss in detail the different reactions that occurred in the steels studied in this investigation. However, there is one particular phase transformation that merits a brief discussion.

The bainitic transformation, while discovered over forty years ago,[22] is still the subject of debate.[6] The nature of bainite, its growth kinetics and mechanisms are still not completely resolved. The importance of the bainitic reaction lies in its effect on the mechanical properties in steels as compared to martensitic steels. The relative merits of various types and morphologies of bainite relative to martensite have been widely discussed and will be discussed here in so far as they affect the fracture toughness of the alloys involved. Bainite is generally defined from a microstructural viewpoint. It is generally accepted that bainite is a non lamellar aggregate of ferrite and carbide with an acicular morphology that is nucleated along austenite grain boundaries. Hence, the amount of grain boundary surface area, the energy of the grain boundary, the presence of impurities, solute atoms, carbides, inclusions, or high temperature decomposition produces such as ferrite can significantly alter the amount and morphology of bainite

nucleated. This can then influence the reaction kinetics for the formation of martensite and vice versa. Thus the austenitizing and quenching procedure can control the very delicate balance between obtaining different microstructures for a particular steel. Two variants of bainite, upper and lower, are widely recognized, although other forms do exist.[23] The first stages of the transformation to upper bainite consists of the formation of a lath of ferrite from the austenite. Often, side by side ferrite laths form to result in a sheaf of parallel laths due to a sympathetic nucleation effect.[24] As the ferrite laths grow, carbon diffuses away in front of the ferrite austenite interface and usually carbides will precipitate parallel to the needles or lath axis. However, in some cases the carbon enrichment can cause austenite to be retained between laths.[25] As the transformation temperature in the upper bainite range decreases, the ferrite laths become narrower because the sideways growth of the laths is restricted by the diffusion of carbon, while the axial length is not affected.[26,27] As the amount of carbon increases, the amount of carbide precipitation increases and the cementite carbide film between laths become more continuous. Two surface investigations have shown that upper bainite forms as needle-like particles whereas lower bainite forms as true plates.[28] On a single plane of polish, upper bainite may appear as either a small more or less retangular section or as long needles. These two different appearances are due to the different interactions of the plane of polish with a single lath-like particle. For some orientations, the structure can have an almost pearlitic appearance.[29]

The morphology of bainite changes discontinuously as lower bainite is formed. Again, two surface studies have shown that these plates can consist of many subunits[4] whereas upper bainite generally doesn't. The lower temperature at which lower bainite forms, limits the amount of diffusion of carbon that can occur. Hence the initial ferrite plates that forms tends to be supersaturated with carbon.[4] This supersaturation is then decreased by subsequent internal precipitation of carbides at an approximate angle of 60° to the ferrite plate.

Often, a distinction can be made between upper and lower bainite from the surface relief of optical metallography.[4] Upper bainite exhibits the multiple relief as expected from the role of sympathetic nucleation of laths rather than by lateral advance of the austenite-bainite interface. This is consistant with the concept that the lath boundaries are semi-coherent interfaces and should be immobile.[24] Lower bainite, on the other hand, exhibits a single uniform surface relief. The plates grow slowly in length and generally thicken from only one side.[4]

The subject of the bainite transformation is actually a microcosm of metallurgy since it covers the whole range of transformation and precipitation reactions including both diffusion controlled and shear nucleation, precipitates on interfaces, dislocations and grain boundaries, and involves the cooperative growth of both precipitate and major phase.

The object of this investigation was to study the effects of various microstructures on the fracture properties of several alloy steels. Utilizing the concepts touched upon in the preceeding paragraphs, on

some particular aspects of the heat treatment and phase transformations in steels, it now remains to interpret the observed fracture toughness results of this study in terms of observed microstructural features. The fracture toughness of high strength alloys has been studied by many people in the last few years.[30-48] These investigations generally compared the fracture toughness of different alloys as a function of tempering temperature and/or strength level. Some compared fracture toughness of different microstructures.[30-37] However, all used accepted heat treatment procedures which in this case consisted of oil quenching after austenitizing from 850-870°C. There have been several attempts to determine whether a fully bainitic structure has a higher fracture toughness than fully martensitic structure.[30,34,37] However, these studies have relied upon Charpy impact data which in many cases is not sensitive enough to measure changes in toughness due to fine microstructural changes, while others attempted to compare different structures such as bainite and martensite which were produced by changing the chemical composition of the alloys.

It is interesting that there are two cases where increasing the austenitizing temperature and hence increasing the grain size has been reported to increase the fracture toughness. Backofen and Ebner[49] investigated the effect of austenitizing temperature on the fracture toughness of 4340. They reported that increasing the grain size from 0.008 mm in diameter to 1.1 mm in diameter generally led to an increase in toughness except for the very coarse grain size. They, however, offered no explanation for these findings. In another study[50] an effect of the quenching temperature was studied on impact resistance. Low

alloy cast steels were quenched from between 860°C and 1100°C. The best impact resistance was found to occur after austenitizing at high temperatures and quenching in water.

The toughness of alloy 4130 has been reported[41] to be 100 ksi-in.$^{1/2}$ for a 1/2 in. thick plate tempered to a yield strength of 158,000 psi, while the toughness of alloy 4340 has been widely studied[38,39,42-47] and its fracture toughness determined as a function of strength. Similarly, the fracture toughness has been reported for alloys 4330,[32] 4140,[39] and 300-M.[44,45] The values reported for these alloys generally agree with the values obtained in this study for the commercially heat treated specimens at the strength levels reported. It is impossible to compare with published reports, the as-quenched fracture toughness determined in this investigation because "as-quenched" martensite is historically very brittle and never used.[40] These beliefs are correct in that as-quenched, untempered martensite is brittle, as shown in Fig. 73. However, their conclusions are fortuitous since few materials in thick sections contain only martensite and also the martensite that does form is always auto-tempered. Indeed, even today with very accurate and high resolution techniques available for determining structure, steels such as 4340 are assumed to be fully martensitic when quenched in oil. The results of this investigation have shown that this is not true. On the contrary, all the alloys studied contained some bainite after austenitizing at 870°C and oil quenching. The reason for poor toughness is not that these structures contain brittle untempered martensite as generally believed, but because they

contain upper bainite consisting of laths of soft ferrite surrounded by an extremely hard film of iron carbide. It has been shown that the cleavage stress is very low in alpha (ferrite) iron and that microcracks propagate by cleavage in ferrite.[51] Thus, these alloys heat treated by an (870, Oil) treatment contain exactly the worst microstructural constituent for resisting fracture. The fracture morphology confirms this in Fig. 89a where the fracture has propagated by transgranular cleavage from grain to grain, consistant with the fact that upper bainite laths extend across the grain diameter.

Also, it is apparent from the results of alloy 4130, that just increasing the cooling rate from oil to IBQLN does not prevent the formation of upper bainite. It is necessary to utilize a high austenitizing temperature too. By combining both the high austenitizing temperature and the (IBQLN) the maximum toughness is achieved. Although a mixed microstructure is still present, the presence of upper bainite seems to be eliminated with only lower bainite and martensite present. Eliminating the upper bainite perferential cleavage sites results in an increase in toughness from 55 to 100 ksi-in.$^{1/2}$. However, if the cooling rate is lower by using an oil quench, then extensive amounts of upper bainite is again observed along prior austenite grain boundaries and is accompanied by a corresponding drop in toughness. The presence of upper bainite along grain boundaries provides easy sites for crack initiation and propagation with very little need for plastic flow (Fig. 72) and hence very little energy absorption.

The presence of a mixed microstructure has been considered deleterious to the fracture toughness of alloys.[32] However, the results of this investigation show that a mixed microstructure need not be detrimental. In fact, Liu[53], showed that the fracture path in lower bainite was much more jagged than through martensite. Thus the presence of lower bainite and martensite can lead to a good fracture resistance microstructure. It has recently been shown[53] that a large grained, fully martensitic 0.3 wt% carbon alloy also has excellent toughness equivalent to that of alloy 4130 for the same (1200, IBQLN) heat treatment. Thus for these two alloys, at least, there does not seem to be any effect on toughness due to a mixed microstructure of lower bainite and martensite, instead of a fully auto-tempered martensite microstructure.

Within the limits of detection by X-ray diffraction using copper radiation and a crystal monochromator, no retained austenite was detected in any of the alloys, except for the alloy 300-M for which an austenite peak was barely resolved. Preliminary transmission electron microscopy on 4340 has revealed that some retained austenite is present between the individual laths. Depending on the amount, the stability, and the distribution of retained austenite present, it can contribute to the fracture toughness of an alloy. The (1200→870, Oil) and the (1200, Oil) heat treatment for 4340 and 4140 respectively were modified to include an immediate refrigeration in liquid nitrogen. Similarily for 4130 a (1200, IBQLN) heat treatment was modified to a (1200, IBQ) treatment without liquid nitrogen refrigeration. In each case, the fracture toughness was not affected. On the other hand, a (1200, Oil+LN) heat treatment for 300M as opposed to a (1200, Oil) treatment did seem to result in a drop in the fracture toughness which

suggests that retained austenite may play an active part. However, a very careful examination of the amount of and distribution of retained austenite as well as additional testing is necessary before the role of retained austenite can be accurately determined.

It is interesting that for alloys 4130, 4140 and 300-M the step quench into oil heat treatment (1200→870, Oil) does not result in as high a fracture toughness as did the direct quench into oil, (1200, Oil). Both the direct and step quenched structures revealed the presence of some bainite, but it is very difficult to tell conclusively whether one structure contained more bainite than the other. Also, 870°C is above the temperature where any precipitation should occur in these alloys. Thus the change in toughness can not be attributed to a precipitation reaction. While not attempting to define what the mechanism is, it is possible to speculate as to several possible reasons. First, it is possible that the added homogeneity that is gained by austenitizing at 1200°C instead of 870°C as normally done, is lost by a re-segregation or re-partition of elements along grain boundaries or in pre-precipitation clusters that form when the material is stepped down to 870°C again. Alternately, it is possible that by quenching directly from 1200°C, the defect structure (i.e., quenched in vacencies) is altered, which could alter the mechanisms involved in plastic flow. In addition to the drop in toughness experienced, when these alloys are step-quenched, they also undergo a drop in toughness if the alloy is directly quenched after austenitizing at 1100°C and not 1200°C. Contractor[10] has shown that there can be a reduction in the amount of residual carbides present by austenitizing at 1200°C rather than 1100°C. Thus it is possible

that this could lead to more alloying elements in solution and hence greater "hardenability".* Alternately, there may be a significant redistribution or change in the partition of elements not tied up in carbides that occurs between 1100 and 1200°C.

There are three additional areas which need to be discussed. These are: 1) the role of inclusions on the fracture toughness, 2) the cause of the catastrophic drop in toughness when certain alloys are tempered above 200°C, and 3) the very low micro yield strength exhibited by all the alloys in the as-quenched condition.

The role that inclusions play on the fracture toughness has been extensively studied for brittle and ductile alloys.[55-64] It has been shown many times that increasing the sulphur content reduces the fracture toughness. The reason for this can be readily explained by referring to the scanning electron fractographs that show MnS particles on the surface. These particles were observed in both ductile regions and on intergranular facets and are rod-like stringers running parallel to both the rolling direction and the bar surface. Hence, while these inclusions are ductile at the forging temperature, they are brittle at room temperature. Thus when a load is applied during the fracture toughness test, these particles may break and form a microcrack. If the inclusion is not located on a brittle interface such as a grain boundary, then ductile flow may occur and failure proceeds by ductile rupture in a cup cone type of pattern. On the other hand, if the particle is situated on a brittle grain boundary, then the microcrack that forms

*Hardenability in this concept refers to bainite hardenability and not pearlite hardenability.[54]

as the particle fractures can initiate a cleavage crack along the grain boundary.[51-65] In either case, the MnS particle causes the formation of a microcrack which can lead to either a ductile type of failure which absorbs strain energy through plastic flow or a brittle type of failure which dissipates strain energy by formation of cleavage cracks. Both cases, however, are detrimental to toughness. It is possible to alter the shape of inclusions through rare earth additions.[55,56] Additions of cerium can result in globular shaped inclusions which can lead to significant increases in toughness. The same effect would be expected through prolonged holding at very high temperatures. However, there is no apparent difference in the inclusion morphology between the 870°C and the 1200°C austenitizing treatments for the alloys studied in this investigation.

The change in fracture toughness with tempering, however, is not so clearly understood. The drop in toughness that several of the alloys studied in this investigation undergo when tempered above 200°C (400°F) is common to many alloys, and is termed "500°F tempered martensite embrittlement". This embrittlement always results in an intergranular type of failure and has been the the subject of many investigations.[57,63,67-78]

A general review of the various theories up to 1966 has been presented by Buchler, et al.[44] In the last four years, with the wide spread use of auger electron emission spectroscopy, various theories of martensite embrittlement due to the interaction of impurity elements with the austenite grain boundaries have been proposed which utilizes

auger analysis. To date, there is no unified theory to explain all the observations reported. However, there are three general categories into which theories fall. First, there is the belief that the carbide film which develops during tempering fails in a brittle manner along austenite grain boundaries. Second, there is the theory that it is the ferrite film that forms adjacent to the carbide film which, when subjected to triaxial stresses, fails by cleavage. And third, there is the impurity segregation theory which in general, hypothesises that the surface energy along grain boundaries is reduced by the presence of certain impurity elements. Unfortunately, most of the tests for embrittlement were Charpy impact tests; some done at low temperatures and some one at room temperature. These factors along with the many different alloys used, make it very difficult to try to explain any particular result in comparison to others. It is impossible to reach any absolute conclusions based on the results of the current study thus far, but there are several important results that will be discussed in conjunction with both the ferrite film theory and the impurity theory.

By referring back to the fracture toughness vs tempering temperature curves for the different alloys studied, several observations can be made. First, alloys 4130, 4140 and 4340 suffered embrittlement when heat treated to produce a large grain size and then tempered above 200°C. Second, alloys 4330 and 300-M did not show this type of catastrophic failure. Third, while the fine grained 4330 alloy exhibited an increase in toughness during the initial tempering treatment, the alloy 4130 showed no response for the same heat treatment

conditions. Fourth, when an alloy did embrittle, its level of toughness dropped all the way down to the level of the fine grain commercial heat treatment. These results are all important and tend to point towards certain possible conclusions.

The only two alloys that did not show a tempered martensite embrittlement reaction were the two alloys containing vanadium. Alloy 300-M did contain silicon which has the well known[79-80] effect of retarding the formation of iron carbide. Since this has possible effects on the embrittlement phenomenon in addition to the vanadium, only alloy 5330 will be compared to the alloys that did exhibit an embrittlement. If one considers the possible effects of vanadium on the ferrite film, carbide film, and impurity theories of embrittlement, an arguement can be rationalized for each. The vanadium may alter the carbide reaction such that it would prevent continuous films from developing, which would also present ferrite films from forming or it could alter the impurity distribution and hence change the critical surface energy balance between grain boundaries and the matrix, in favor of the matrix. Thus resulting in a transgranular failure path.

By limiting ourselves to just the first two initial observations, then it is impossible to favor any one theory. However, by jumping ahead to the fourth observation an important point can be made; that is, that in the embrittled specimens, the toughness drops to the level of the fine grain microstructure containing upper bainite, which consists of laths of ferrite connected by carbide films. In addition, the fractographs show that the embrittled fracture mode is an intergranular

type of cleavage and that for the fine grain material containing upper bainite, the fracture mode was also that of cleavage only along ferrite laths instead of along grain boundaries. This then suggests that as tempering preceeds, the ferrite film thickens until a critical thickness is achieved which enables cleavage to initiate in the ferrite.

The lack of response of the fine grained (870, Oil) alloy 4130 to tempering as compared to the other alloys can be explained in light of the fact that its extremely low alloy content and low hardenability[54] results in an almost entirely bainitic structure, which, since it already consists of an aggregate of ferrite and carbides, would not be expected to show any response to low tempering temperatures that produce a carbide precipitation in martensite. On the other hand, the more highly alloyed steels contain primarily martensite with some bainite present. This results in an increase in toughness when they are tempered due to relaxation of strain in the martensite and the beneficial effect of a slight amount of discontinuous precipitation. The tensile test results are the last results which need to be discussed.

The values of the yield stress obtained for an alloy is a relative value, since it depends on the techniques used to measure it, the sample size and the way in which it is defined. Due to the widespread commercial use of the alloys used in this study, there are many reports which include the yield strength of several of these alloys as a function of tempering temperature. These published values fall into two categories, one being that the as-quenched yield strength is very low, and the other that the yield strength is very

high and at a maximum in the as-quenched condition. Unfortunately, very few papers tell the method used in determing their observed value other than the size of the specimens. Bucher, et al.[45] reported that in the as-quenched condition 4340 has a yield strength of 233,000 psi and that 300-M has a yield strength of 240,000 psi. Klinger, et al.[33] have reported that 4340 has an as-quenched yield strength of 240,000 psi, while 4330 has an as-quenched yield strength of 220,000 psi. Hall,[48] on the other hand, reports that the yield strength of as-quenched 4340 is high, while 300-M has an as-quenched yield strength of about 160,000 psi. Shih, Averback and Cohen[80] have reported that both 4340 and 300-M have low yield strengths of about 160,000 psi when tested in the as-quenched condition. Most reports, however, agree that the yield strength increases to a maximum when tempered at 200°C. There have been several studies which investigate the occurrance of micro-yielding in alloys[81-83] using very sensitive techniques such as etch pit observations and highly sensitive extensometers. Etch pit techniques give information about individual slip bands, their distribution and density, but does not reveal a quantitative picture of their cumulative effect. Highly sensitive extensometers, on the other hand, measure cumulative micro-displacement at each stress.

Many times macroscopic yield strength data has been used to explain strengthening mechanisms based on very specific dislocation-precipitation interactions. The discrepencies that surround the yield strength of these alloys are important when considering whether martensite containing carbon in solution is hard or soft, or when applying linear elastic fracture mechanics concepts to alloys where the actual yield

stress may be as much as 75,000 psi lower than commonly believed.

There are two theories governing the flow stress of as-quenched martensite. First, that dislocation motion is difficult because of lattice resistance due to solid solution effects,[83,84] in which case the macro yield stress would be close to the macroscopic yield stress. The second theory is that the micro-yield strength is very low, but that a very high rate of work hardening results in a very high macro-yield strength.[85,86]

Johnson, et al.[87] have shown that the as-quenched structure does exhibit a very low yield stress and that the stress-strain curve is essentially shaped like a parabola. Also, they reported that the initial portion of the curves are insensitive to the carbon content, and that the effect of carbon only manifests itself in the macroscopic range. They conclude that the lattice resistance from carbon in solution is small and that the high macroscopic yield strength results from a rapid rate of strain hardening involving a large number of dislocations introduced during transformation. Furthermore, both Nessler, et al.[88] and Ansell, et al.[89] have reported that very high quenching rates result in marked softening of as-quenched martensite. They have concluded that if the quenching rate is fast enough, carbon segregation in the austenite can be avoided and also the re-arrangement of carbon atoms to dislocations during quenching can be prevented.

The results obtained in this investigation have shown that the as-quenched yield strength is indeed very low, with the stress strain curve having no real linear region. However, as the material is

tempered the stress strain curve straightens out until, at high enough tempering temperature, a definite yield point is observed. At these higher temperatures the yield point is pronounced enough so that even on the load vs stroke curve the yield point is observed. Thus for these conditions an accurate estimation of the yield strength can be determined without the use of an extensometer. It has also been shown in this study that, if for the load vs total crosshead or stroke control method described earlier, the error due to the displacement of the loading in the grips and threads is subtracted from the total load vs crosshead movement, then the difference between the micro and macro yield stress is reduced by an average of about 50%.

The discrepencies in the yield strength of the as-quenched materials that appear in the literature can be explained from the results obtained in this investigation. First, by just using total crosshead movement, enormous errors can be introduced. However, in many cases, the measured yield strength in each report may be accurate, but there still may be large differences from report to report. This can be explained on the following basis. If one considers that low tempering temperature (i.e., up to 200°C) results in an increase in strength for these alloys, then the same reasoning can be applied to the as-quenched specimens. That is, aging can occur at low temperatures below room temperature, and in some cases leads to higher yield strengths. Also, the exact way in which the specimen is quenched from the austenitizing temperature can affect the yield strength. The cooling rate in water is extremely sensitive to the water temperature. Similarly, the size of the specimen

affects its cooling rate. These factors all contribute to the observed yield strength in that they affect the amount of aging and hence strengthening that occurs in the specimens. This is reflected in the results of this study in that 1/4 in. round tensile specimens machined and then heat treated resulted in a macro yield strength 25,000 psi higher than for 3/8 in. round tensile specimens cut from a previously heat treated plate for alloy 4340. Variations in procedures such as these not only can change the amount of auto tempering that occurs, but can involve the testing of totally different structures in each case. Oftentimes, people test the yield strength of material using very small specimens and then do fracture tests on much larger specimens while assuming the strength is the same for both cases. Not only may the strength be different, but the entire structure may be different. Finally, for the alloy 4340, three duplicate tests were done at a later date than the rest of the specimens and are marked by an asterick in the table. These specimen were machined from square stock instead of being ground while flooded with water. They were, however, made from the same piece of bar so that they have the same composition as the others. The "micro" yield strengths of these alloys tested in the as-quenched condition was found to be much higher than for the specimens tested earlier that were ground. This is probably due to more heat being generated by the tool bit, resulting in a larger amount of tempering occurring. This then illustrates the final point that the as-quenched yield strength is extremely sensitive to small changes in the preparation, heat treatment, and testing program. Thus the scatter

in the reported yield strength data can be expected. This is unfortunate and can be very misleading. For example, many people compare fracture toughness of different alloys based on equivalent yield strength levels. This can lead to erroneous conclusions and misconceptions as to which microstructure or alloy has better toughness.

V. SUMMARY AND CONCLUSIONS

This investigation has shown that while the as-quenched and low tempered fracture toughness of several commercial alloy steels is very low, large increases in the fracture toughness can be achieved by altering the heat treatment. This is due to a microstructure which is much more resistant to fracture. Many important conclusions have been reached. These are summarized below, although not in any particular order of importance.

1. The term tempered martensite should not be applied to these alloys as they are normally heat treated.
2. The normally used heat treatment for all alloys results in a mixed microstructure consisting of either blocky ferrite, pro-eutectoid ferrite, upper bainite, lower bainite or auto tempered martensite or some combination of these.
3. It was not possible to avoid some decomposition product along prior austenite grain boundaries in a 5/8 in. thick fracture toughness specimen for any of the alloys investigated.
4. A mixed microstructure does not necessarily imply poor fracture toughness.
5. The fracture toughness of all the alloys investigated can be substantially increased by austenitizing at higher temperatures than normally used.
6. A higher quenching rate when used in conjunction with an increased austenitizing temperature can further increase the toughness for some alloys.

7. The Charpy V-notch impact test is not sensitive to changes in microstructure which significantly alter the fracture toughness of the alloys.
8. There is no correlation between Charpy V-notch impact test and the plane strain fracture toughness for the alloys investigated.
9. The alloys without vanadium exhibited a severe intergranular embrittlement when tempered above 200°C, while those alloys that contained vanadium did not show any signs of embrittlement.
10. The as-quenched tensile specimens had very low micro yield strengths which rapidly approached the macro yield strengths when slightly tempered.
11. A 100% martensite untempered structure is brittle.

ACKNOWLEDGEMENTS

This research was performed partially under the auspices of the U. S. Atomic Energy Commission through the Inorganic Materials Research Division of the Lawrence Berkeley Laboratory, Contract No. W-7405-eng-48 and partially under the auspices of the Army Materials and Mechanics Research Center, Watertown, MA, Contract No. DAAG46-7-C-0220.

REFERENCES

1. E. C. Bain and H. W. Paxton, Alloying Elements in Steel (American Society for Metals, 1939).
2. Annual Book of ASTM Standards (American Society for Testing and Materials, Philadelphia, 1972) p. 955, part 31.
3. Annual Book of ASTM Standards (American Society for Testing and Materials, Philadelphia, 1972) p. 959, part 31.
4. R. F. Hehemann, Phase Transformations (American Society for Metals, 1970) p. 397.
5. F. B. Pickering, Transformation and Hardenability in Steels (Climax Molybdenum Co., 1967) p. 109.
6. R. F. Hehemann, K. R. Kinsman and H. I. Aaronson, Met. Trans. 3, 1077 (1972).
7. G. Agricola, De Re Metallica (Dover Publishers, Inc., New York, 1950).
8. J. Barford and W. S. Owen, J. Iron Steel Inst. 198, 146 (1961).
9. R. V. Fostini and F. I. Schoen, Transformation and Hardenability in Steels (Climax Molybdenum Co., 1967) p. 195.
10. A. S. Sastri and D. R. F. West, J. Iron Steel Inst. 203, 138 (1965).
11. G. P. Contractor, E. G. Schempp and W. A. Morgan, Trans. Amer. Soc. Metals 54, 208 (1961).
12. R. A. Grange and H. M. Stewart, Metals Technology, Tech. Paper 1996, 467 (1946).
13. T. Wada, H. Wada, J. F. Elliot and J. Chipman, Met. Trans. 3, 2715 (1972).

14. H. B. Aaron and G. R. Kotler, Met. Trans. 2, 393 (1971).

15. B. R. Banerjee, J. Iron Steel Inst. 203, 166 (1965).

16. E. C. Rollason, Fundamental Aspects of Molybdenum on Transformation of Steel (Climax Molybdenum Co., 1962).

17. L. J. Habraken and M. Economopoulos, Transformation and Hardenability in Steel (Climax Molybdenum Co., 1967) p. 69.

18. Isothermal Transformation Diagrams, (United States Steel, 1963).

19. D. J. Blickewede and R. C. Hess, Trans. Amer. Soc. Metals 49, 427 (1957).

20. R. V. Fostini and M. Sernchyshen, Trans. Amer. Soc. Metals 57, 632 (1964).

21. M. Cohen, Trans. Amer. Soc. Metals 41, 35 (1949).

22. E. S. Davenport and E. C. Bain, Trans. AIME 90, 117 (1930).

23. R. F. Mehl, Hardenability of Alloy Steels (American Society for Metals, 1939) p. 1.

24. H. I. Aaronson, Decomposition of Austenite by Diffusional Processes, V. F. Zackay and H. I. Aaronson, ed. (Interscience Publishers, New York, 1962) p. 387.

25. J. M. Oblak and R. F. Hehemann, Transformation and Hardenability in Steel (Climax Molybdenum Co., 1967) p. 27.

26. G. R. Speich and M. Cohen, Trans. AIME 218, 1050 (1960).

27. G. R. Speich, Decomposition of Austenite by Diffusional Processes, V. F. Zackay and H. I. Aaronson, ed. (Interscience Publishers, New York, 1962) p. 353

28. J. M. Oblak, R. H. Goodenow and R. F. Hehemann, Trans. AIME 230, 258 (1964).

29. D. N. Shackleton and P. M. Kelly, Physical Properties of Martensite and Bainite, I. S. I. Spec. Rpt. No. 93 (The Iron and Steel Institute, London, 1965) p. 126.

30. K. J. Irvine, Steel Strengthening Mechanisms (Climax Molybdenum Co., 1969) p. 55.

31. F. B. Pickering, Toward Improved Ductility and Toughness (Climax Molybdenum Co., 1971) p. 9.

32. J. S. Pascover and S. J. Matas, Structure and Properties of Ultrahigh-Strength Steels, ASTM STP 370 (American Society for Testing and Materials, Philadelphia, 1965) p. 33.

33. L. J. Klinger, W. J. Barnett, R. P. Frohmberg and A. R. Troiano, Trans. Amer. Soc. Metals 46, 1557 (1953).

34. C. R. Simcoe and J. P. Sheehan, Armour Research Foundation Report No. ASD-TDR-63-458, Af 33 (657)-8426, May 1963.

35. Y. H. Liu, Trans. Amer. Soc. Metals 62, 55 (1969).

36. K. Firth, R. D. Garwood, Fracture Toughness of High Strength Materials: Theory and Practice, I. S. I. Spec. Report No. 120 (The Iron and Steel Institute, London, 1970) p. 81.

37. G. E. Pellissier, ENG. Fracture Mech. 1, 55 (1968).

38. J. N. Robinson, C. W. Tuck, ENG. Fracture Mech. 4, 377 (1972).

39. E. A. Steigerwald, ENG. Fracture Mech. 1, 473 (1969).

40. R. H. Aborn, Trans. Amer. Soc. Metals 48, 51 (1956).

41. S. T. Rolfe and S. R. Novak, United States Applied Research Lab. Report B-63102, DMIC No. 69502 (1967).

42. L. E. Hays and E. T. Wessel, Applied Materials Research 2, 99 (1963).

43. P. Kenny and J. D. Campbell, Progress in Materials Science 13, 135 (1967).

44. J. H. Bucher, Application of Fracture Toughness Parameters to Structural Metals, Herman D. Greenberg, ed. (Gordon and Breach, New York, 1966) p. 323.

45. J. H. Bucher, G. W. Powell and J. W. Spretnak, Trans. AIME 233, 884 (1965).

46. G. A. Miller, Trans. Amer. Soc. Metals 62, 651 (1969).

47. R. W. Senn, Fracture Toughness of 4340 Steel as a Function of Tempering Temperature (Pitman-Dunn Research Lab., Frankford Arsenal, 1966).

48. A. M. Hall, Introduction to Todays Ultra High Strength Structural Steels, ASTM STP 498 (Americal Society for Testing and Materials, Philadelphia, 1971).

49. W. A. Backoften and M. L. Ebner, Metallurgical Aspects of Fracture of High Strength Steels, Final Tech. Report (Watertown Arsenal Lab., Mass., 1963).

50. A. I. Shedunov and N. F. S. Lant'eva, Metallovedenie i Term. Obrat. Metallov. No. 10, 63 (1966).

51. C. J. McMahon, Jr. and M. Cohen, ACTA Met. 13, 591 (1965).

52. Y. H. Liu, Trans. Amer. Soc. Metals 62, 544 (1969).

53. R. Goolsby, W. Wood, V. F. Zackay and E. R. Parker, Electron Microscopy and Structure of Materials, G. Thomas, ed (Univ. of California Press, 1972) p. 298.

54. J. H. Holloman and L. D. Jaffee, Trans. AIME 167, 601 (1946).

55. I. R. Sprung and K. R. Olen, Met. Trans. 3, 2939 (1972).

56. L. Luyskx, J. Bell, A. McLean and M. Korchynsky, Met. Trans. 1, 3241 (1970).

57. E. B. Kula and A. A. Anctil, J. Mater. 4, 817 (1969).

58. J. M. Hodge, R. H. Frazier and F. W. Boulger, Trans. AIME 215, 745 (1959).

59. A. J. Birkle, R. P. Wei and G. E. Pellissier, Trans. Amer. Soc. Metals 59, 981 (1966).

60. J. M. Capus and C. Mayer, J. Iron Steel Inst. 203, 1254 (1965).

61. C. L. M. Cottrell, Fracture Toughness of High Strength Materials: Theory and Practice, I.S.I. Spec. Report No. 120 (The Iron and Steel Institute, London, 1970) p. 112.

62. H. G. Baron and S. Turner, J. Iron Steel Inst. 203, 1229 (1965).

63. B. R. Banerjee, Structure and Properties of Ultrahigh-Strength Steels, ASTM STP 370 (The American Society for Testing and Materials, Philadelphia, 1965) p. 94.

64. G. E. Gaza and F. R. Larson, U. S. Army Materials Research Agency, Report AMRA TR65-22, Watertown, Mass. (DMIC 62251), 1965.

65. C. J. McMahon, Jr., J. R. Rellick and B. Shultz, Proceedings of the Second International Conference on Fracture, Brighton, 1969 P. L. Pratt, ed. (Chapman and Hall, London, 1969) paper 23.

66. E. Hornbogen, Trans. Amer. Soc. Metals 55, 719 (1962).

67. D. F. Stein, A. Joshi and R. P. LaForce, Trans. Amer. Soc. Metals 62, 776 (1969).

68. R. Viswanathan, Met. Trans. 2, 899 (1971).

69. J. R. Low, Jr., Trans. AIME 245, 2481 (1969).

70. M. E. Fine and H. L. Marcus, Met. Trans. 2, 1473 (1971).

71. J. M. Capus, J. Iron Steel Inst. 200, 922 (1962).

72. B. R. Banerjee, J. Iron Steel Inst. 203, 166 (1965).

73. A. J. Baker, F. J. Lauta and R. P. Wei, Structure and Properties of Ultrahigh-Strength Steels, ASTM STP 370 (The American Society of Testing and Materials, Philadelphia, 1965) p. 3.

74. A. J. Baker, Metals ENG. Quarterly 6, 24 (1966).

75. M. A. Grossman, Trans. AIME 167, 39 (1946).

76. J. M. Capus, J. Iron Steel Inst. 201, 53 (1963).

77. J. M. Capus and G. Mayer, Metallurgia 62, 133 (1960).

78. G. R. Speich and W. C. Leslie, Met. Trans. 3, 1043 (1972).

79. C. J. Alstetter, M. Cohen and B. L. Averbach, Trans. Amer. Soc. Metals 55, 287 (1962).

80. C. H. Shih, B. L. Averback and M. Cohen, Trans. Amer. Soc. Metals 48, 86 (1956).

81. W. D. Brentnall and W. Rostoker, Acta Met. 13, 187 (1965).

82. R. Sejnoha, Sbornik, Vedeckych praci Vysoke' Školy báňske V Ostravé Ročnik XIII, Cislo 1, 331 (1967).

83. P. G. Winchell and M. Cohen, Trans. Amer. Soc. Metals 55, 303 (1962).

84. P. G. Winchell and M. Cohen, Trans. Amer. Soc. Metals 55, 995 (1962).

85. S. T. Kishkin, Izvestya Akad. Nauk. USSR, Otdelnie Tekn. Nauk 12, 1799 (1946).

86. N. H. Polakowski, J. Iron Steel Inst. 185, 67 (1957).

87. T. L. Johnson, A. S. Tetelman and A. J. McEvily, Jr., High Strength Materials, V. F. Zackay, ed. (John Wiley and Sons, 1964) p. 363.

88. R. W. Messler, G. S. Ansell and V. I. Lisunov, Trans. Amer. Soc. Metals 62, 362 (1969).

89. C. S. Ansell and E. H. Breinan, Trans. Amer. Soc. Metals 58, 110 (1965).

Table I. Chemical Composition of Alloys (given in wt.%)

Alloy	C	Mn	Cr	Ni	Mo	S	Si	Cu	P	V
4130	.30	.46	.85	.08	.20	.010	.28	.13	.008	*
4130-A	.31	.57	.85	.15	.18	.009	.28	.21	.008	*
4130-B	.33	.63	.90	.15	.18	.009	.27	.19	.008	*
4140-A	.40	.94	.90	.09	.22	.012	.28	.17	.008	*
4140-B	.42	1.02	.85	.17	.23	.012	.28	.13	.009	*
4330	.28	1.02	.85	1.80	.40	.005	.28	.10	.009	.07
4340-A	.40	.80	.72	1.65	.24	.010	.24	.19	-	*
4340-B	.40	.85	.72	1.73	.24	.010	.22	.14	.004	*
3140	.41	.85	.68	1.24	.02	.009	.35	.04	-	*
300-M	.41	.79	.75	1.85	.43	.002	1.59	.04	.008	.08
D6-AC	.46	.68	.98	.58	.93	.003	.25	—	.009	.11

* less than .005%

Table II. Heating data from room temperature to 1200°C, and furnace cooling data from 1200°C to 870°C. Taken from the midsection of a fracture toughness specimen 5/8" thick.

Run 1			Run 2				
Time	Thermocouple A Temp. °C	Thermocouple B Temp. °C	Time	Thermocouple A Temp. °C	Thermocouple B Temp. °C	Time	Temp. °C
(sec.)			(sec.)			(sec.)	
0	27	27	0	26	23	0	1204
30	484	482	8	128	126	15	1093
45	553	549	15	183	180	60	1007
60	609	603	22	234	233	90	974
75	659	654	30	285	282	120	949
90	698	694	37	331	330	150	929
105	733	728	45	381	377	180	921
120	746	743	52	421	418	210	907
135	761	756	60	459	458	240	899
150	804	800	68	496	493	270	893
165	855	848	75	527	527	300	889
180	897	893	82	556	557	360	879
195	928	923	90	579	588	420	874
210	957	754	97	604	618	480	871
225	979	972	105	624	642	540	869
240	997	992	117	651	664		
225	1022	1013	120	672	684		
270	1034	1031	135	715	717		
285	1052	1048	150	743	742		
300	1071	1067	165	754	754		
315	1079	1076	180	791	786		
330	1092	1088	195	847	843		
345	1101	1099	210	893	892		
360	1111	1109	225	934	932		
375	1119	1117	240	965	967		
390	1128	1125	255	992	997		
405	1135	1133	270	1019	1020		
420	1143	1142	285	1041	1041		
450	1151	1151	300	1058	1059		
480	1159	1159	315	1074	1076		

Table II. Continued

Time	Run 1 Thermocouple A Temp.	Run 1 Thermocouple B Temp.	Time	Run 2 Thermocouple A Temp.	Run 2 Thermocouple B Temp.	Time	Temp.
(sec.)	°C	°C	(sec)	°C	°C	(sec.)	°C
510	1167	1167	330	1088	1089		
540	1174	1173	345	1100	1101		
570	1177	1177	360	1110	1111		
620	1182	1181	375	1120	1122		
630	1182	1182	390	1128	1130		
660	1181	1181	405	1136	1138		
			420	1142	1143		
			435	1149	1151		
			450	1153	1156		
			465	1157	1161		
			480	1162	1166		
			495	1167	1169		
			510	1169	1171		
			525	1171	1174		

Table III. Oil and water quench cooling data from midsection of a fracture toughness specimen 5/8" thick.

Time	Oil Quench from 1200°C Thermocouple		Water Quench from 1200°C Thermocouple		Oil Quench from 870°C Thermocouple		Water Quench from 870°C Thermocouple	
	A	B	A	B	A	B	A	B
(sec.)	°C	°C	°C	°C	°C	°C	°C	°C
0.0	1217	1210	1214	1214	879	879	883	883
3.0	1209	1202	1201	1210	868	847	824	852
6.0	1193	1192	1151	1168	798	783	646	703
9.0	1154	1151	1015	1042	707	718	513	527
12.0	1091	1091	861	892	619	632	405	388
15.0	1023	1028	665	708	543	526	291	276
18.0	945	954	476	532	483	493	202	177
21.0	759	764	379	408	421	416	113	116
24.0	726	746	230	259	347	353	90	86
27.0	621	626	153	172	298	293	78	78
30.0	527	532	107	126	263	251	71	64
33.0	471	461	93	93	231	219	64	59
36.0	409	425	78	86	208	197	57	59
42.0	309	330	66	66	178	166	49	57
48.0	237	241	57	57	157	147	44	49
54.0	199	194			142	130		
60.0	176	162	41	50	129	126		
66.0	164	154			122	118		
72.0	152	142			122	107		
78.0	139	133			104	101		
84.0	133	126			104	101		
90.0	126	117			101	96		
150.0	107	100			80	70		
180.0	100	86						

Table IV. Ice brine quench cooling data from midsection of a fracture toughness specimen 5/8" thick.

Time (sec.)	Run 1 Thermocouple A Temp. °C	Run 1 Thermocouple B Temp. °C	Run 2 Thermocouple A Temp. °C	Run 2 Thermocouple B Temp. °C	Run 3 Thermocouple A Temp. °C	Run 3 Thermocouple B Temp. °C
0.0			1187	1191	1204	1201
0.8	1186	1184	1186	1191		
1.5	1184	1184	1186	1189		
2.3	1184	1183	1183	1186		
3.0	1183	1181	1176	1181	1192	1108
3.8	1176	1174	1162	1166		
4.5	1156	1159	1129	1134		
5.3	1099	1101	1053	1033		
6.0	981	985	940	948	919	941
6.8	870	868	828	838		
7.5	778	776	729	738		
8.3	689	681	644	651		
9.0	613	603	568	575	669	674
9.8	546	538	503	513		
10.5	487	481	450	460		
11.3	434	428	411	421		
12.0	373	369	387	397	466	482
12.8	360	356	368	379		
13.5	342	336	354	365		
14.3	322	319	335	346		
15.0	309	309	309	323	308	357
15.8	291	285	279	296		
16.5	268	265	252	269		
17.3	223	223	227	244		
18.0	205	207	209	223	202	242
18.8	191	193	189	204		
19.5	179	180	177	188		
20.3	166	168				
21.0	153	156	151	159	142	161
21.8	142	147				
22.5	128	134	129	141		
23.3	121	121				

Table IV. Continued

Time (sec.)	Run 1 Thermocouple A Temp. °C	Run 1 Thermocouple B Temp. °C	Run 2 Thermocouple A Temp. °C	Run 2 Thermocouple B Temp. °C	Run 3 Thermocouple A Temp. °C	Run 3 Thermocouple B Temp. °C
24.0	117	114		128	99	87
24.8	112	108				
25.5	109	104		126		
26.3	104	99				
27.0	101	98		126	80	73
27.8	97	96		125		
30.0					64	57
33.0					49	44
36.0					41	33
42.0					33	28

Table V. Approximate cooling rates, degrees centigrade per second, at different temperatures taken from the mid-section of a 5/8" thick fracture toughness specimen.

Austenitizing Temperature °C	Quench	900 °C	705* °C	500 °C	300 °C	150 °C
1200	Ice Brine	125	125	69	32	15
1200	Water	100	100	46	37	17
1200	Oil	38	38	23	13	22
870	Oil		32	21	14	22
870	Water		100	43	32	10

* 705°C = 1300°F

Table VI. Room temperature fracture toughness properties for alloy 4130

Austenitizing Temperature °C	Quench	Tempering Temperature °C	Test Specimen Number	$\frac{P_m}{P_Q}$	Plane Strain Fracture Toughness K_{IC} ksi-in.$^{\frac{1}{2}}$	Critical Stress Intensity K_{crit} ksi-in.$^{\frac{1}{2}}$	$\frac{K_{IC}}{\sigma_{ys}}$
1200	Oil	A Q***	2	1.22	83.5	111	.41
		A Q	5	1.05	89.4	101	.44
		A Q	31	1.06	86.5	117	
1200	IBQLN	A Q	1	1.21	98.5	142	.46
		A Q	4	1.11	99.5	108	.46
		A Q	24	1.15	81.0	107	.38
		A Q	26	1.16	81.0	103	.38
		200	28	1.10	96.0	130	.45
		200	12	1.11	110.0*	154	.51
		225	22	1.07	91.0	103	.44
		280	13	1.06	79.0	95.0	.41
		280	32	1.20	71.0	92.5	.40
		350	16	1.09	67.5	80.5	.38
1200	IBQ **	A Q	25	1.12	78.0	112	.38
		A Q	27	1.07	80.3	111	.38
1100	IBQLN	A Q	21	1.02	69.0	74.9	.32

* These values are apparent ones (K_Q) and do not meet the requirements specified in the ASTM standards.

** Specimens were quenched in ice brine only and not refrigerated in liquid nitrogen.

*** AQ refers to the as quenched condition.

Table VI. Continued

Austenitizing Temperature °C	Quench	Tempering Temperature °C	Test Specimen Number	$\frac{P_m}{P_Q}$	Plane Strain Fracture Toughness K_{IC} ksi-in.$^{\frac{1}{2}}$	Critical Stress Intensity K_{crit} ksi-in.$^{\frac{1}{2}}$	$\frac{K_{IC}}{\sigma_{ys}}$
1200-870	Oil	A Q	7	1.12	72.8	96.8	.35
		200	18	1.05	74.3	82.8	.35
		280	19	1.07	61.3	75.2	.29
		350	20	1.04	64.6	76.0	.31
1200-870	IBQLN	A Q	6	1.10	82.2	108.3	.38
870	Oil	A Q	3	1.17	58.0	76.5	.29
		A Q	9	1.03	55.1	63.0	.27
		A Q	29	1.00	47.5	47.5	.23
		200	30	1.03	51.4	60.0	.24
		200	10	1.03	55.2	61.5	.25
		225	23	1.05	57.6	68.7	.27
		280	11	1.00	63.5	63.5	.29
		350	17	1.01	67.5	83.3	.36
870	IBOLN	A Q	8	1.00	52.8	52.8	.25

Table VII. Room temperature fracture toughness properties for alloy 4140

Austenitizing Temperature °C	Quench	Tempering Temperature °C	Test Specimen Number	$\frac{P_m}{P_Q}$	Plane Strain Fracture Toughness K_{IC} ksi-in.$^{\frac{1}{2}}$	Critical Stress Intensity K_{crit} ksi-in.$^{\frac{1}{2}}$	$\frac{K_{IC}}{\sigma_{ys}}$
1200	Oil	A Q	4	1.13	53.1	67.5	.22
		A Q	18	1.04	49.8	54.7	.21
		190	19	1.10	64.5	80.0	.28
		200	10	1.00	90.4	90.4	.39
		200	22	1.10	71.7	83.4	
		245	13	1.02	68.0	75.8	.30
		245	15	1.05	64.2	74.2	.29
		325	11	1.08	48.5	59.0	.23
		350	9	1.12	53.2	67.5	.25
1200	IBQLN	A Q	3	1.12	43.2	52.6	.18
1200	Oil + LN	A Q	20	1.02	50.8	57.6	.21
1100	Oil	A Q	17	1.08	33.5	46.7	.14
		200	21	1.01	59.2	66.8	.26
		245	16	1.02	57.3	66.4	.25
		245	14	1.00	46.8	46.8	.21
1200-870	Oil	A Q	5	1.12	33.0	41.0	.14
1200-870	IBQLN	A Q	2	1.08	37.9	49.0	.16

Table VII. Continued

Austenitizing Temperature °C	Quench	Tempering Temperature °C	Test Specimen Number	$\frac{P_m}{P_Q}$	Plane Strain Fracture Toughness K_{IC} ksi-in.$^{\frac{1}{2}}$	Critical Stress Intensity K_{crit} ksi-in.$^{\frac{1}{2}}$	$\frac{K_{IC}}{\sigma_{ys}}$
870	Oil	A Q	6	1.04	27.1	34.0	.11
		200	7	1.00	39.9	46.7	.19
		280	8	1.00	50.0	50.0	.22
		396	12	1.06	50.6	62.5	.23

Table VIII. Room temperature fracture toughness properties for alloy 4330

Austenitizing Temperature °C	Quench	Tempering Temperature °C	Test Specimen Number	P_m/P_Q	Plane Strain Fracture Toughness K_{IC} ksi-in.$^{\frac{1}{2}}$	Critical Stress Intensity K_{crit} ksi-in.$^{\frac{1}{2}}$	K_{IC}/σ_{ys}
1200	Oil	A Q	2	1.28	87.5	131.5	.42
1200	IBQLN	A Q	1	1.12	102.5	147.5	.49
		200	10	1.12	108.5 *	151.0	.53
		200	13	1.11	113 *	157.0	.55
		280	11	1.02	107 *	130	.57
		280	14	——	106.5 *	——	.57
		350	12	1.13	106.5 *	141	.59
1200-870	Oil	A Q	4	1.29	79.4	136.1	.35
1200-870	IBQLN	A Q	3	1.18	75.8	116	.35
870	Oil	A Q	5	1.08	60.0	76.3	.26
		A Q	6	1.10	67.1	94.6	.29
		200	7	1.06	88	114	.40
		280	8	1.10	99.4	132	.48
		280	15	1.04	94.0	106	.47
		350	9	1.13	104.0 *	141	.53

* K_Q values, did not meet thickness requirements for valid K_{Ic} test.

Table IX. Room temperature fracture toughness properties for alloy 4340

Austenitizing Temperature °C	Quench	Tempering Temperature °C	Test Specimen Number	$\frac{P_m}{P_Q}$	Plane Strain Fracture Toughness K_{IC} ksi-in.$^{\frac{1}{2}}$	Critical Stress Intensity K_{crit} ksi-in.$^{\frac{1}{2}}$	$\frac{K_{IC}}{\sigma_{ys}}$
1200	Oil	A Q	1	1.12	65.3	81.8	.29
		A Q	2	1.15	60.9	88.9	.27
		A Q	39	1.08	49.6	62.8	.22
		245	40	1.05	82.4	88.8	.37
		280	50	1.12	62.8	79.0	
1200	water	A Q	5		quench cracked		
		A Q	6		quench cracked		
1200	IBOLN	A Q	3		quench cracked		
		A Q	4	1.19	49.8	51.7	.22
1100	Oil	A Q	41	1.07	40.0	45.3	.18
1200-870	Oil	A Q	9	1.02	63.8	69.4	.29
		A Q	10	1.01	66.6	68.7	.29
		A Q	35	1.11	52.0	65.3	.23
		A Q	46	1.00	61.2	61.2	.26
		175	26	1.10	72.9	87.0	.33
		200	31	1.06	76.9	87.5	.34
		200	47	1.04	76.7	110.0	.34
		280	32	1.06	57.8	74.3	.26
		280	48	1.10	62.3	78.5	.26
		350	33	1.12	60.2	78.0	.27
		350	42	1.19	61.4	80.0	.28

Table IX. Continued

Austenitizing Temperature °C	Quench	Tempering Temperature °C	Test Specimen Number	$\frac{P_m}{P_Q}$	Plane Strain Fracture Toughness K_{IC} ksi-in.$^{\frac{1}{2}}$	Critical Stress Intensity K_{crit} ksi-in.$^{\frac{1}{2}}$	$\frac{K_{IC}}{\sigma_{ys}}$
1100-870	Oil	245	36	1.04	54.4	56.3	.25
1200-870	Oil + LN	A Q	43	1.07	55.6	63.7	.25
1200-870	Water	A Q	11	1.14	59.3	74.6	.26
		A Q	12	1.31	59.8	97.5	.27
1200-870	IBOLN	A Q	7	1.14	60.5	84.5	.27
		A Q	8	1.24	52.2	85.4	.23
870	Oil	A Q	15	1.08	31.1	38.8	.14
		A Q	16	1.00	39.0	39.4	.17
		A Q	34	1.00	32.3	32.3	.14
		175	27	1.00	62.0	62.0	.27
		200	49	1.00	59.5	59.5	
		280	44	1.00	60.3	60.3	.27
		280	29	1.02	61.4	71.6	.28
		350	30	1.01	79.8	84.3	.32
		395	38	1.04	91.2	94.5	.44
870	Oil + LN	A Q	45	1.00	33.1	33.1	.14
870	Water	A Q	17		quench cracked		
		A Q	18		quench cracked		

Table IX. continued

Austenitizing Temperature °C	Quench	Tempering Temperature °C	Test Specimen Number	P_m/P_Q	Plane Strain Fracture Toughness K_{IC} ksi-in.$^{\frac{1}{2}}$	Critical Stress Intensity K_{crit} ksi-in.$^{\frac{1}{2}}$	K_{IC}/σ_{ys}
870	IBQLN	A Q	13		quench cracked		
		A Q	14		quench cracked		
1200-870-870*	Oil	A Q	37	1.08	38.9	46.5	.17

* Step quenched into oil (1200-870) and then re-austenitized at 870°C for 1 hour and oil quenched.

Table V. Room temperature fracture toughness properties for alloy 300-M

Austenitizing Temperature °C	Quench	Tempering Temperature °C	Test Specimen Number	$\frac{P_m}{P_Q}$	Plane Strain Fracture Toughness K_{IC} ksi-in.$^{\frac{1}{2}}$	Critical Stress Intensity K_{crit} ksi-in.$^{\frac{1}{2}}$	$\frac{K_{IC}}{\sigma_{ys}}$
1200	OQ	A Q	4	1.00	48.0	48.0	.23
		A Q	19	1.00	34.5	34.5	.16
		A Q	20	1.00	44.8	44.8	
		200	17	1.00	75.0	75.0	.34
		245	5	1.04	69.2	74.0	.30
		245+245	9	1.03	71.8	78.6	.31
		325	10	1.00	75.5	75.5	.32
		396	13	1.00	74.7	74.7	.31
1200	OQ + LN	A Q	18	1.00	35.0	35.0	.16
1200-870	OQ	A Q	6	1.00	37.1	37.1	.17
		245	7	1.08	45.2	60.9	.20
		245+245	8	1.07	50.6	56.7	.22
		325	14	1.00	52.7	52.7	.22
		396	15	1.00	63.5	63.5	.27
870	OQ	A Q	16	1.00	23.0	23.0	
		A Q	21	1.00	23.7	23.7	
		245	2	1.00	34.8	34.8	.15
		245+245	3	1.00	34.3	34.3	.14
		300	22	1.00	59.4	59.4	
		325	11	1.00	64.8	64.8	.19
		396	12	1.00	60.9	60.9	.25

Table XI. Room temperature fracture toughness properties for alloy 4350

Austenitizing Temperature °C	Quench	Tempering Temperature °C	Test Specimen Number	$\frac{P_m}{P_Q}$	Plane Strain Fracture Toughness K_{IC} ksi-in.$^{\frac{1}{2}}$	Critical Stress Intensity K_{crit} ksi-in.$^{\frac{1}{2}}$	$\frac{K_{IC}}{\sigma_{ys}}$
1200-870	Oil	A Q	4	1.10	31.1	42.2	
		200	5	1.14	47.1	58.8	
1200-870	IBQLN	A Q	1		quench cracked		
870	Oil	A Q	3	1.03	23.7	28.2	
		200	6	1.09	37.9	44	

Table XII. Room temperature fracture toughness properties for alloy 3140

Austenitizing Temperature °C	Quench	Tempering Temperature °C	Test Specimen Number	$\frac{P_m}{P_Q}$	Plane Strain Fracture Toughness K_{IC} ksi-in.$^{\frac{1}{2}}$	Critical Stress Intensity K_{crit} ksi-in.$^{\frac{1}{2}}$	$\frac{K_{IC}}{\sigma_{ys}}$
1200	Oil	A Q	7	1.23	61.4	97.5	
		200	2	1.09	91.6	129.0	
		350	3	1.12	46.3	56.7	
1200	IBQLN	A Q	5	1.27	53.1	76.6	
1200-870	Oil	A Q	8	1.13	53.4	78.4	
870	Oil	A Q	9	1.09	41.4	51.1	
		200	10	1.04	54.3	65.1	
		350	1	1.01	48.3	52.5	
870	IBQLN	A Q	4	1.14	36.3	56.1	

Table XIII. Room temperature Charpy V-notch impact properties.

Austenitizing Temperature °C	Quench	Tempering Temperature °C	CVN Impact Energy (ft.-lbs) Alloy 4130	Alloy 4330	Alloy 4340	Alloy 300-M	Alloy D6-AC
870	Oil	A Q	8.0	11.5	7.5	5.8	4.2
			5.9	12.7	6.1	6.8	4.8
		115	8.5	20.4	9.0	7.4	5.7
			11.9	25.5	9.9	8.6	6.9
		165	17.3	28.2	11.5	10.5	6.6
			20.0	27.1	19.3	9.6	7.0
		200	8.0	26.1	15.2	11.6	8.5
			11.3	19.0	16.4	17.0	9.3
		280	7.8	26.2	15.0	10.4	6.7
			10.1	17.7	13.0	10.6	6.6
		350	12.6	16.9	17.4	8.5	6.9
			12.7	20.0	16.7	11.7	6.4
1200	Oil	A Q	8.4	17.5	5.7	5.5	4.2
			6.6	20.0	5.4	4.2	4.8
		115	13.8		10.3	4.6	5.7
			16.5		7.4	4.4	6.9
		165	15.1		14.5	6.2	6.6
			18.0		17.0	10.4	7.0
		200	14.1	27.7	10.5	8.0	8.5
			13.0	29.7	10.9	10.9	9.3
		280	6.0		4.9	6.7	6.7
			7.0	22.3	4.2	10.4	6.6
		350	9.9	18.2	4.3	6.9	6.9
			6.8	15.8	5.1	10.3	6.4

Table XIII. Continued

Austenitizing Temperature °C	Quench	Tempering Temperature °C	CVN Impact Energy (ft.-lbs) Alloy 4130	Alloy 4330	Alloy 4340	Alloy 300-M	Alloy D6-AC
1200-870	Oil	A Q	8.0	17.2	5.4	4.4	3.7
			6.6	18.2	6.0	3.8	
		115	11.3		8.0		
			7.9		11.1		
		165	10.8		8.7		
			12.7		11.9		
		200	9.3	25.0	8.6	6.4	7.3
			6.2	23.0	8.8	6.0	6.7
		280	4.3	8.7	5.9	5.9	5.3
			4.5	13.6	4.8	5.2	5.4
		350	3.4	10.7	5.5	6.4	6.3
			4.1	11.2	4.4	8.5	6.3
1200-870	Water	A Q	5.7	14.3		2.5	
			6.8	13.3		2.7	
		115	10.2	16.7			
			11.1	15.3			
		165		19.1			
				21.8			
		200	8.4	24.7		6.3	
			13.2	24.3		5.8	
		280	4.3	13.0		5.5	
			4.9	15.8		5.6	
		350	5.0	11.7		6.8	
			5.9	10.6		7.0	

Table XIII. Continued

Austenitizing Temperature °C	Quench	Tempering Temperature °C	CVN Impact Energy (ft.-lbs) Alloy 4130	Alloy 4330	Alloy 4340	Alloy 300-M	Alloy D6-AC
1200-870	IBQLN	A Q	7.1	14.0	3.6		
			7.0	17.0	3.7		
		115			4.2		
		165			7.6		
		200	11.9	22.3	6.7		
			12.0	19.5	6.5		
		280	4.7	9.8	4.4		
			4.4	13.4	4.9		
		350	7.6	12.7	5.0		
			6.3	10.7	6.0		
1200	IBQLN	A Q		16.9			
			8.7	16.7			
		115	11.8				
			16.1				
		165	18.6				
			20.8				
		200	14.9	26.3			
			14.5	30.5			
		280	7.6	22.5			
			7.0	14.6			
		350	7.5	11.0			
			6.1				

Table XIII. Continued

Austenitizing Temperature °C	Quench	Tempering Temperature °C	CVN Impact Energy (ft.-lbs) Alloy 4130	Alloy 4330	Alloy 4340	Alloy 300-M	Alloy D6-AC
1200	Water	A Q	10.4 10.1				
		115	10.5 12.7				
		165	17.7 16.8				
		200	17.4 17.6				
		280	6.6 5.0				
		350	5.7 6.5				

Table XIV. Room temperature longitudinal tensile properties for alloy 4130

Austenitizing Temperature °C	Quench	Tempering Temperature °C	Test Specimen Number	.2% Yield Strength ksi micro	.2% Yield Strength ksi macro	Ultimate Tensile Strength ksi	Elongation %	Reduction of Area %	True Fracture Strain
1200	IBQLN	A Q	1	172	219	245	1.4 *	5.5	.04
		A Q	2	162	210	252	1.8 *	7.6	.07
		200	3	186	210	257	4.5 *	13.0	.12
		280	4	183	195	230	7.6	21.0	.23
		280	5	185	192	220	2.2 *	6.7	.06
		350	6	180	180	209	9.8	37.0	.45
1200	Water	A Q	13	166	218	280	6.5	15.0	.15
		A Q	14	168	219	277	5.0	13.0	.12
		200	15	210	213	258	9.7	—	—
		280	16	180	190	225	10.8	38.7	.08
		280	17	185	195	231	1.7 *	8.8	.11
		350	18	180	180	210	9.8	25.2	.42
1200	Oil	A Q	7	165	203	282	5.4	10.9	.10
		A Q	8	158	206	270	5.8	8.8	.08
		200	9	176	210	262	7.5	18.1	.19
		280	10	195	210	246	8.0	24.0	.26
		280	11	192	210	245	7.9	26.9	.30
		350	12	182	192	222	7.7	30.6	.35
1200-870	IBQLN	A Q	19		210	285	6.6	12.0	.07
		A Q	20	170	225	273	— *	2.4	.01
		200	21	195	213	261	3.7 *	7.6	.07
		280	22	183	189	226	7.8	25.9	.29
		280	23	186	196	234	5.2 *	6.7	.06
		350	24	200	203	210	9.3	32.4	.38

* quench cracks visible

Table XIV. Continued

Austenitizing Temperature °C	Quench	Tempering Temperature °C	Test Specimen Number	.2% Yield Strength ksi micro	.2% Yield Strength ksi macro	Ultimate Tensile Strength ksi	Elongation %	Reduction of Area %	True Fracture Strain
1200-870	Water	A Q	31	164	222	282	6.2	6.7	.06
		A Q	32	160	207	273	4.3	7.6	.07
		200	33	195	217	261	7.6	19.0	.20
		280	34	190	198	234	-	27.7	.32
		280	35	189	200	234	6.9	21.1	.23
		350	36	180	-	209	9.6	35.2	.42
1200-870	Oil	A Q	25	159	217	280	7.0	7.6	.06
		A Q	26	153	202	270	2.1	6.7	.06
		200	27	174	210	258	5.2	7.6	.07
		280	28	192	213	252	3.6	9.7	.10
		280	29	198	219	255	4.2	8.8	.08
		350	30	198	207	237	5.2	16.1	.16
870	Oil	A Q	37	165	207	284	12.0	34.2	.41
		A Q	38	162	195	284	10.8	31.6	.37
		200	39	192	219	274	13.2	8.8	.08
		280	40	170	185	-	9.5	45.5	.59
		280	41	200	210	246	10.6	45.5	.59
		350	42	177	186	210	12.0	53.4	.75

Table XV. Room temperature longitudinal tensile properties for alloy 4330

Austenitizing Temperature °C	Quench	Tempering Temperature °C	Test Specimen Number	.2% Yield Strength ksi micro	.2% Yield Strength ksi macro	Ultimate Tensile Strength ksi	Elongation %	Reduction of Area %	True Fracture Strain
1200	IBQLN	A Q	1	168	210	222	0.8*	5.5	.04
		A Q	2	178	–	–	0.4*	1.2	–
		200	3	177	205	252	12.0	37.9	.46
		280	4	180	190	228	3.7*	13.0	.12
		280	5	177	187	225	2.9*	8.8	.08
		350	6	170	180	210	4.6	10.9	.10
1200	Water	A Q	13	160	232	245	1.4*	5.5	.04
		A Q	14	183	219	250	2.9*	3.4	.02
		200	15	183	210	257	11.3	37.9	.46
		280	16	177	192	230	5.0*	7.6	.07
		280	17	182	196	230	2.7*	12.0	.11
		350	18	170	185	214	10.1	38.7	.48
1200	Oil	A Q	7	153	210	280	8.1	12.0	.11
		A Q	8	157	207	285	7.4	15.0	.15
		200	9	189	213	267	9.1	25.9	.29
		280	10	182	195	242	9.0	28.8	.33
		280	11	174	222	238	8.8	30.6	.35
		350	12	183	187	227	7.5	28.8	.33
1200-870	IBQLN	A Q	19	170	215	230	10.5*	33.4	.02
		200	20	193	215	260	1.0*	3.4	.39
		200	21	–	–	–	1.1*	2.4	.01
		280	22	177	190	228	10.7	37.9	.46
		280	23	177	189	228	2.3*	4.5	.03
		350	24	171	186	217	5.2	15.0	.14

* quench cracks visible

Table XV. Continued

Austenitizing Temperature °C	Quench	Tempering Temperature °C	Test Specimen Number	.2% Yield Strength ksi micro	.2% Yield Strength ksi macro	Ultimate Tensile Strength ksi	Elongation %	Reduction of Area %	True Fracture Strain
1200-870	Water	A Q	31	162	216	302	5.4	12.0	.11
		A Q	32	173	240	295	2.8	12.0	.11
		2 J	33	-	202	256	11.4	32.4	.38
		280	34	175	186	228	5.1	36.0	.43
		280	35	175	195	234	9.5	34.2	.41
		350	36	174	166	216	-	27.0	.45
1200-870	Oil	A Q	25	165	190	286	7.4	14.1	.14
		A Q	26	160	205	285	3.2	12.0	.11
		200	27	185	205	257	10.2	29.8	.34
		280	28	182	195	235	8.8	27.7	.32
		280	29	182	197	239	8.2	28.8	.33
		350	30	178	187	220	9.1	34.2	.41
870	Oil	A Q	37	160	247	285	12.7	-	-
		A Q	38	165	220	282	13.5	43.0	.55
		200	39	198	220	273	12.6	51.0	.70
		280	40	203	205	245	12.9	51.0	.70
		280	41	201	210	247	13.0	53.4	.75
		350	42	201	201	223	14.1	55.6	.80

Table XVI. Room temperature longitudinal tensile properties for alloy 4140

Austenitizing Temperature °C	Quench	Tempering Temperature °C	Test Specimen Number	.2% Yield Strength ksi micro	.2% Yield Strength ksi macro	Ultimate Tensile Strength ksi	Elongation %	Reduction of Area %	True Fracture Strain
1200	Oil	A Q	10	170	240	320	2.6	5.5	.04
		A Q	14	170	240	330	2.5	4.5	.03
		200	15	200	230	292	6.2	3.4	.02
		280	16	205	215	263	4.9	13.0	.12
		280	17	218	225	266	4.7	12.0	.11
		350	18	202	210	245	4.5	14.1	.14
		350	19	202	210	245	4.1	4.5	.03
1200-870	Oil	A Q	7	170	230	298	2.1	5.5	.04
		A Q	8	175	240	290	-	-	-
		200	9	205	240	298	3.0	4.5	.03
		280	12	205	215	258	4.0	7.6	.07
		280	11	205	225	270	3.4	5.5	.04
		350	13	195	205	235	2.0	3.4	.02
870	Oil	A Q	1	185	240	335	11.6	28.8	.33
		A Q	2	175	250	340	4.5	19.7	.10
		200	3	210	245	302	13.3	-	-
		280	4	230	230	267	12.5	47.9	.64
		280	5	233	230	267	13.1	51.0	.70
		350	6	222	220	248	13.3	52.7	.73

Table XVII. Room temperature longitudinal tensile properties for alloy 4340

Austenitizing Temperature °C	Quench	Tempering Temperature °C	Test Specimen Number	.2% Yield Strength ksi micro	macro	macro'**	Ultimate Tensile Strength ksi	Elongation %	Reduction of Area %	True Fracture Strain %
1200	Oil	A Q	13	165	220	195	326	6.9	5.5	.04
		200	14	200	227	220	288	8.5	19.0	.20
		280	15	202	212	210	256	7.7	24.0	.26
		350	16	195	207	200	238	6.8	20.0	.21
1200-870	Oil	A Q *	17	190	210	180	315		12.0	.11
		A Q *	18	200	218	200	308	3.0	13.0	.12
		A Q *	19	200	220	212	320	3.9	8.8	.08
		A Q	7	160	230	188	318	2.6	6.7	.06
		A Q	8	163	232	200	318	3.7	8.8	.08
		200	9	195	230	225	290	7.1	13.0	.12
		280	10	197	215	205	253	7.7	21.0	.23
		280	11	208	225	217	265	6.7	12.0	.11
		350 *	20	200	200	200	232	7.3	20.1	.21
		350 *	21	202	200	200	236	6.1	21.1	.23
		350	12	196	205	200	235	6.6	15.0	.04
870	Oil	A Q	1	180	237	210	323	10.6	17.0	
		A Q	2	171	225	205	320	7.4	44.6	.18
		200	3	195	235	225	290	13.5	54.8	.58
		280	4	210	210	210	235	13.4	47.1	.79
		280	5	225	230	230	262	12.8	55.6	.62
		350	6	217	217	217	242	13.9	6.7	.80

* These specimens were heat treated at a later date than the other specimens and were machined instead of ground.

** Corrected macro yield strength, explained in text.

Table XVIII. Room temperature longitudinal tensile properties for alloy 300-M

Austenitizing Temperature °C	Quench	Tempering Temperature °C	Test Specimen Number	.2% Yield Strength ksi micro	.2% Yield Strength ksi macro	Ultimate Tensile Strength ksi	Elongation %	Reduction of Area %	True Fracture Strain
1200	Oil	A Q	1	190	207	338	-	6.4	.07
		A Q	2	191	218	330	1.5	8.7	.10
		200	3	219	218	300	-	15.0	.16
		280	4	238	238	290	6.9	17.1	.19
		280	5	237	235	288	6.3	20.1	.23
		350	6	243	242	287	6.3	19.1	.21
1200-870	Oil	A Q	13	195	225	335			
		A Q	14	190	218	333	3.3	7.7	.08
		110	28	206	218	332	-	8.7	.10
		165	29	225	228	331	5.0	6.6	.07
		165	30	228	232	318	6.4	6.1	.18
		200	15	230	232	292	7.6	17.1	.19
		280	16	240	240	290	6.0	19.1	.21
		280	17	238	241	288	7.8	15.0	.16
		350	18	241	240	286	6.6	19.1	.21
1200-870	Water	A Q	19		quench cracked				
		A Q	20		quench cracked				
		200	21	227	233	280	2.3*	7.7	.08
		280	22	233	235	282	8.5	26.0	.30
		280	23		quench cracked				
		350	24	237	239	263	1.5*	5.5	.06

* quench cracks visible

Table XVIII. Continued

Austenitizing Temperature °C	Quench	Tempering Temperature °C	Test Specimen Number	.2% Yield Strength ksi micro	.2% Yield Strength ksi macro	Ultimate Tensile Strength ksi	Elongation %	Reduction of Area %	True Fracture Strain
870	Oil	A Q	7	190	230	348	-	9.8	.10
		A Q	8	177	215	340	14.4	16.1	.18
		110	25	200	215	335	9.3	25.0	.29
		165	26	226	228	318	-	39.7	.51
		165	27	229	233	322	12.9	37.1	.46
		200	9	236	238	303	13.6	45.6	.61
		280	10	243	240	288	12.0	47.3	.64
		280	11	210	243	289	12.0	47.3	.64
		350	12	252	250	290	12.7	48.9	.67

Table XIX. Room temperature longitudinal tensile properties for alloy D6-AC

Austenitizing Temperature °C	Quench	Tempering Temperature °C	Test Specimen Number	.2% Yield Strength ksi micro	.2% Yield Strength ksi macro	Ultimate Tensile Strength ksi	Elongation %	Reduction of Area %	True Fracture Strain
1200	Oil	A Q	1	176	227	333	2.2*	4.4	.04
		A Q	2	174	225	333	-	4.4	.04
		200	3	228	225	303	4.9	8.7	.10
		280	4	224	220	272	4.3	8.7	.10
		280	5	226	225	277	1.5*	8.7	.10
		350	6	218	218	260	3.3	9.8	.10
1200-870	Oil	A Q	13	210	218	321	1.5	5.5	.06
		A Q	14	193	217	318	1.7	4.4	.04
		110	22	201	213	322	2.0	4.4	.04
		165	23	227	233	322	2.0	4.4	.07
		165	24	228	235	320	2.0	6.6	.06
		200	15	231	233	303	3.8	7.7	.08
		280	16	225	222	275	3.8	9.8	.10
		350	17	227	227	276	3.3	7.7	.08
		350	18	217	217	258	3.7	8.7	.10
870	Oil	A Q	7	202	227	349	-	17.1	.19
		A Q	8	213	238	348	-	9.8	.10
		110	19	213	232	340	4.5	7.7	.08
		165	20	240	245	331	9.4	15.0	.16
		165	21	233	244	328	-	33.5	.41
		200	9	249	247	310	-	32.6	.39
		280	10	243	243	280	12.1	47.6	.64
		280	11	245	243	258	11.6	47.3	.64
		350	12	233	233	262	12.4	49.6	.69

* quench cracks visible

FIGURE CAPTIONS

Fig. 1. Vertical tube controlled atmosphere furnaces used to austenitize test specimens.

Fig. 2. Schematic of a fracture toughness specimen in which two thermocouples were placed, in order to measure midthickness cooling rates.

Fig. 3. ASTM specification for compact tension fracture toughness specimens.

Fig. 4. Schematic of the orientation in which Charpy V-notch blanks were cut from the bar and wired together for heat treatment.

Fig. 5. Schematic of the orientation in which tensile specimen blanks were cut from the bar and wired together for heat treatment before being ground to size.

Fig. 6. ASTM specification for Charpy V-notch specimen.

Fig. 7. Schematic of the orientation of the final Charpy V-notch specimen relative to the blank specimen and the bar.

Fig. 8. ASTM specification for 3/8 in. diameter round tensile specimen.

Fig. 9. Dual extensometer arrangement used to determine the "micro" yield strength of the tensile specimens.

Fig. 10. Apparatus used to calibrate the output of the extensometers, ampliers and x-y recorder.

Fig. 11. Crack opening displacement, v, vs crack length, a, calibration curve.

Fig. 12. Temperature vs time during heating from room temperature and cooling from 1200°C to 870°C measured at the midsection of a 5/8 in. thick fracture toughness specimen.

Fig. 13. Temperature vs time during quenching from 870°C in either oil or water measured at the midsection of a 5/8 in. thick fracture toughness specimen.

Fig. 14. Temperature vs time during quenching from 1200°C into either oil, water or ice brine measured at the midsection of a 5/8 in. thick fracture toughness specimen.

Fig. 15. Schematic of three general types of load vs crack opening displacement curves obtained from fracture toughness tests.

Fig. 16. Plane strain fracture toughness vs tempering temperature for 4130.

Fig. 17. Plane strain fracture toughness vs tempering temperature for 4140.

Fig. 18. Plane strain fracture toughness vs tempering temperature for 4330.

Fig. 19. Plane strain fracture toughness vs tempering temperature for 4340.

Fig. 20. Plane strain fracture toughness vs tempering temperature for 300-M.

Fig. 21. Plane strain fracture toughness vs tempering temperature for 3140.

Fig. 22. Charpy V-notch impact energy vs tempering temperature for 4130.

Fig. 23. Charpy V-notch impact energy vs tempering temperature for 4330.

Fig. 24. Charpy V-notch impact energy vs tempering temperature for 4340 and 300-M.

Fig. 25. Charpy V-notch impact energy vs tempering temperature for D6-AC.

Fig. 26. "Micro" and "macro" yield and ultimate strength vs tempering temperature for 4130.

Fig. 27. "Micro" and "macro" yield and ultimate strength vs tempering temperature for 4330.

Fig. 28. "Micro" and "macro" yield and ultimate strength vs tempering temperature for 4140.

Fig. 29. "Micro" and "macro" yield and ultimate strength vs tempering temperature for 4340.

Fig. 30. "Micro" and "macro" yield and ultimate strength vs tempering temperature for 300-M.

Fig. 31. "Micro" and "macro" yield and ultimate strength vs tempering temperature for D6-AC.

Fig. 32. Typical stress-strain curve for both an as-quenched specimen and a specimen tempered at 350°C, (A) "micro" stress-strain using extensometers, (B) "macro" stress-strain curve using crosshead movement.

Fig. 33. As-quenched martensitic structure of a 0.027 in. thick section of 4340 after austenitizing for 1 hour at 1200°C and ice brine quenching followed by refrigeration in liquid nitrogen (1200°C, IBQLN) heat treatment.

Note: All micrographs were taken from sections cut from the middle of fracture toughness specimens, except where noted.

Fig. 34. As-quenched microstructure of 4130 after a (1200°C, IBQLN) heat treatment.

Fig. 35. As-quenched microstructure of 4130 after a (1200°C, IBQLN) heat treatment showing a grain boundary decomposition product (indicated by arrow) along a prior austenite grain boundary.

Fig. 36. As-quenched microstructure of 4130 after a (1200°C, IBQLN) heat treatment showing a grain boundary decomposition product (indicated by arrow) along a prior austenite grain boundary.

Fig. 37. As-quenched microstructure of 4130 after a (1200°C, Oil) heat treatment showing upper bainite (marked by arrow) nucleated along grain boundaries.

Fig. 38. As-quenched microstructure of 4130 after a (1200°C, Oil) heat treatment showing upper bainite (marked by arrow) nucleated along grain boundaries.

Fig. 39. As-quenched microstructure of 4130 after a (1200°C, Oil) heat treatment showing upper bainite (marked by arrow) nucleated along grain boundaries.

Fig. 40. As-quenched microstructure of 4130 after a (1200°C, Oil) showing upper bainite that has nucleated from a grain boundary.

Fig. 41. As-quenched microstructure of 4130 after a (1200°C, Oil) showing upper bainite that has nucleated from a grain boundary.

Fig. 42. Enlargement of micrograph in Fig. 41.

Fig. 43. As-quenched microstructure of 4130 after a (1200→870°C, Oil) heat treatment showing regions of upper bainite marked by arrows.

Fig. 44. As-quenched microstructure of 4130 after a (1200→870°C, Oil) heat treatment showing regions of upper bainite marked by arrows.

Fig. 45. As-quenched microstructure of 4130 after an (870°C, IBQLN) heat treatment which results in a small prior austenite grain size and a fine upper bainitic structure, marked by arrows.

Fig. 46. (A) As-quenched microstructure of 4130 after an (870°C, IBQLN) heat treatment showing the upper bainite structure marked by arrows, (B) higher magnification of same area as (A).

Fig. 47. Enlargement of Fig. 46.

Fig. 48. Interference contrast micrograph of the as-quenched structure of 4130 after an (870°C, IBQLN) heat treatment, showing the parallel laths of upper bainite extending across individual prior austenite grains.

Fig. 49. As-quenched microstructure of 4130 after an (870°C, Oil) heat treatment, showing the bainitic structure with parallel laths indicated by arrows (micrograph taken near the surface of the specimen).

Fig. 50. As-quenched microstructure of 4130 after an (870°C, Oil) heat treatment showing ferrite and upper bainite, marked by arrows.

Fig. 51. As-quenched microstructure of 4330 after a (1200°C, IBQLN) heat treatment showing small regions of a decomposition product clearly nucleated along grain boundaries similar to Figs. 34 through 36.

Fig. 52. Interference contrast micrograph of as-quenched microstructure of 4330 after a (1200°C, Oil) heat treatment showing bainite, marked by arrows.

Fig. 53. As-quenched microstructure of 4330 after a (1200°C, Oil) heat treatment showing bainite, marked by arrows.

Fig. 54. As-quenched microstructure of 4330 after a (1200°C, Oil) heat treatment showing bainite and a ferrite film along a grain boundary, marked by arrow.

Fig. 55. As-quenched microstructure of 4330 after a (1200→870°C, Oil) heat treatment showing bainite and ferrite along grain boundaries, marked by arrow.

Fig. 56. As-quenched microstructure of 4330 after a (870°C, Oil) heat treatment showing upper bainite, marked by arrows.

Fig. 57. As-quenched microstructure of 4140 after a (870°C, Oil) heat treatment showing bainite, marked by arrows.

Fig. 58. As-quenched microstructure of 4140 after a (1200°C, Oil) heat treatment with a typical region of bainite marked by an arrow.

Fig. 59. Higher magnification micrograph of Fig. 58.

Fig. 60. Interference contrast micrograph of same area as Fig. 58 and 59.

Fig. 61. As-quenched microstructure of 4140 after a (1200°C, Oil) heat treatment showing the grain boundary network of bainite which surrounds many grains.

Fig. 62. Interference contrast micrograph of the same area as Fig. 61 showing the presence of very fine subunits, marked by arrows, growing outward along the edge of the bainite.

Fig. 63. As-quenched microstructure of 4340 after a (1200→870°C, Oil) heat treatment showing the grain boundary network of bainite, marked by arrows, similar to that of alloy 4140, Fig. 61.

Fig. 64. As-quenched microstructure of 4340 after a (1200→870°C, Oil) heat treatment showing the feathery structure of bainite, marked by arrows.

Fig. 65. As-quenched microstructure of 4340 after a (1200→870°C, Oil) heat treatment showing bainite originating from grain boundaries, marked by arrows.

Fig. 66. As-quenched microstructure of 4340 after a (1200→870°C) heat treatment showing the feathery type of structure associated with bainite (indicated by the upper arrow), an apparent ferrite film along the prior austenite grain boundary, and a particle located on the grain boundary (marked by the lower arrow).

Fig. 67. As-quenched structure of 4340 after a (1200 870°C, Oil) heat treatment with several dark etching plates marked by arrows.

Fig. 68. Interference contrast micrograph of the same area as Fig. 67 showing that the plates marked by arrows in Fig. 67 actually consist of many parallel closely spaced subunits.

Fig. 69. As-quenched microstructure of 4340 after a (870°C, Oil) heat treatment showing a dark etching structure, marked by arrows, extending across the prior austenite grains, similar to Figs. 46 and 57.

Fig. 70. As-quenched microstructure of 300-M after a (1200°C, Oil) heat treatment showing bainite, marked by arrows, originating from the site of a prior austenite grain boundary.

Fig. 71. Interference contrast micrograph of the same area as Fig. 70, showing that each dark etching region is actually composed of many parallel subunits.

Fig. 72. Profiles of nickel plated fracture surfaces of a fracture toughness specimen of 4130 after a (1200°C, Oil) heat treatment showing (A) evidence of plastic deformation and a jagged type of transgranular fracture path and (B) a smooth intergranular type of fracture path that occurs when upper bainite is present along grain boundaries.

Fig. 73. Photomacrograph showing the amount of bending that a 0.027 in. thick sheet of 4340 will undergo after a (1200°C, IBQLN) and a (870°C, Oil) heat treatment; the (1200°C, IBQLN) heat treated specimen is extremely brittle and broke without bending at all, while the (870°C, Oil) heat treated specimen was bent 90° without cracking.

Fig. 74. Typical fracture surfaces represented by 4130 for three different heat treatments. The top corresponds to a (870°C, Oil) tempered at 200°C heat treatment with K_{IC} 55 ksi-in.$^{1/2}$, the middle specimen corresponds to a (1200°C, IBQLN) tempered at 200°C heat treatment with K_{IC} = 110 ksi-in.$^{1/2}$, and the bottom specimen corresponds to a (1200°C, IBQLN) tempered at 350°C heat treatment with K_{IC} = 60 ksi-in.$^{1/2}$.

Fig. 75. Fractograph of 4130 after a (1200°C, IBQLN) heat treatment tested in the as-quenched condition showing intergranular, quasi-cleavage and ductile rupture.

Fig. 76. A and B, fractographs of 4130 after a (1200°C, Oil) heat treatment tested in the as-quenched condition showing the presence of particles located in the bottom of many dimples.

C through E, fractographs showing MnS particles extending from the fracture surface of a region that has failed intergranularly.

Fig. 77. Fractograph of 4130 after an (870°C, Oil) heat treatment tested in the as-quenched condition showing primarily cleavage (A), with regions of ductile rupture with Mn particles again visible (B).

Fig. 78. Fractograph of 4130 after an (870°C, Oil) heat treatment tested after tempering at 350°C, showing primarily quasi-cleavage with MnS particles visible

Fig. 79. Fractograph of 4130 after a (1200°C, IBQLN) heat treatment tested after tempering at 200°C showing primarily ductile rupture with large amounts of plastic flow associated with dimples initiated by particles as compared to Figs. 76 and 78A.

Fig. 80. Fractograph of 4130 after a (1200°C, IBQLN) heat treatment tested after tempering at 280°C (A and B) and 350°C (C and D) showing the transition from a primarily ductile type of failure, Fig. 79, to a completely intergranular brittle type of failure.

Fig. 81. Fractograph of 4330 after a (1200°C, IBQLN) heat treatment tested in the as-quenched condition, showing a completely ductile type of failure with particles visible.

Fig. 82. Fractograph of 4330 after an (870°C, Oil) heat treatment tested in the as-quenched condition showing a borderline case of quasi-cleavage and ductile rupture in which the quasi-cleavage facets lose their flat appearance as in Fig. 78B and become almost cone shaped.

Fig. 83. Fractograph of 4330 after a (1200°C, IBQLN) heat treatment (A and B), and (C) an (870°C, Oil) heat treatment, all tested after tempering at 350°C, showing a ductile type of failure in each case.

Fig. 84. Fractograph of 4340 after a (1200°C, Oil) heat treatment tested in the as-quenched condition showing the intergranular nature of a quench crack.

Fig. 85. Fractograph of 4340 after a (1200→870°C, Oil) heat treatment tested in the as-quenched condition showing intergranular facets, quasi-cleavage, and regions of ductile rupture with many MnS particles visible.

Fig. 86. Fractograph of 4340 after an (870°C, Oil) heat treatment tested in the as-quenched condition, showing primarily cleavage with isolated regions of ductile rupture with some particles visible.

Fig. 87. Fractograph of 4340 after (1200→870°C, Oil) heat treatment tested after tempering at 200°C to achieve maximum toughness, showing all the features as the as-quenched specimen, Fig. 85, except that there are more regions of ductile rupture and within these regions there is extensive plastic flow around each particle E and F.

Fig. 88. Fractograph of 4340 after a (1200→870°C, Oil) heat treatment tested after tempering at 280°C, showing the intergranular type of failure associated with tempered martensite embrittlement, and the presence of MnS particles along grain boundaries.

Fig. 89. Fractograph of 4140, (A) after an (870°C, Oil) heat treatment tested in the as-quenched condition, (B) after a (1200°C, Oil) heat treatment tested in the as-quenched condition, (C and D) after a (1200°C, Oil) heat treatment tested after tempering at 200°C, showing cleavage and quasi-cleavage for all conditions.

Fig. 90. Fractograph of 4140, (A) after an (870°C, Oil) heat treatment tested after tempering at 280°C, (B) same as (A) except tempered at 390°C, (C) higher magnification of the particle visible in (B), and (D) after a (1200°C, Oil) heat treatment tested after tempering at 350°C. The (870°C, Oil) heat treatment becomes progressively more ducitle as the tempering temperature is increased, while the (1200°C, Oil) heat treatment fails intergranularly when tempered at 280°C.

Fig. 91. Fractograph of 300-M, (A) after an (870°C, Oil) heat treatment tested in the as-quenched condition, (B) after a (1200°C, Oil) heated treatment tested in the as-quenched condition, (C and D) after a (1200°C, Oil) heat treatment tested after tempering at 325°C.

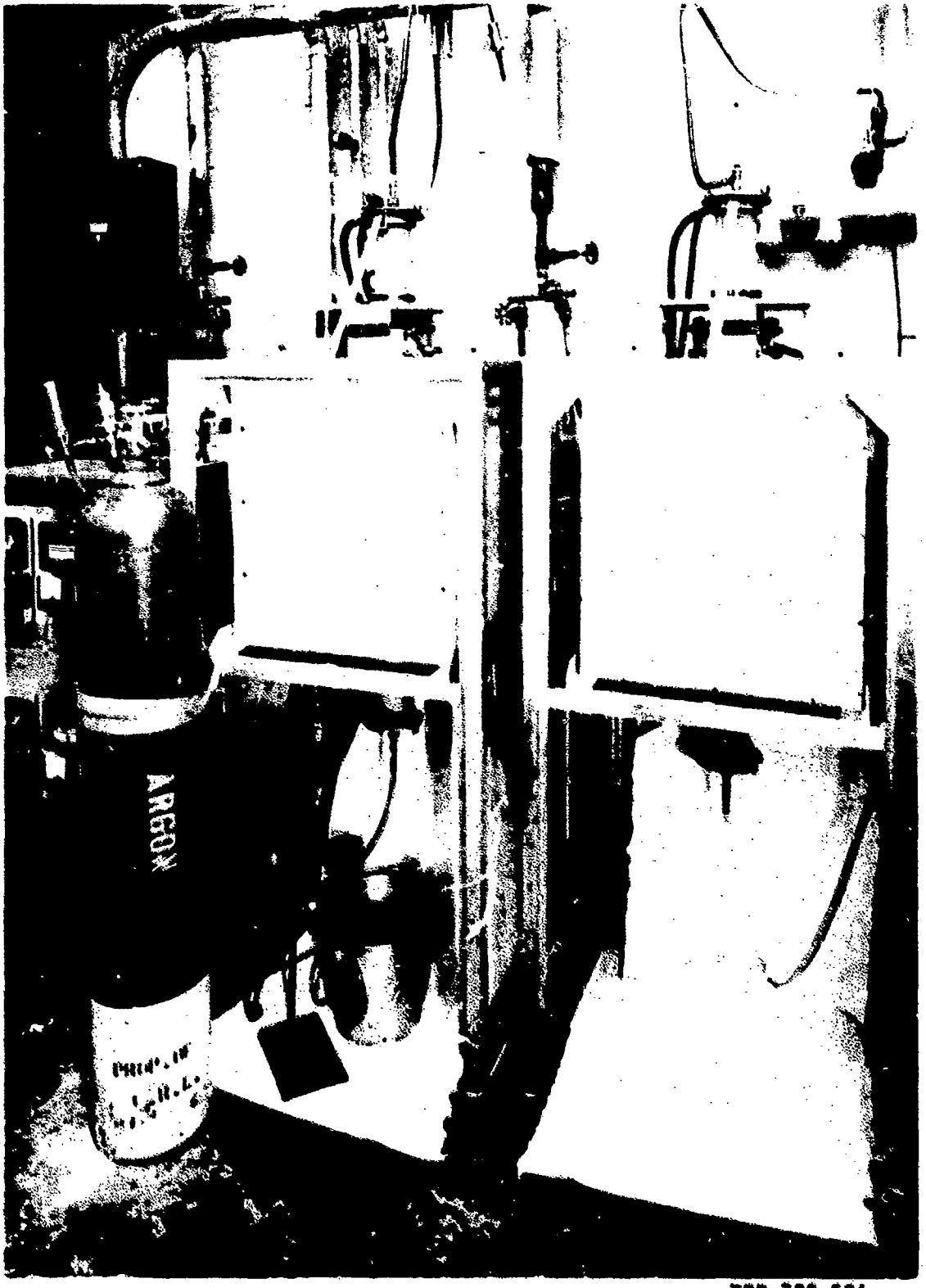

XBB 732-504

Fig. 1

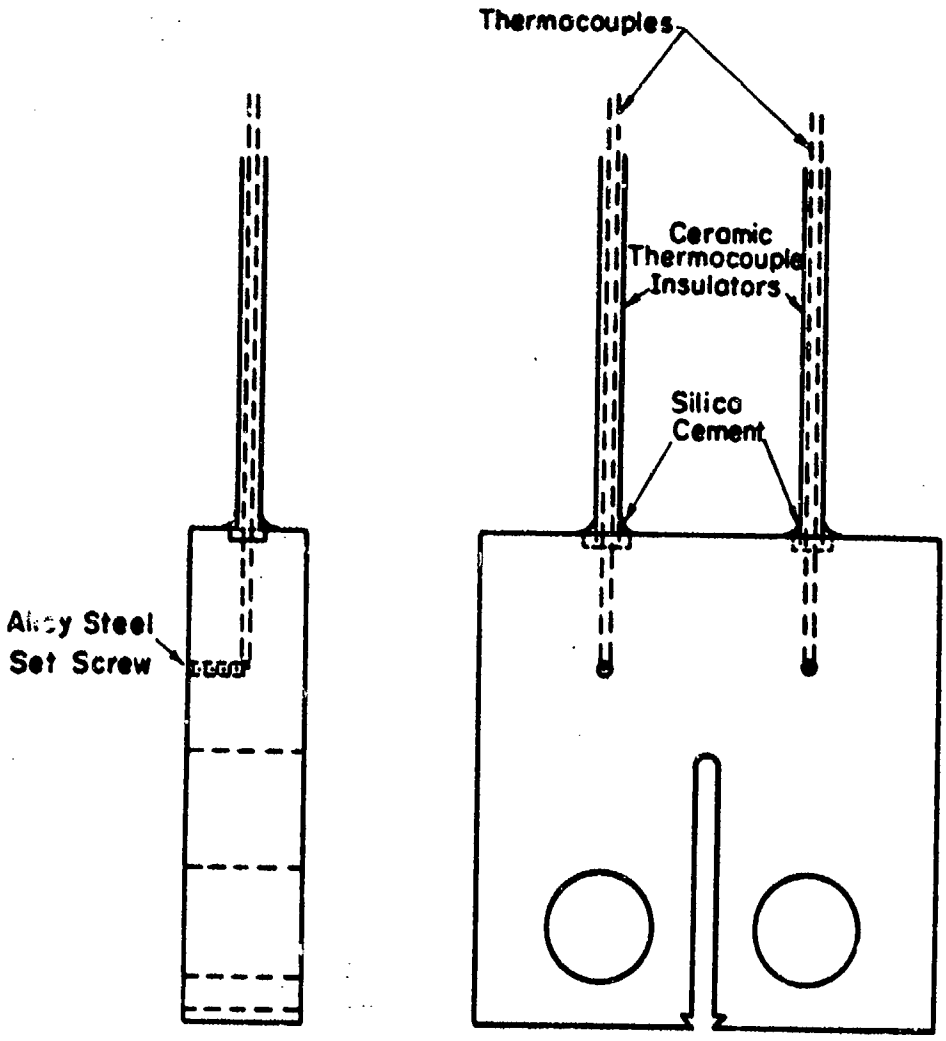

XBL 734-5992

Fig. 2

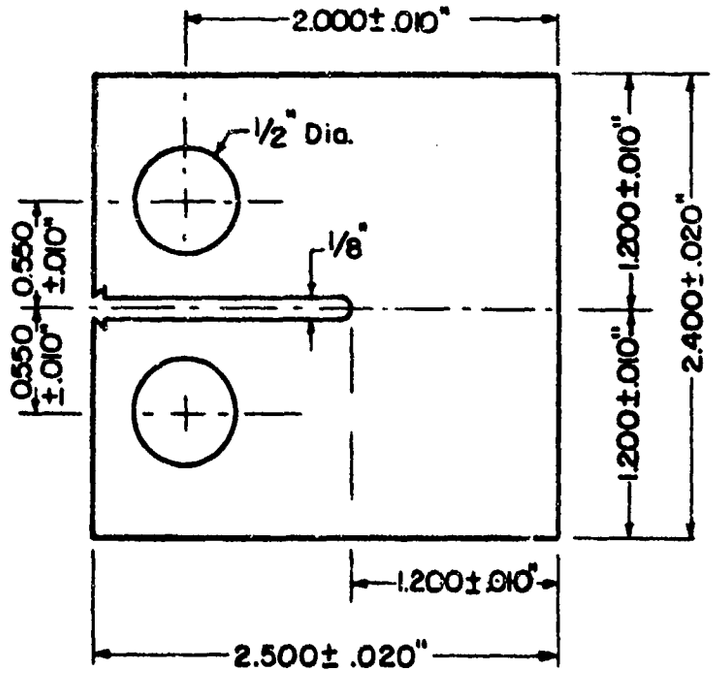

XBL 734-5986

Fig. 3

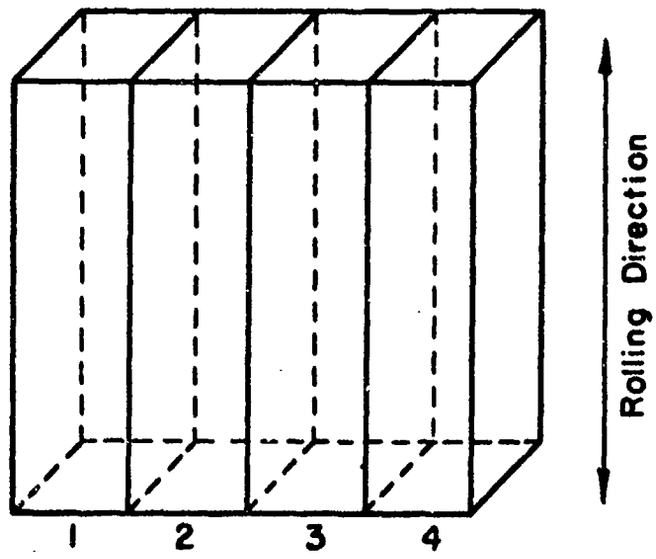

XBL 734-5989

Fig. 4

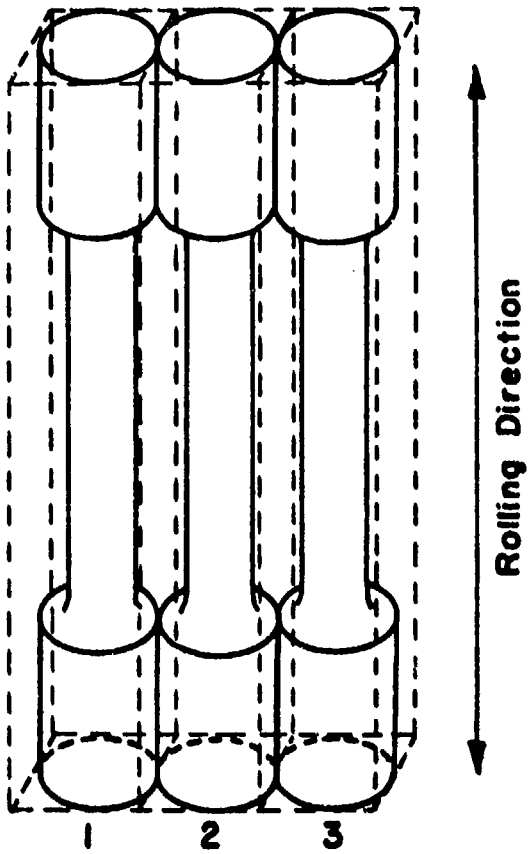

XBL 734-5987

Fig. 5

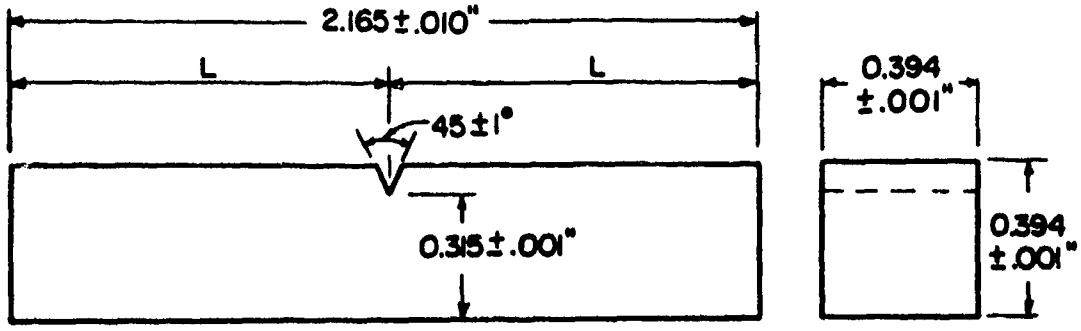

Fig. 6

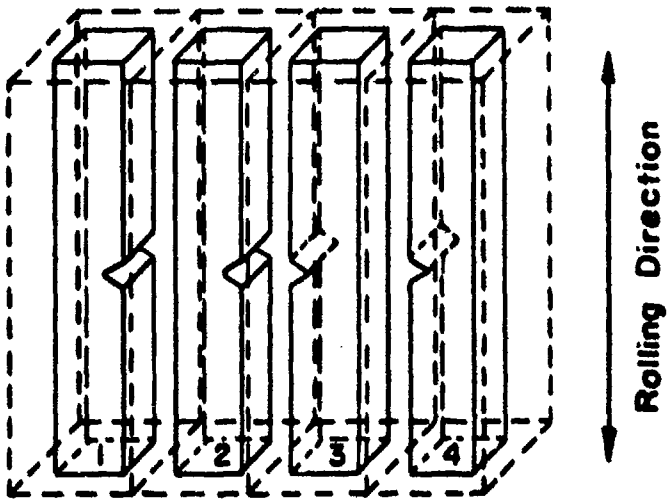

XBL 734-5988

Fig. 7

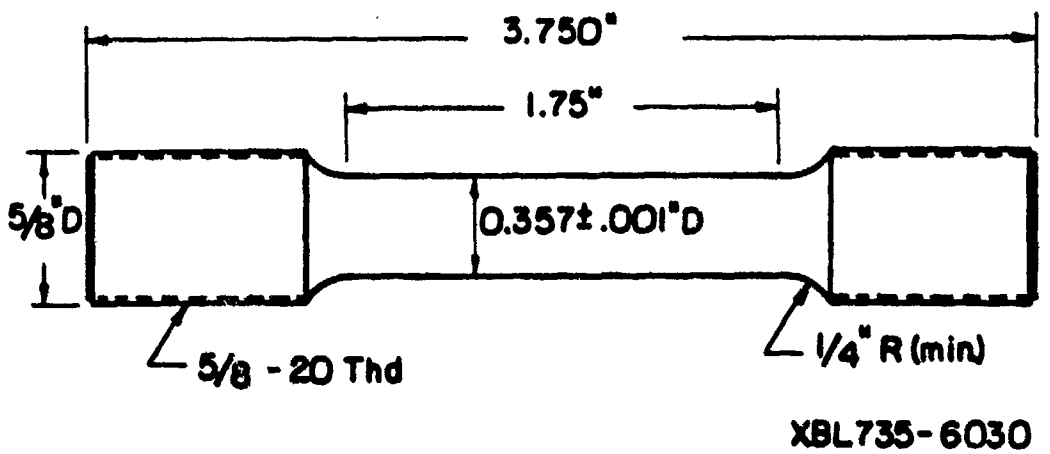

Fig. 8

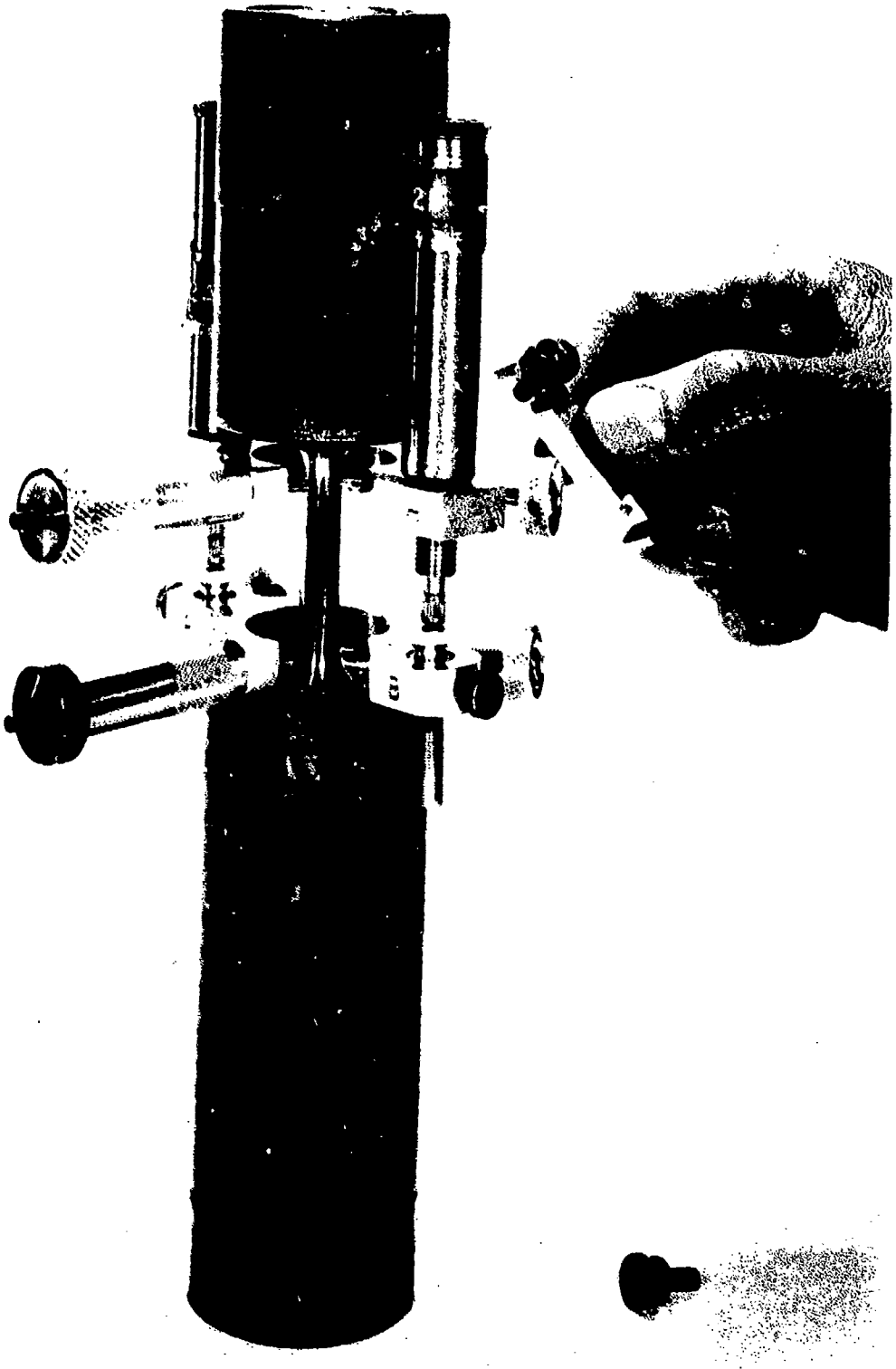

XBB 732-505

Fig. 9

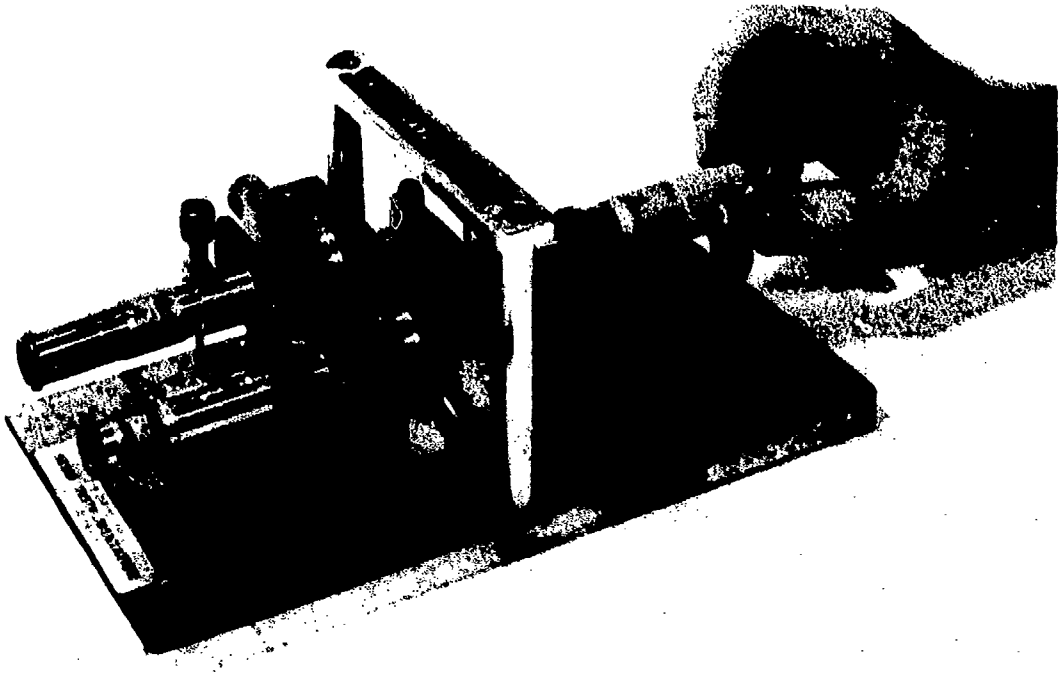

XBB 732-508

Figure 10

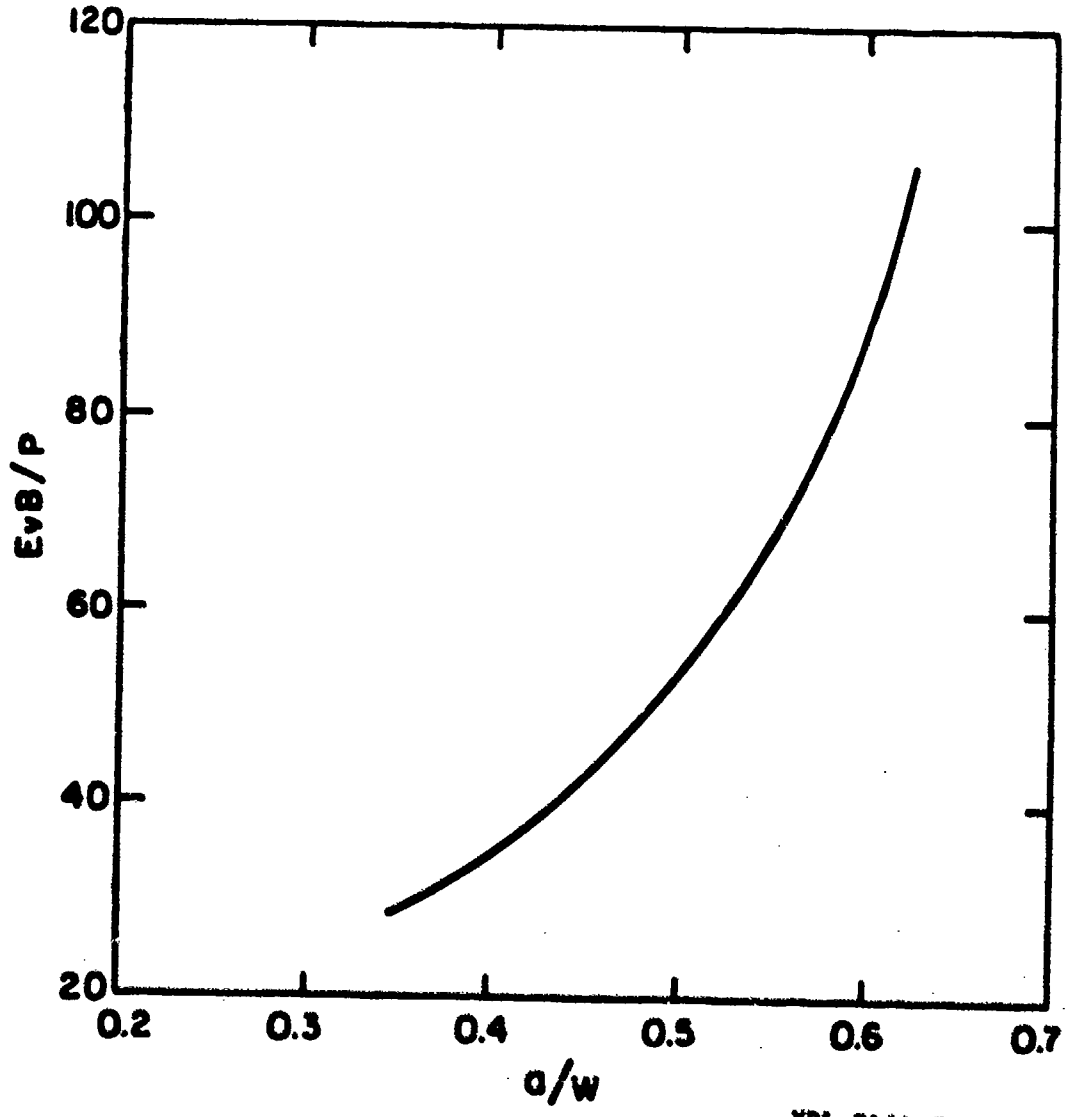

XBL 7111-7614

Fig. 11

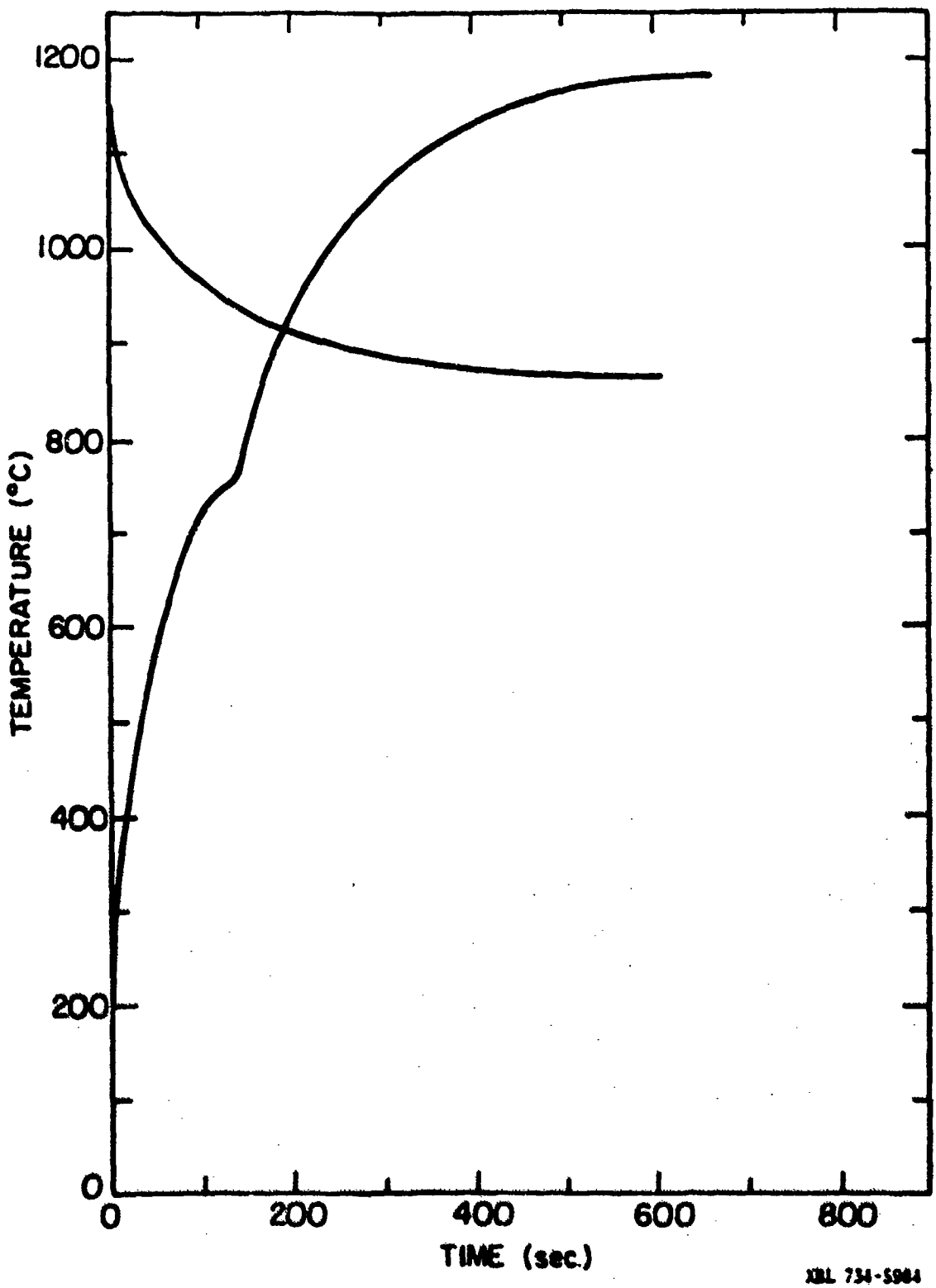
1200
1000
800
600
400
200
0
TEMPERATURE (°C)
0
200
400
600
800
TIME (sec.)
XBL 734-5984

Fig. 12

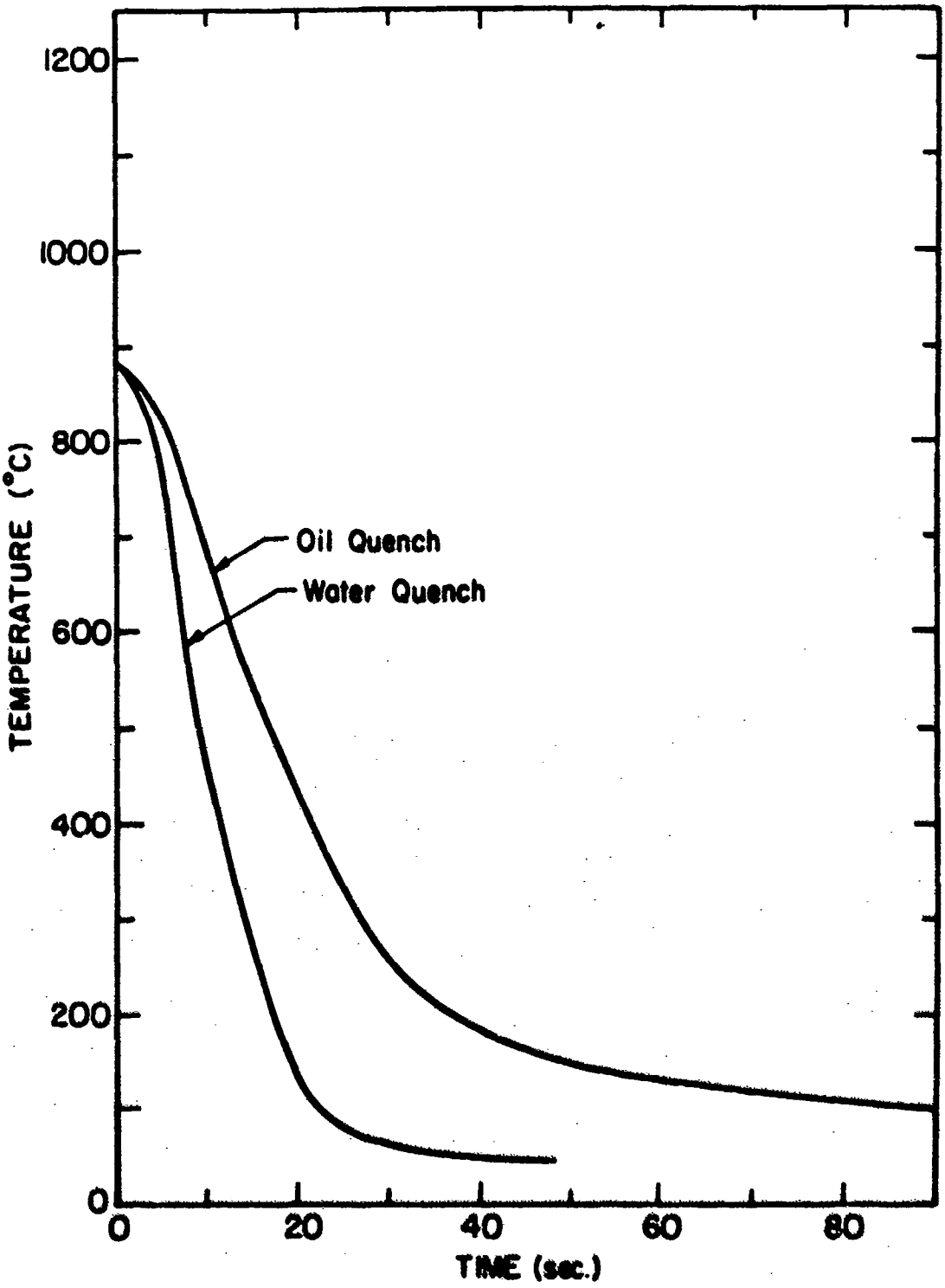
1200
1000
800
600
400
200
0
TEMPERATURE (°C)
Oil Quench
Water Quench
0
20
40
60
80
TIME (sec.)

Fig. 13

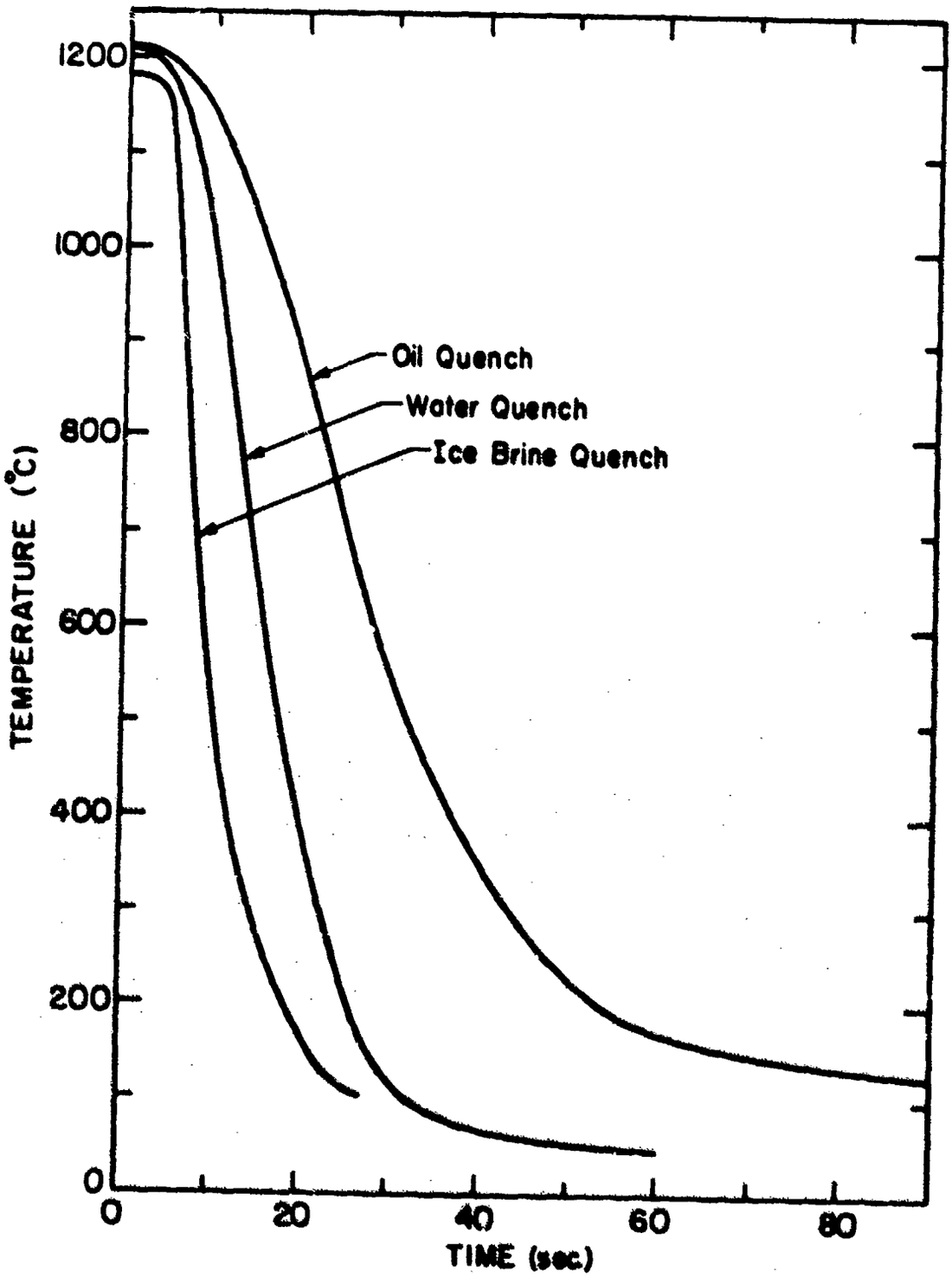
1200
1000
800
600
400
200
0
TEMPERATURE (°C)
0
20
40
60
80
TIME (sec.)
Oil Quench
Water Quench
Ice Brine Quench

Fig. 14

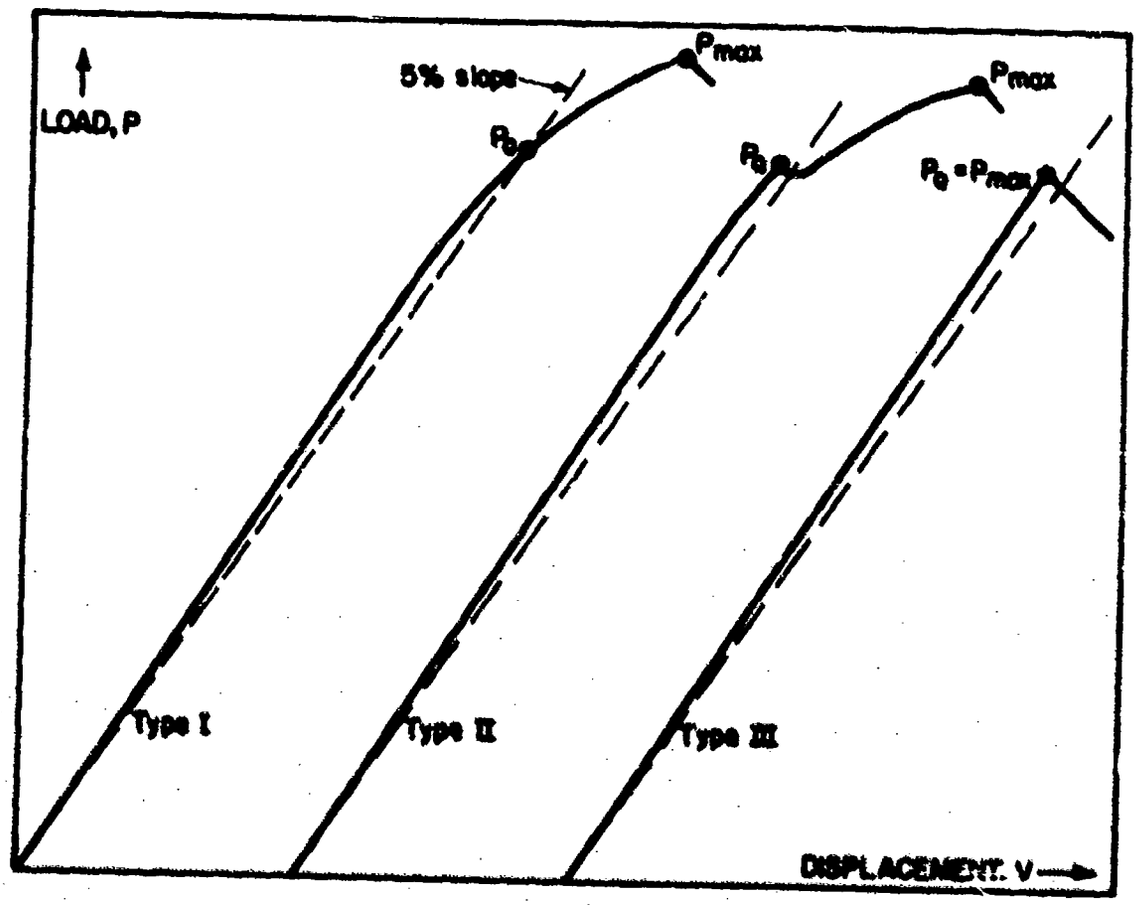

XBL 734-5085

Fig. 15

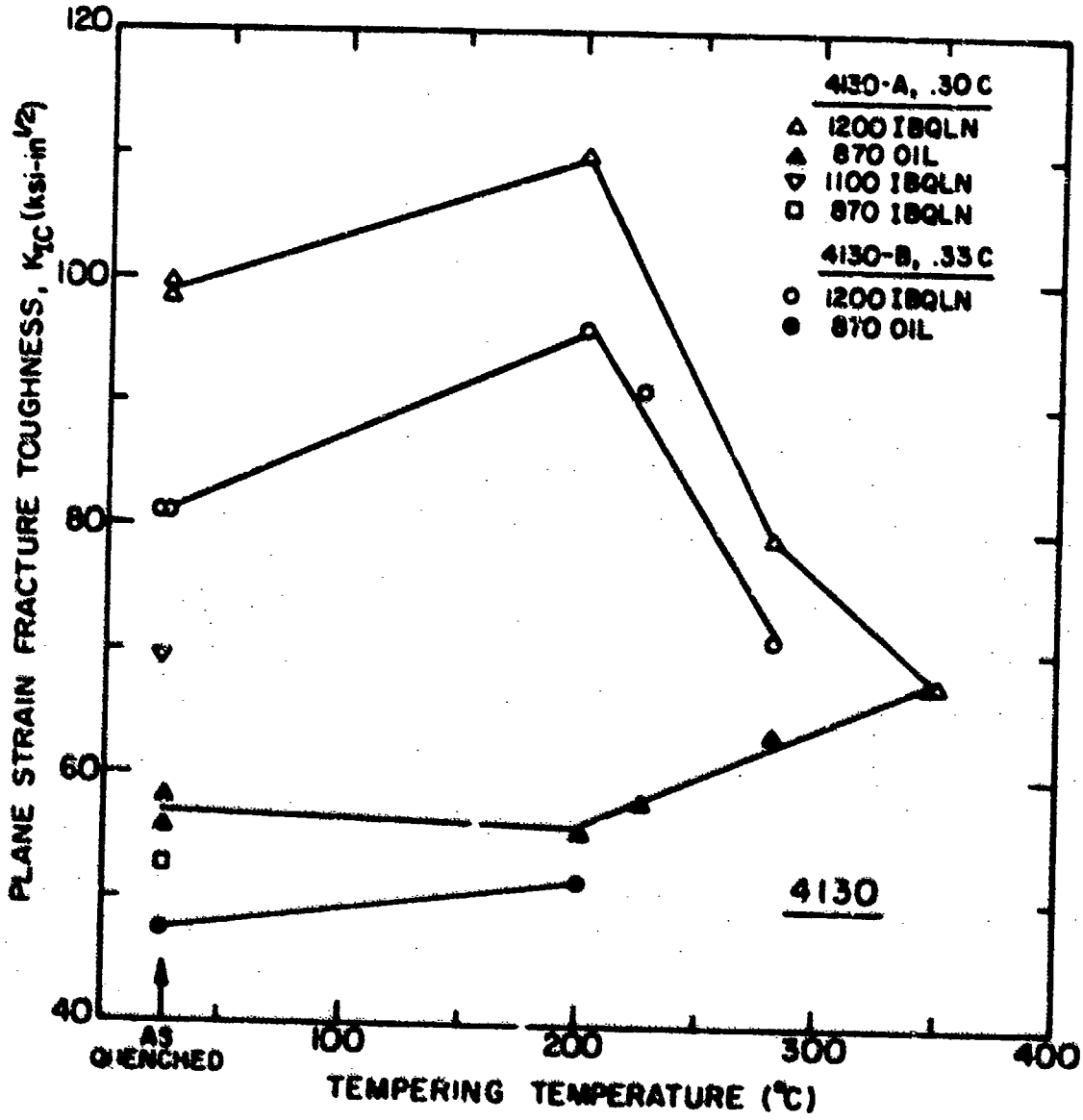

XBL 734-5971

Fig. 16

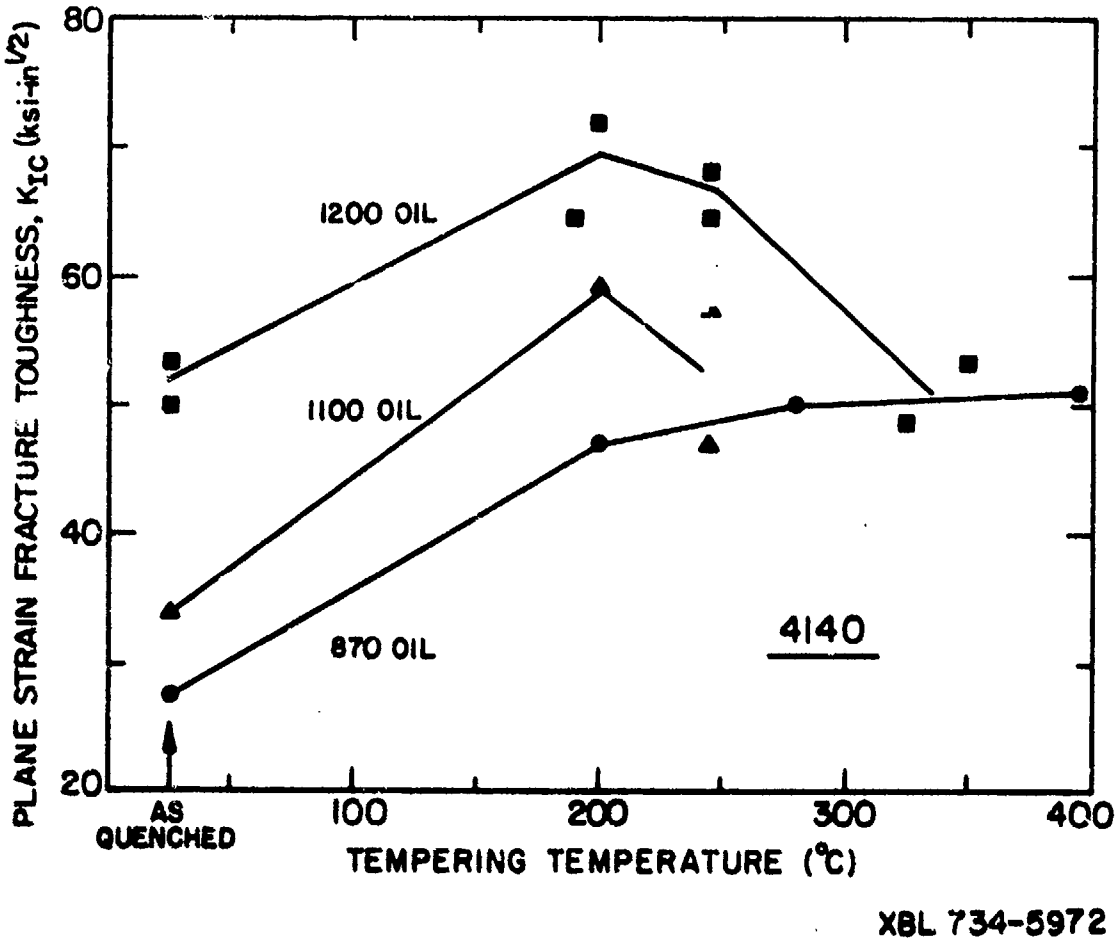

XBL 734-5972

Fig. 17

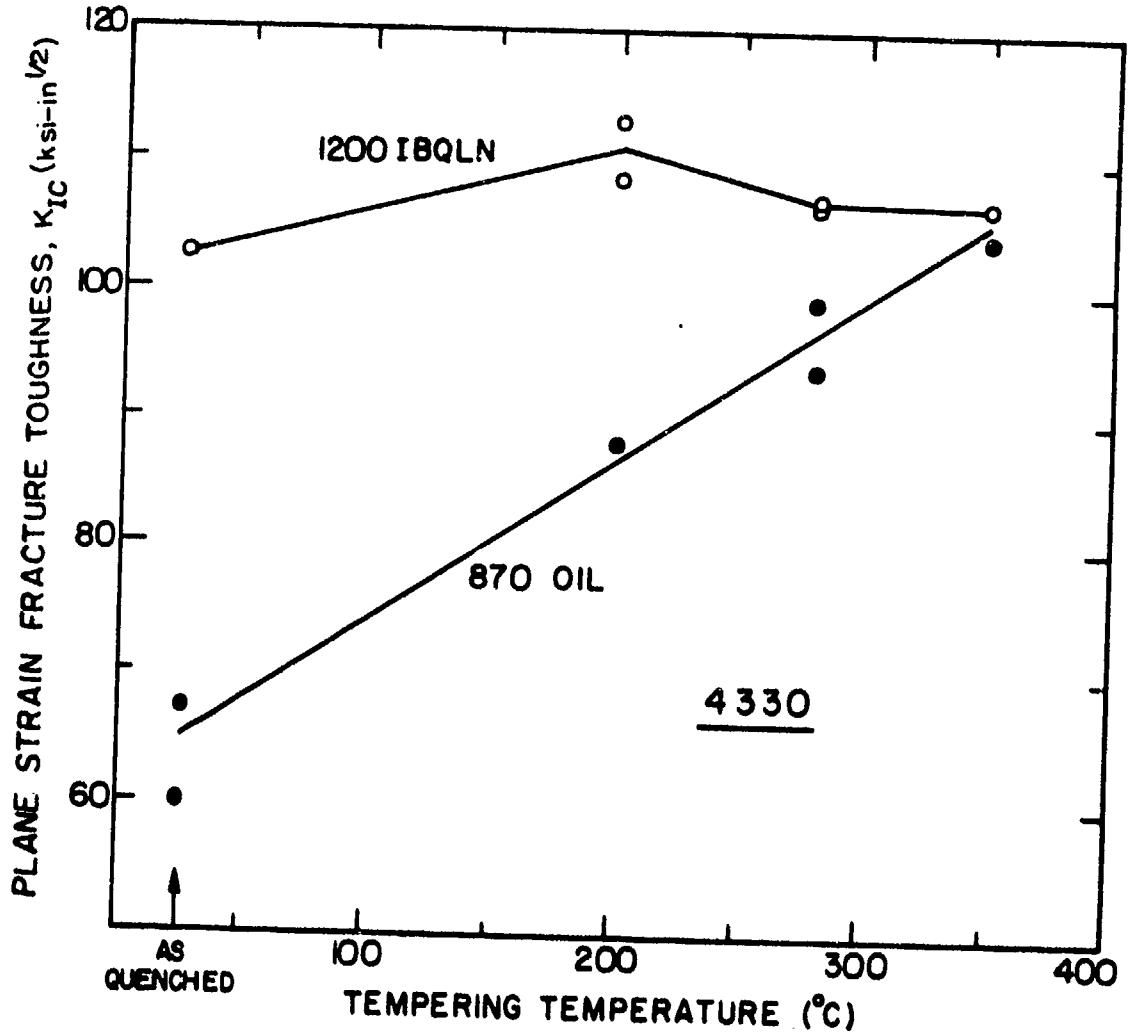

XBL 734-5973

Fig. 18

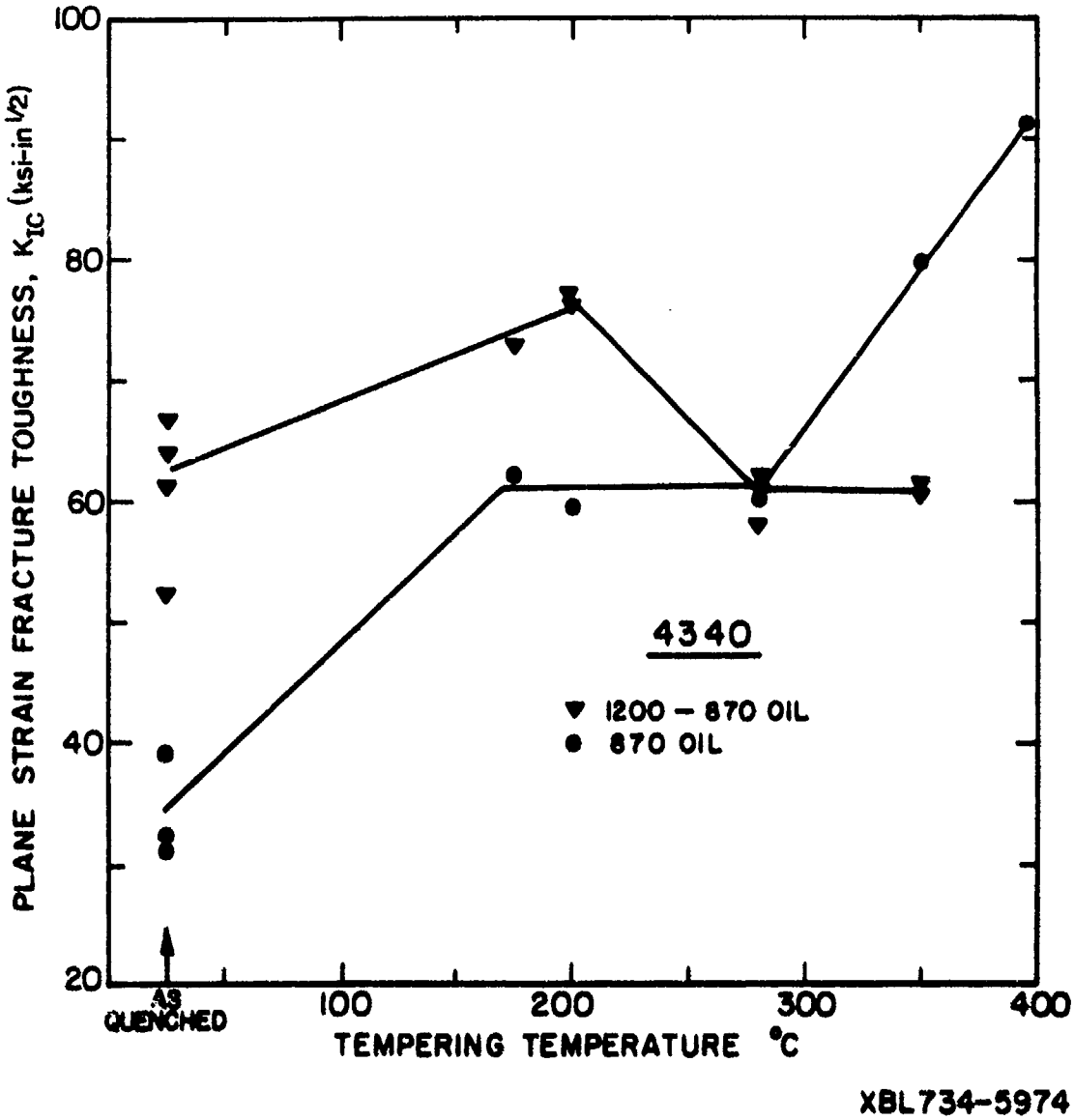
100
80
60
40
20
PLANE STRAIN FRACTURE TOUGHNESS, K_{IC} (ksi-in$^{1/2}$)
AS QUENCHED
100
200
300
400
TEMPERING TEMPERATURE °C
4340
1200 – 870 OIL
870 OIL
XBL734-5974

Fig. 19

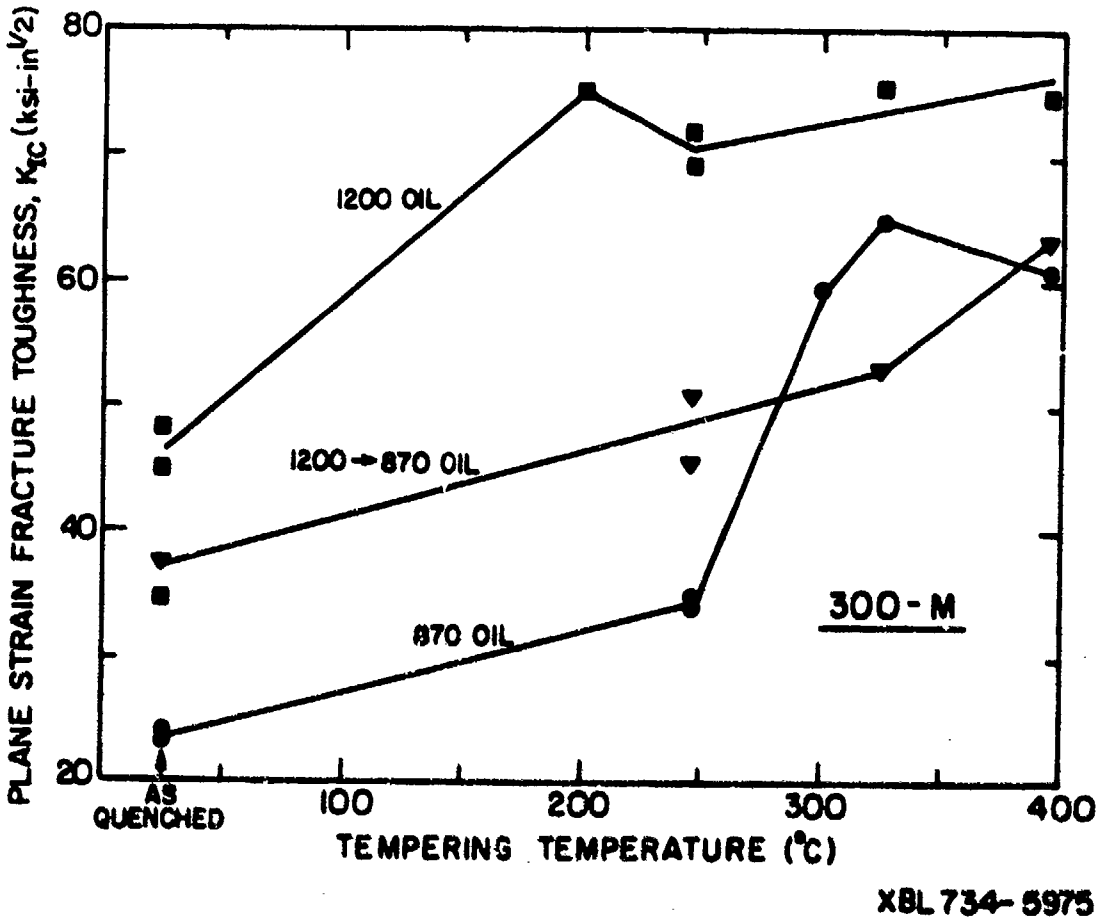
PLANE STRAIN FRACTURE TOUGHNESS, K_{IC} (ksi-in$^{1/2}$)
80
60
40
20
1200 OIL
1200→870 OIL
870 OIL
300-M
AS QUENCHED
100
200
300
400
TEMPERING TEMPERATURE (°C)
XBL 734-5975

Fig. 20

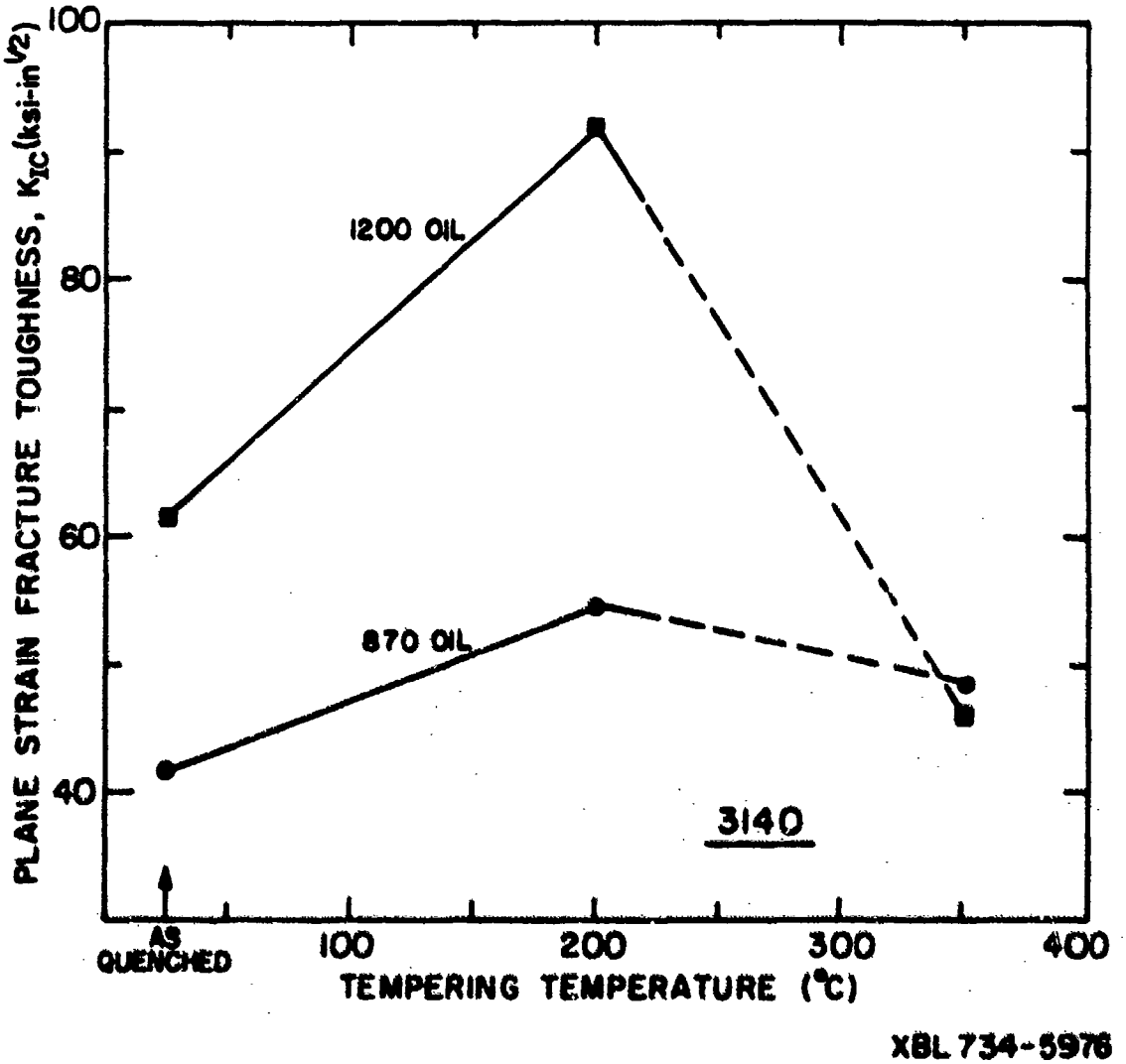

XBL 734-5976

Fig. 21

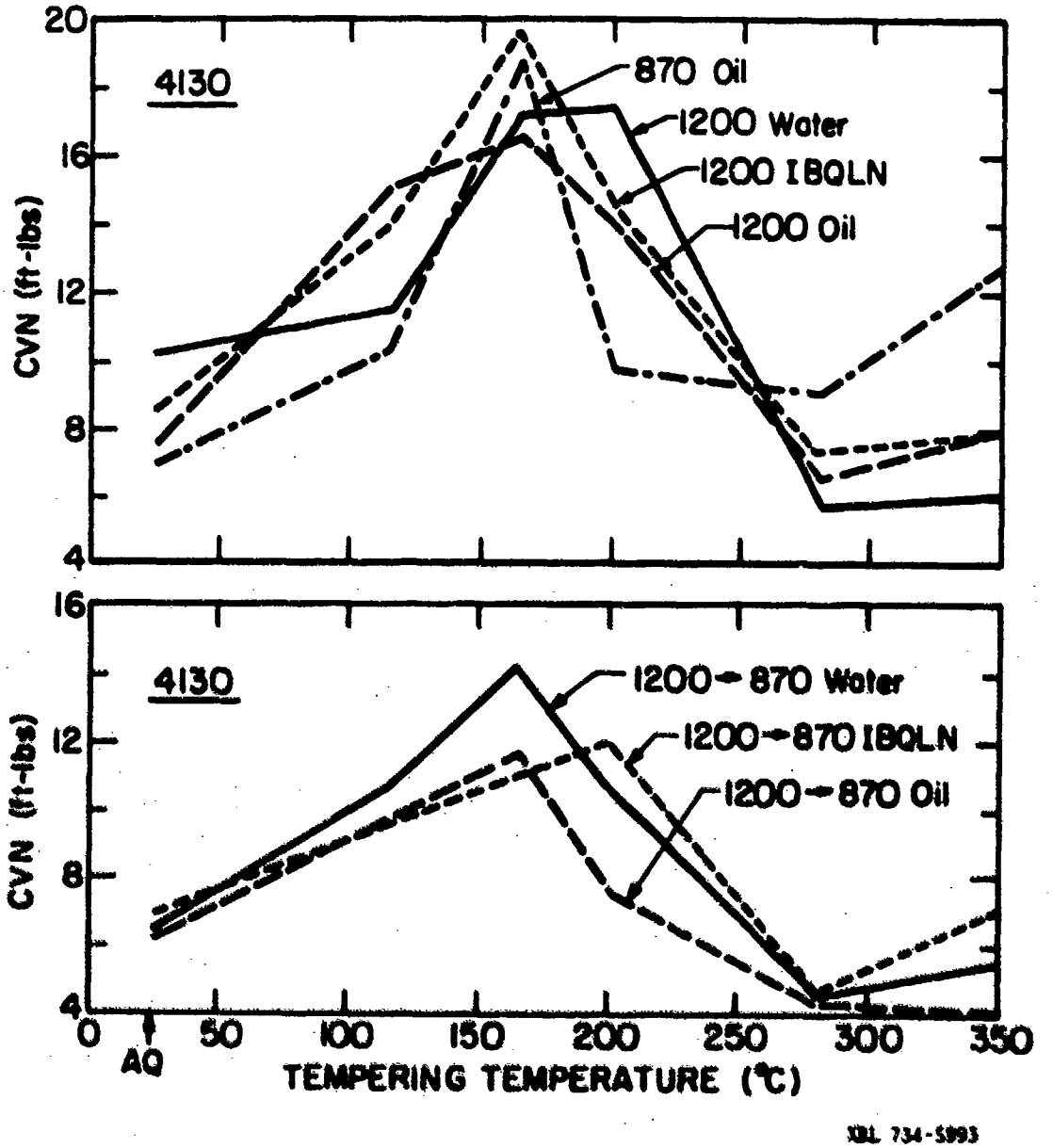

XBL 734-5993

Fig. 22

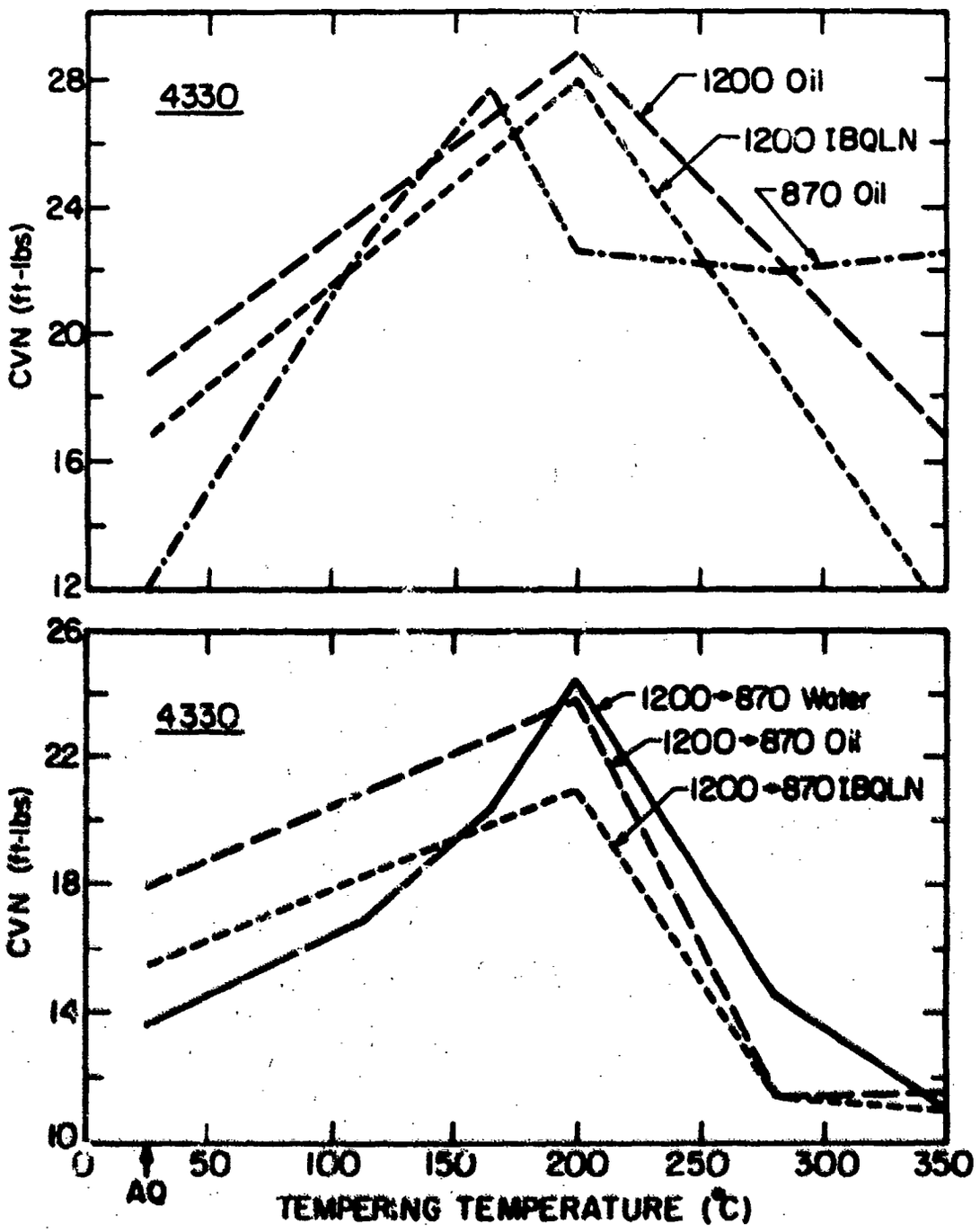

XBL 734-5990

Fig. 23

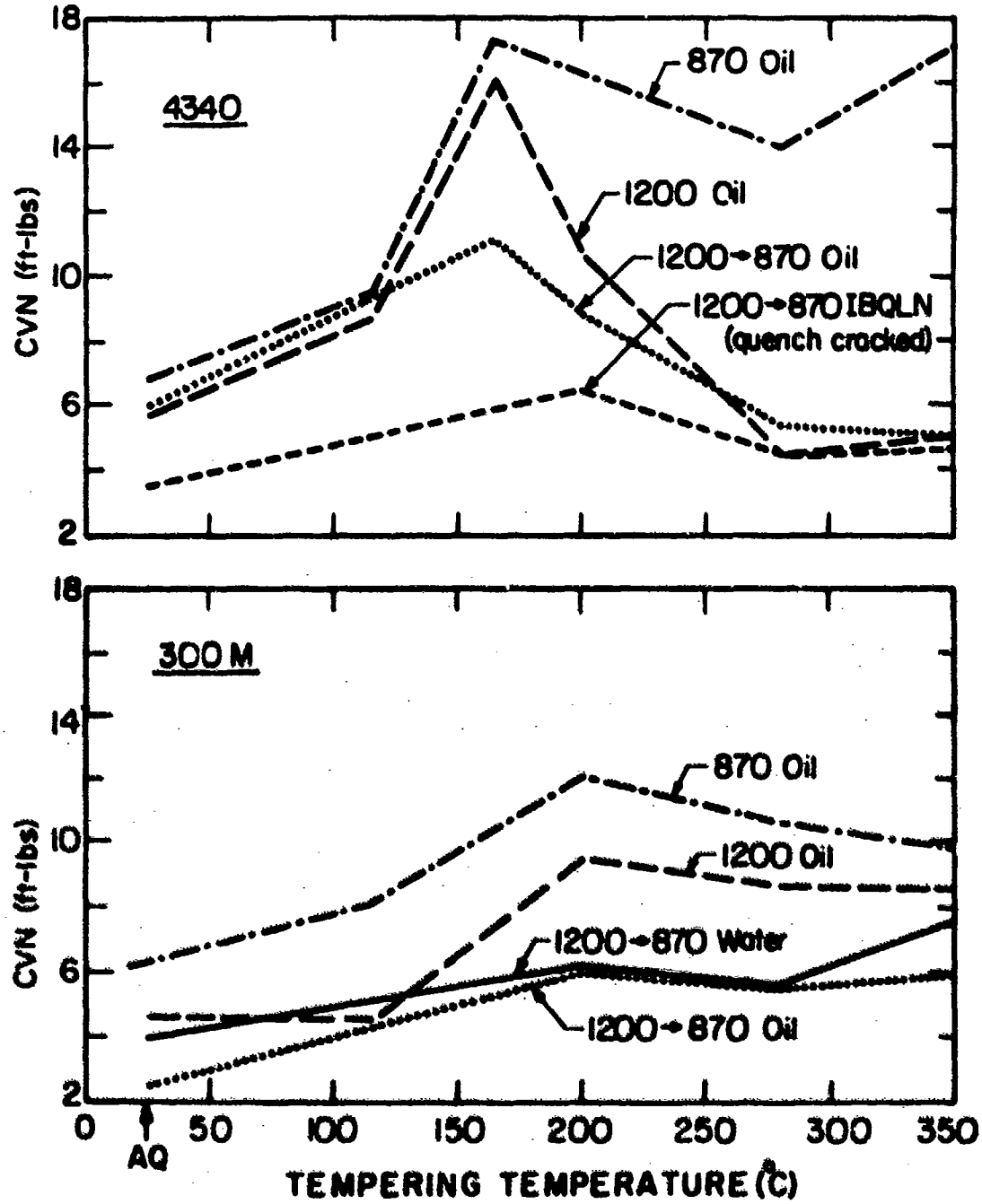

XBL 735-6029

Fig. 24

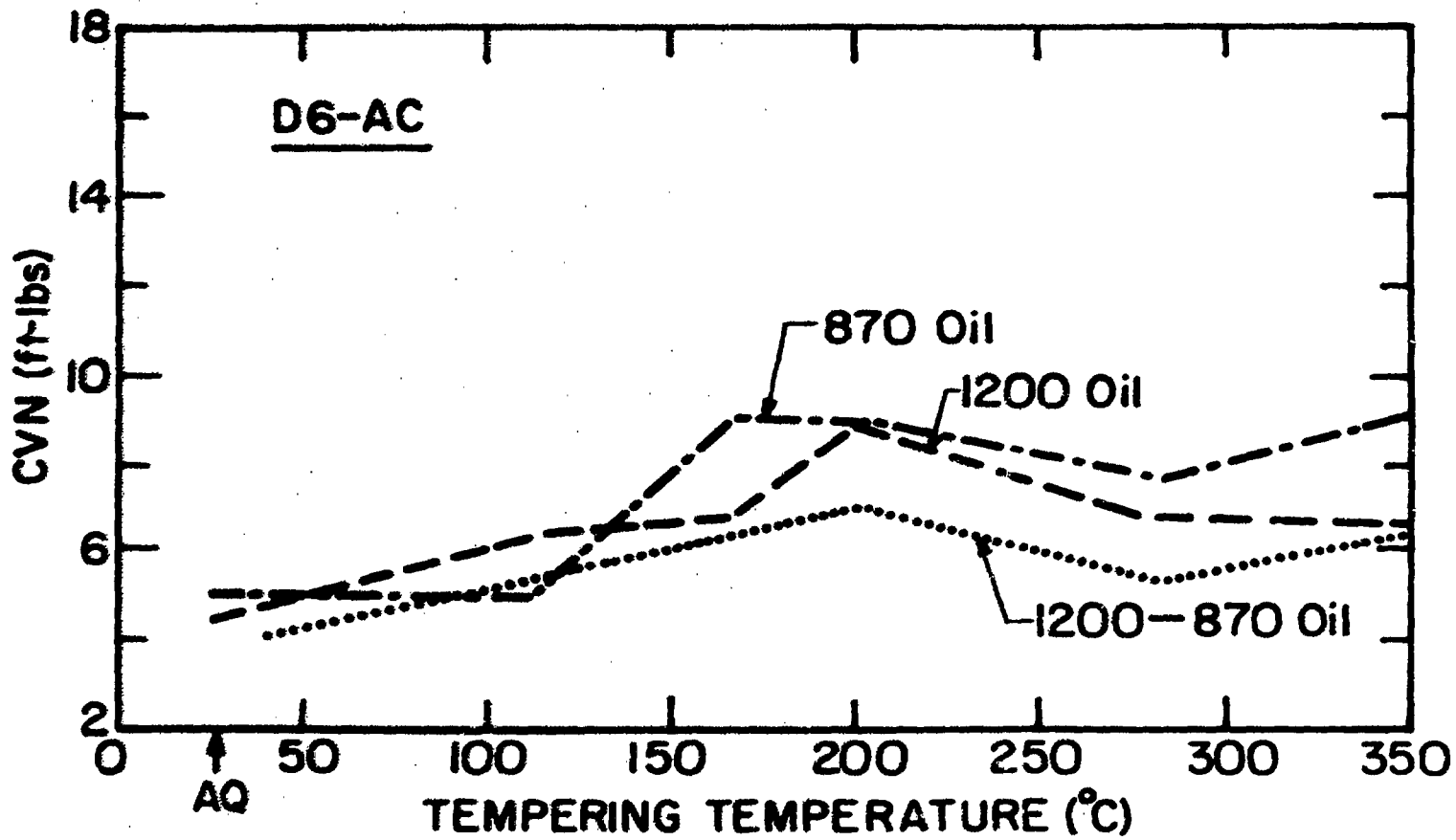

XBL 734-5991

Fig. 25

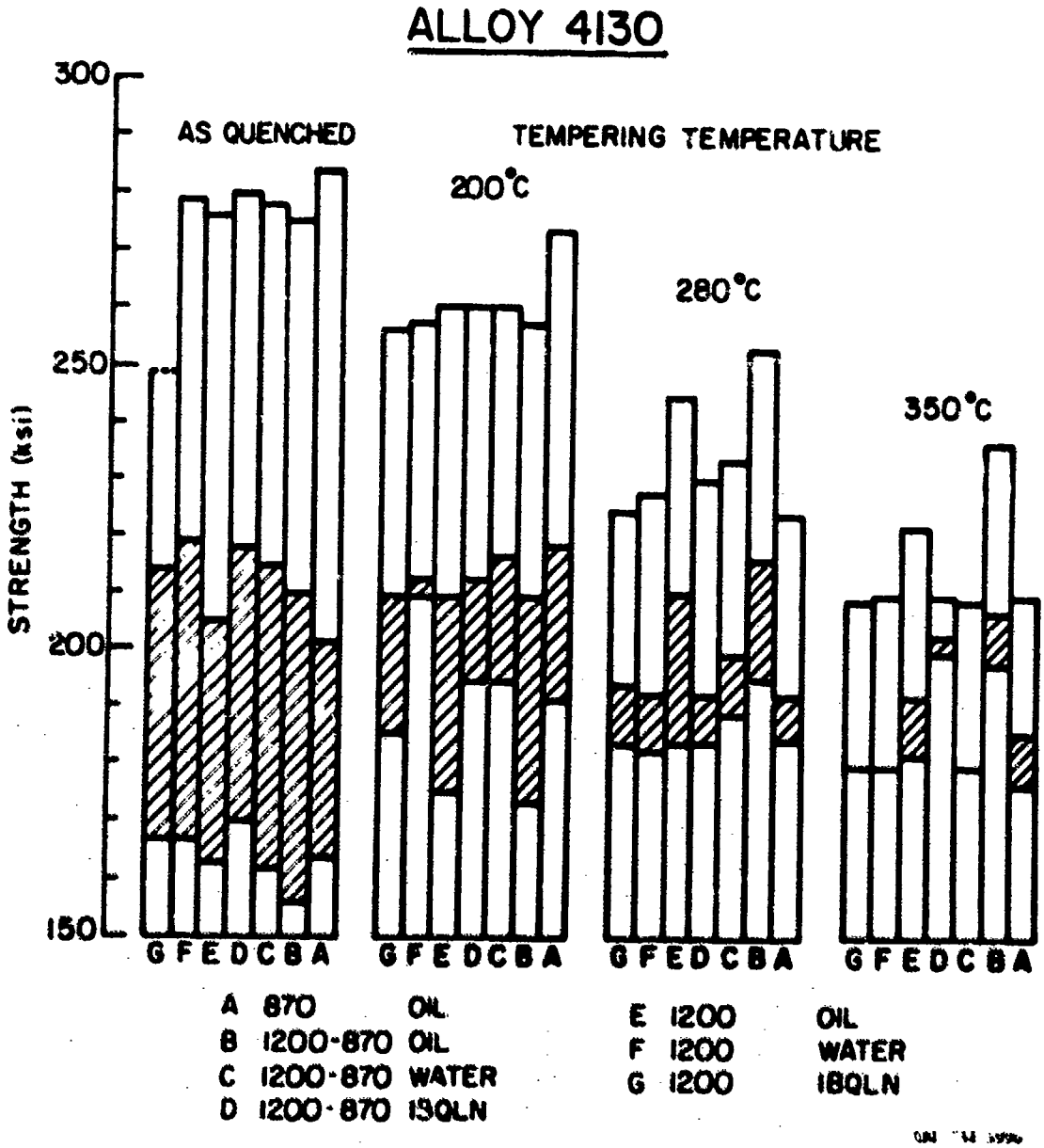
ALLOY 4130
300
250
200
150
STRENGTH (ksi)
AS QUENCHED
TEMPERING TEMPERATURE
200°C
280°C
350°C
G F E D C B A
A 870 OIL
B 1200-870 OIL
C 1200-870 WATER
D 1200-870 ISQLN
E 1200 OIL
F 1200 WATER
G 1200 IBQLN

Fig. 26

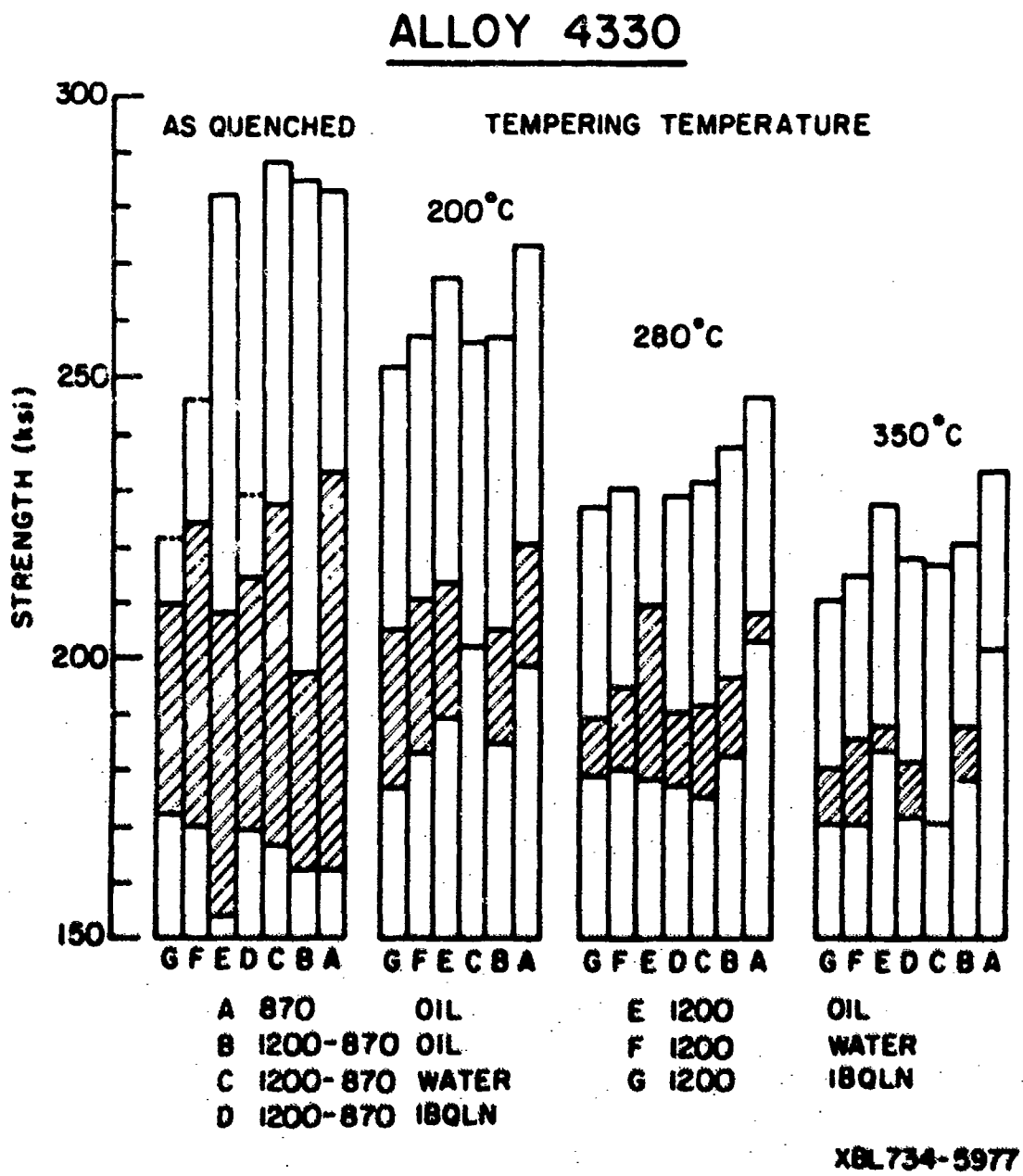
ALLOY 4330
AS QUENCHED
TEMPERING TEMPERATURE
200°C
280°C
350°C
STRENGTH (ksi)
300
250
200
150
G F E D C B A
G F E C B A
G F E D C B A
G F E D C B A
A 870 OIL
B 1200-870 OIL
C 1200-870 WATER
D 1200-870 IBQLN
E 1200 OIL
F 1200 WATER
G 1200 IBQLN
XBL734-5977

Fig. 27

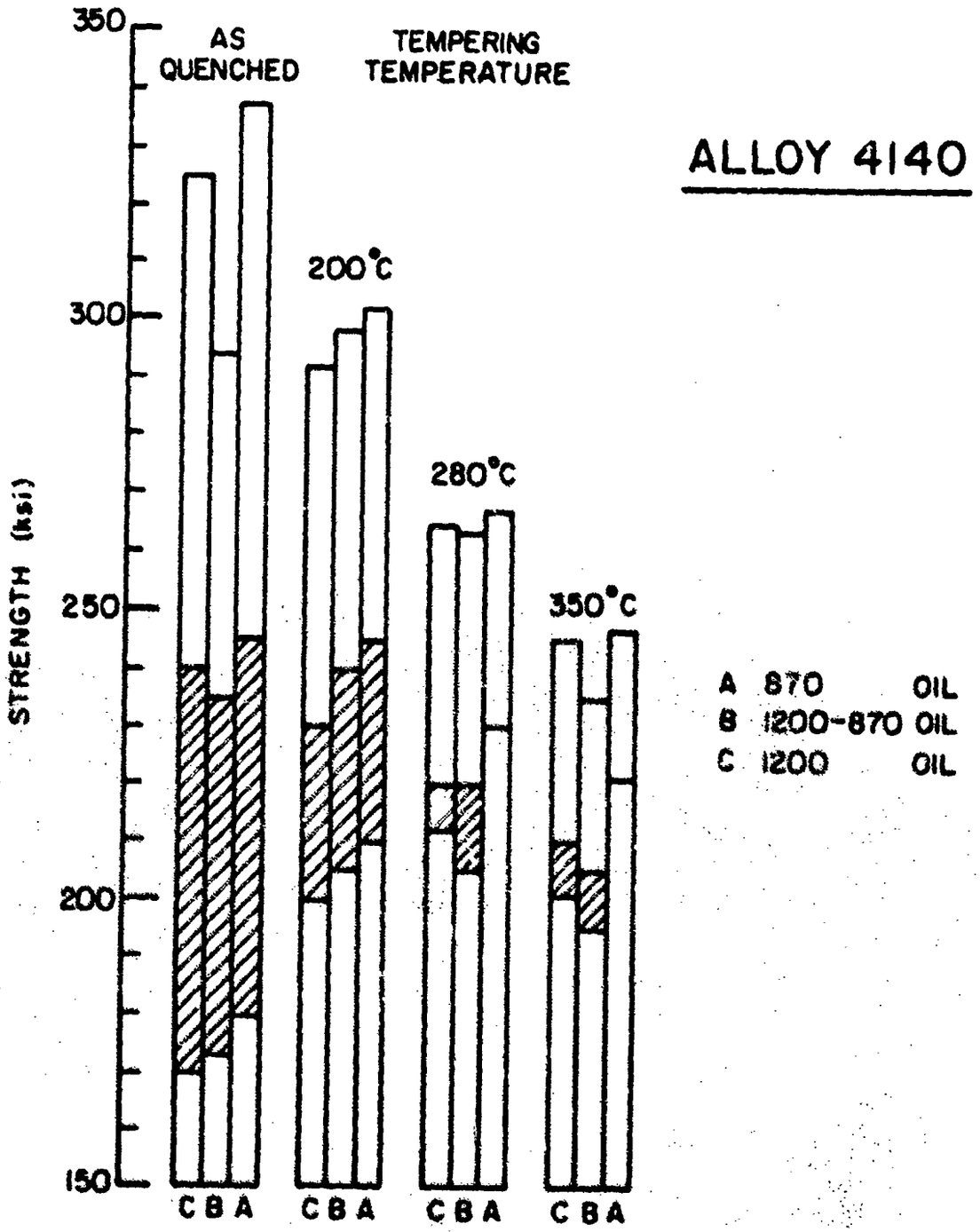

XBL 734-5978

Fig. 28

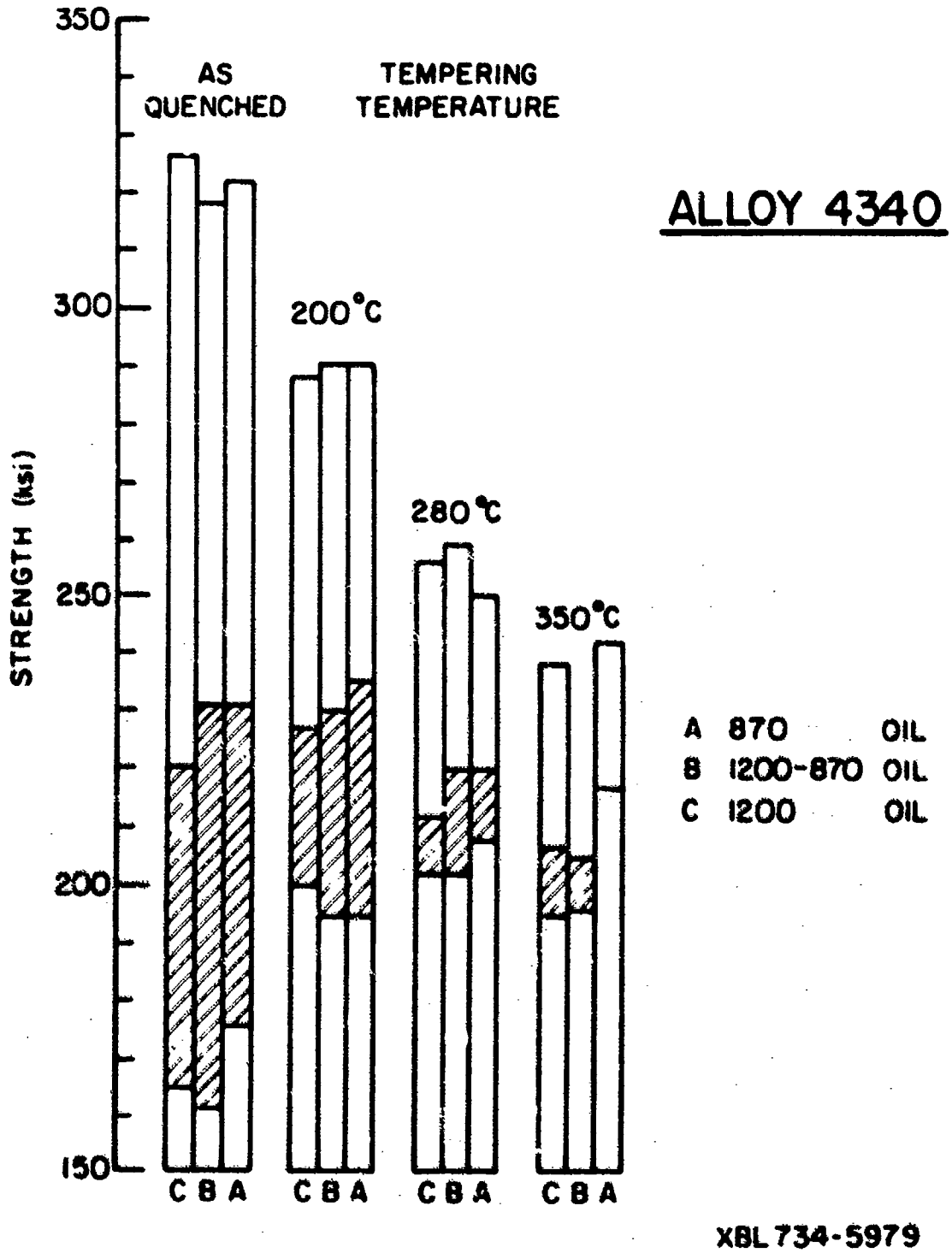
350
300
250
200
150
STRENGTH (ksi)
AS QUENCHED
TEMPERING TEMPERATURE
ALLOY 4340
200°C
280°C
350°C
C B A
C B A
C B A
C B A
A 870 OIL
B 1200-870 OIL
C 1200 OIL
XBL 734-5979

Fig. 29

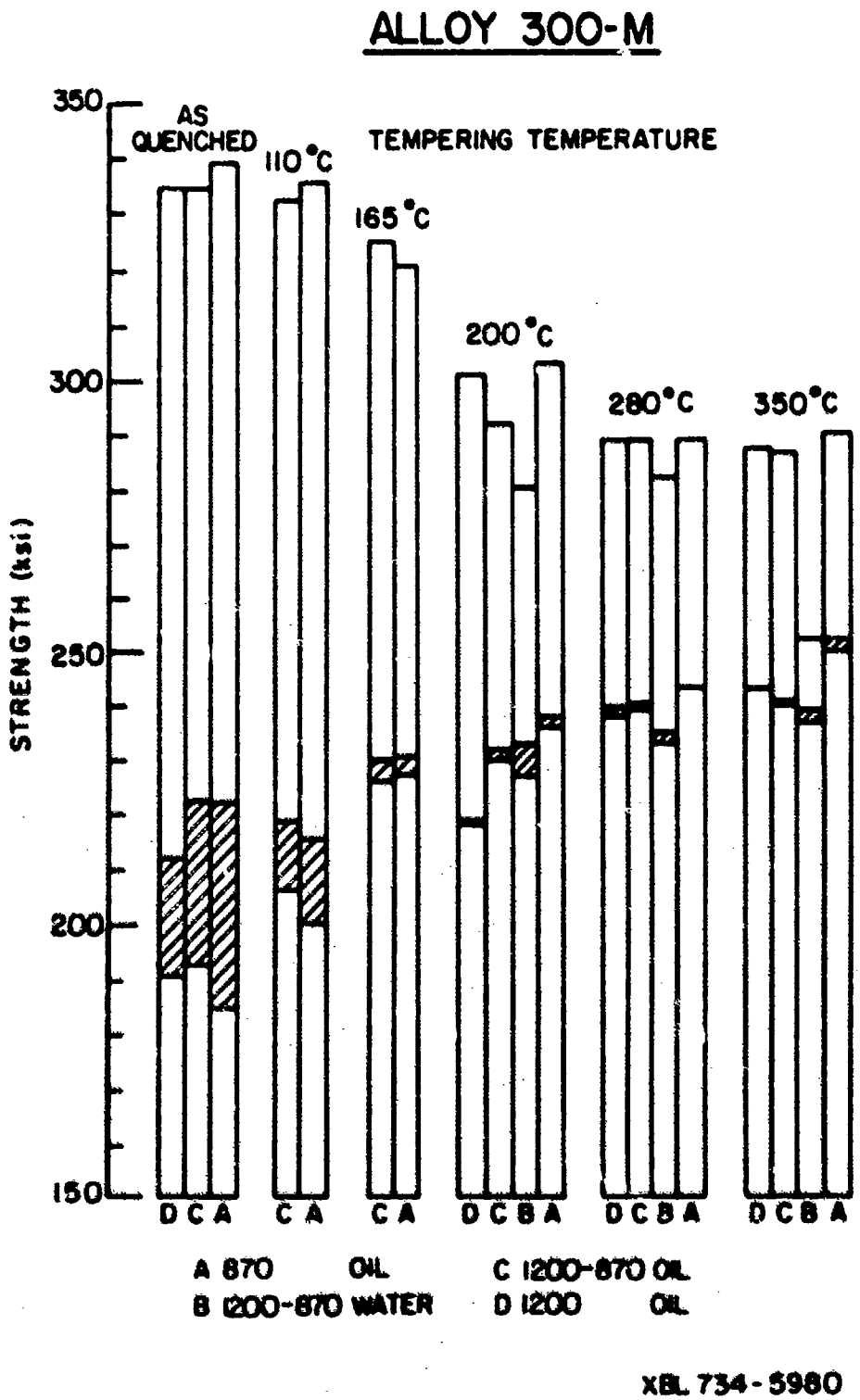
ALLOY 300-M
TEMPERING TEMPERATURE
AS QUENCHED
110°C
165°C
200°C
280°C
350°C
STRENGTH (ksi)
350
300
250
200
150
D C A
C A
C A
D C B A
D C B A
D C B A
A 870 OIL
B 1200-870 WATER
C 1200-870 OIL
D 1200 OIL
XBL 734-5980

Fig. 30

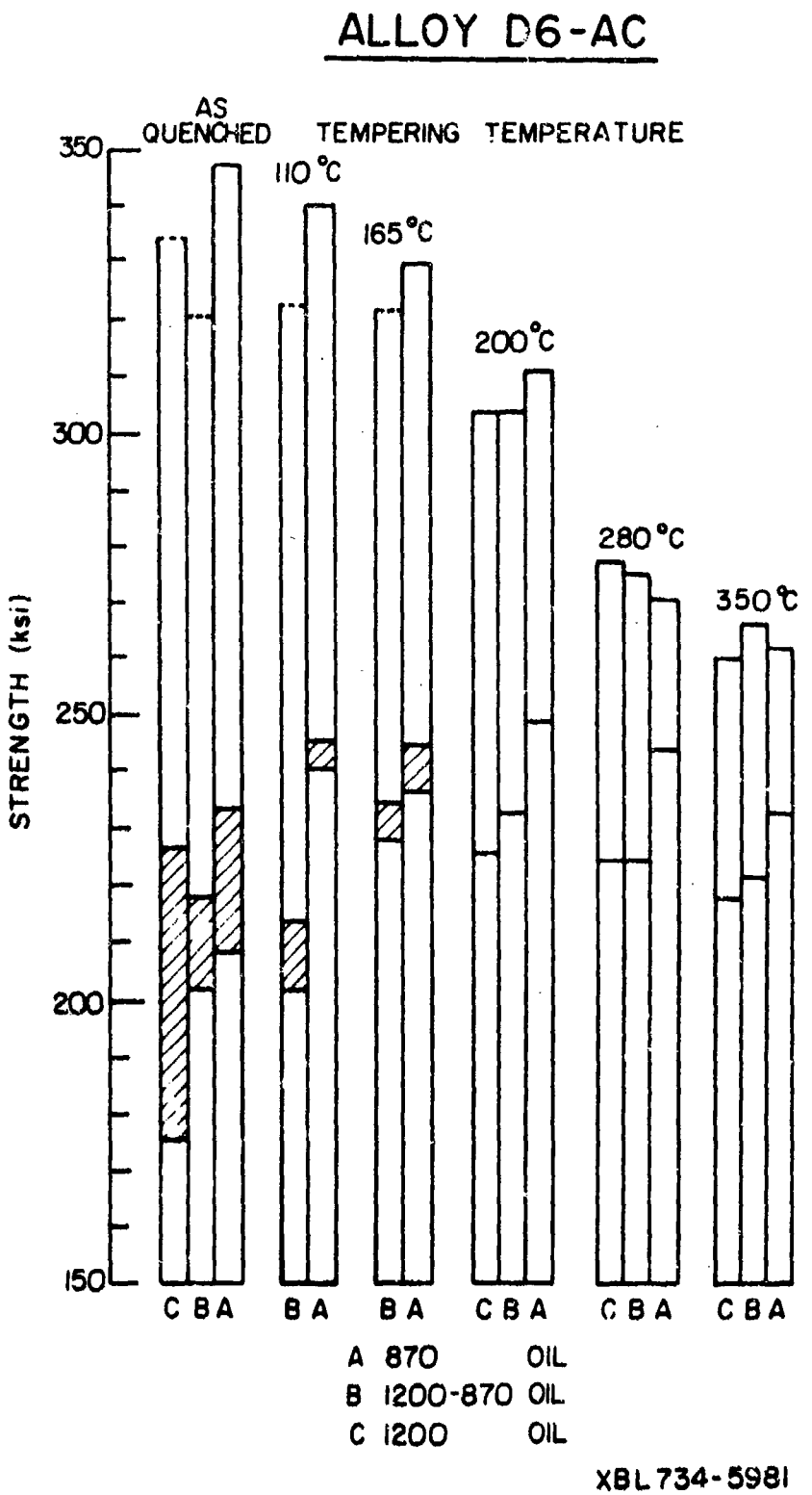
ALLOY D6-AC
AS QUENCHED
TEMPERING TEMPERATURE
110 °C
165 °C
200 °C
280 °C
350 °C
STRENGTH (ksi)
350
300
250
200
150
C B A
B A
B A
C B A
C B A
C B A
A 870 OIL
B 1200-870 OIL
C 1200 OIL
XBL 734-5981

Fig. 31

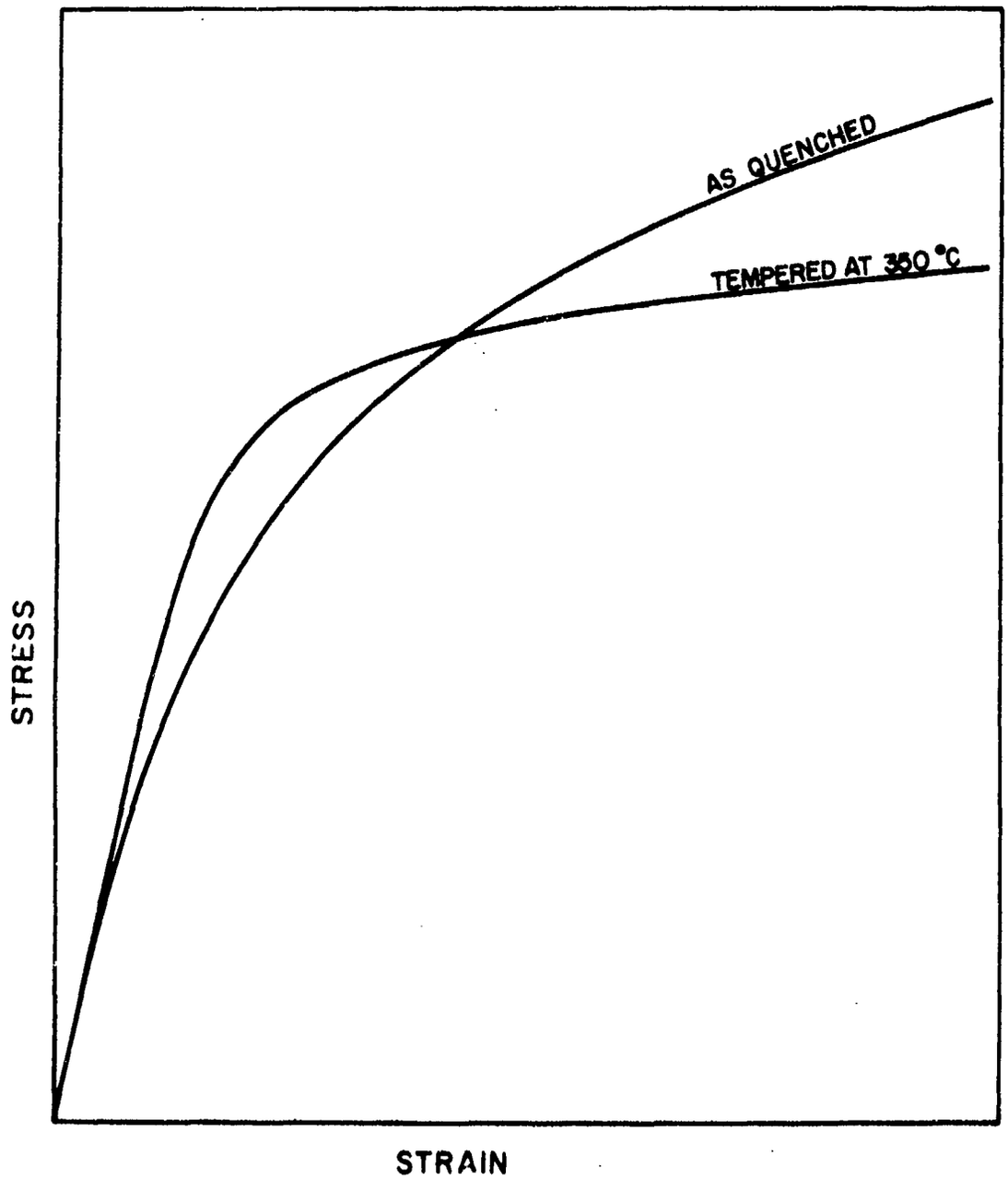

XBL 734-5982

Fig. 32A

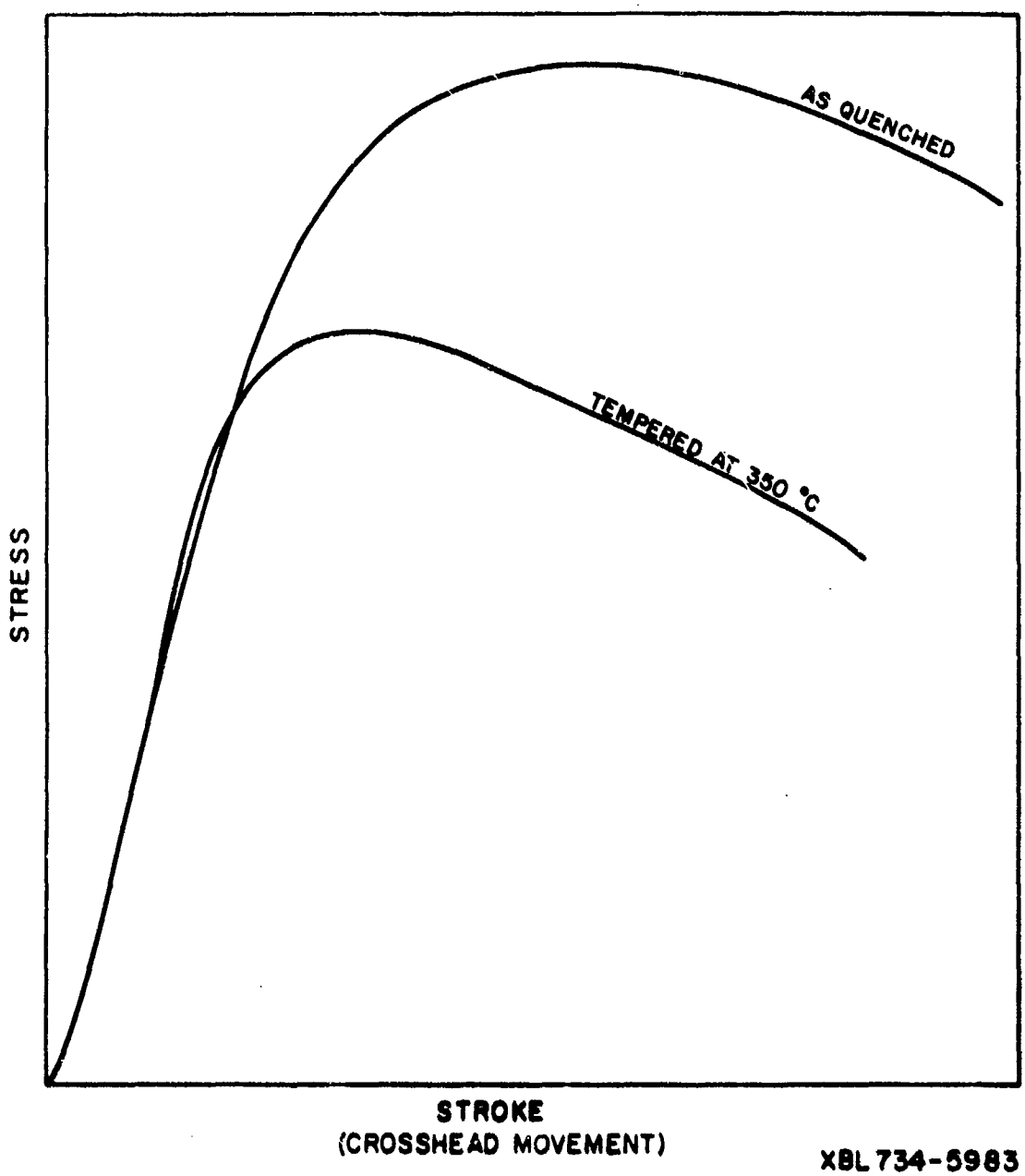
AS QUENCHED
TEMPERED AT 350 °C
STRESS
STROKE
(CROSSHEAD MOVEMENT)
XBL 734-5983

Fig. 32B

XBB 732-1159

4340 (1200, IBQLN) AQ, 0.027 in. thick

Fig. 33

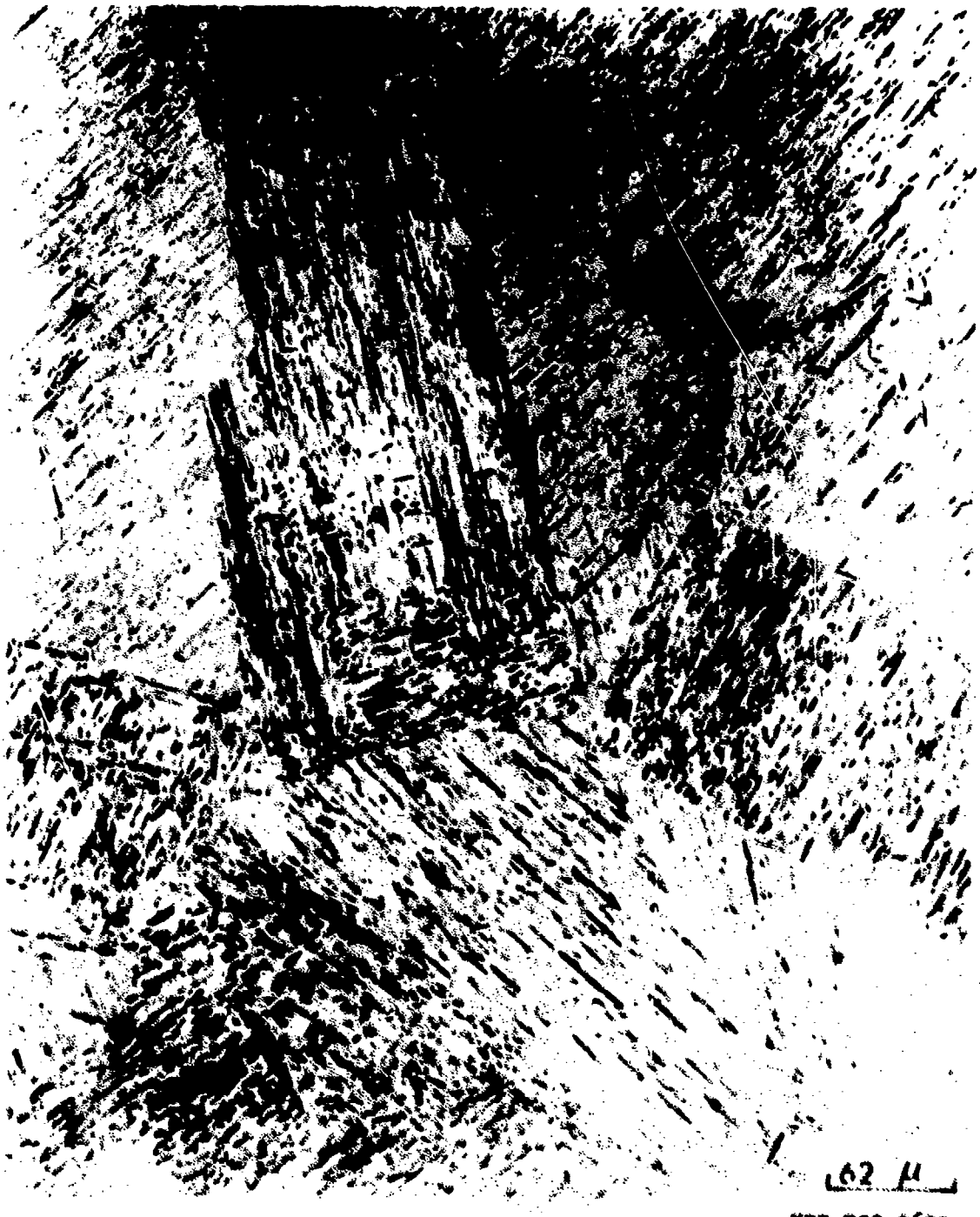

XBB 732-0620

4130 (1200, IBQLN) AQ

Fig. 34

XBB 732-0622

4130 (1200, IBQLN) AQ

Fig. 35

4130 (1200, IBQLN) AQ

Fig. 36

XBB 732-0626

4130 (1200, Oil) AQ

Fig. 37

XBB 732-0624

4130 (1200, Oil) AQ

Fig. 38

XBB 732-635

4130 (1200, Oil) AQ

Fig. 39

XBB 732-0625

4130 (1200, O11) AQ

Fig. 40

XBB 732-653

4130 (1200, 011) AQ

Fig. 41

XBB 732-652

4130 (1200, Oil) AQ

Fig. 42

XBB 732-610

4130 (1200+870, 011) AQ

Fig. 43

XBB 732-651

4130 (1200→870, Oil) AQ

Fig. 44

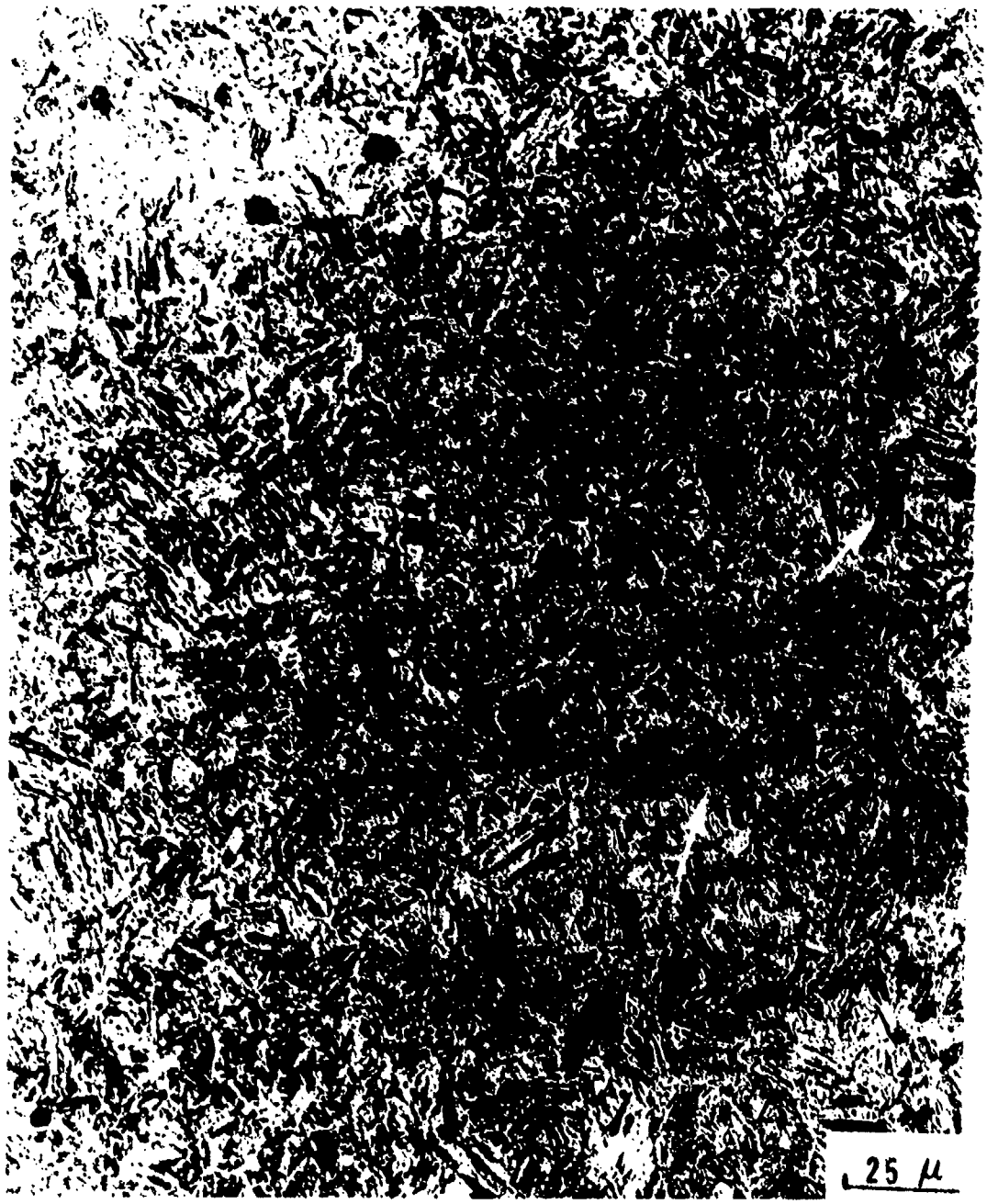

XBB 732-654

4130 (870, IBQLN) AQ

Fig. 45

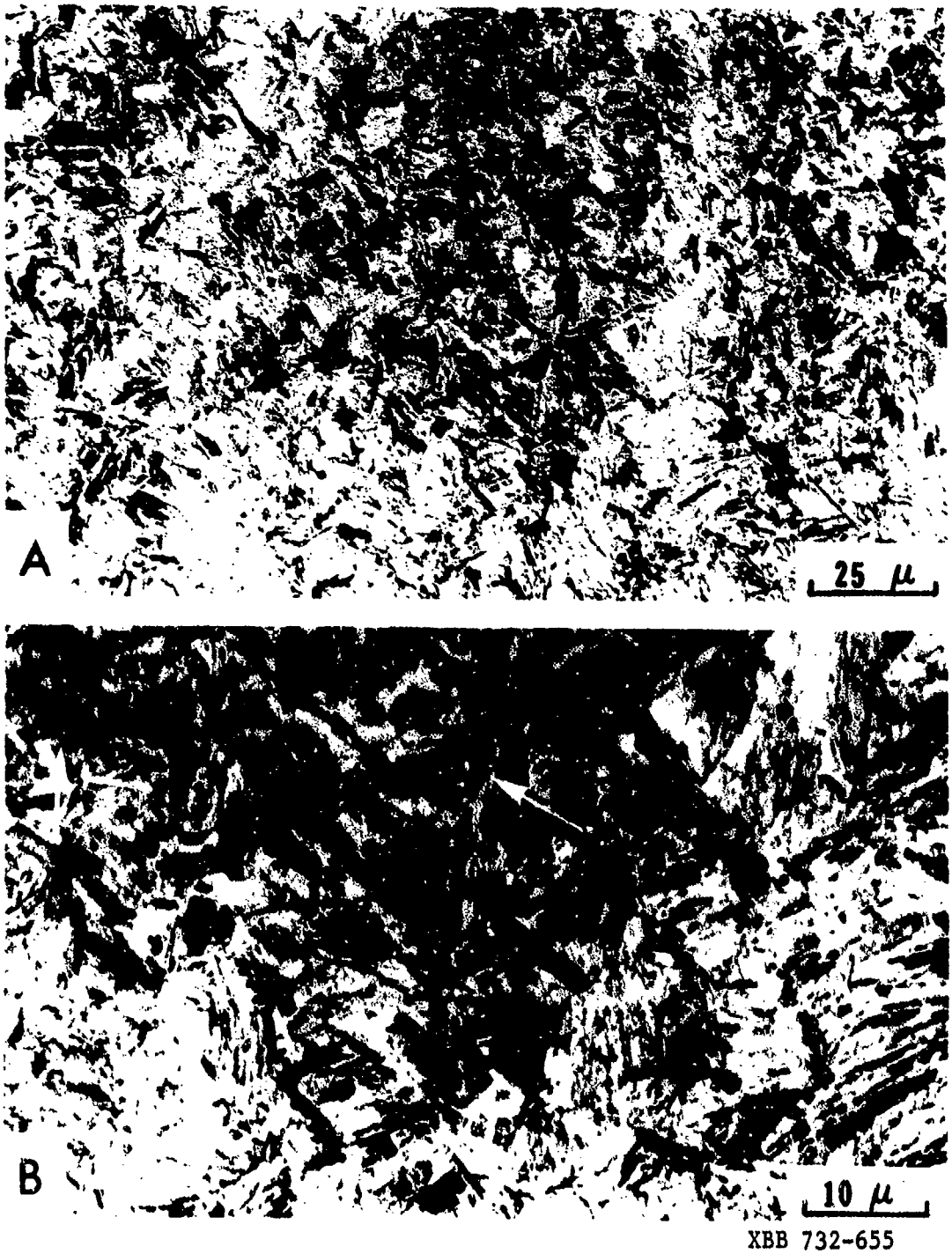

XBB 732-655

4130 (870, IBQLN) AQ

Fig. 46

XBB 732-656

4130 (870, IBQLN) AQ

Fig. 47

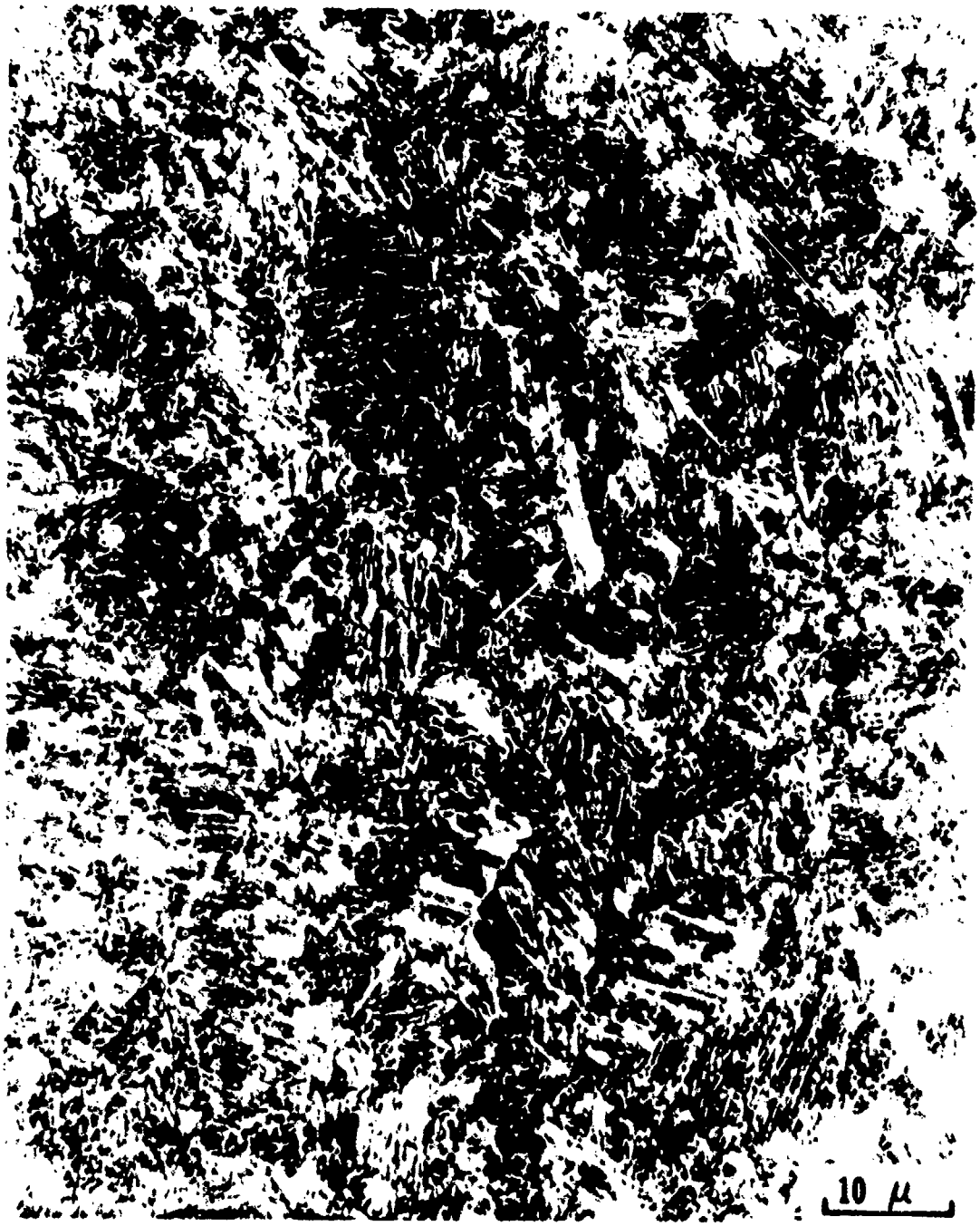

XBB 732-657

4130 (870, IBQLN) AQ

Fig. 48

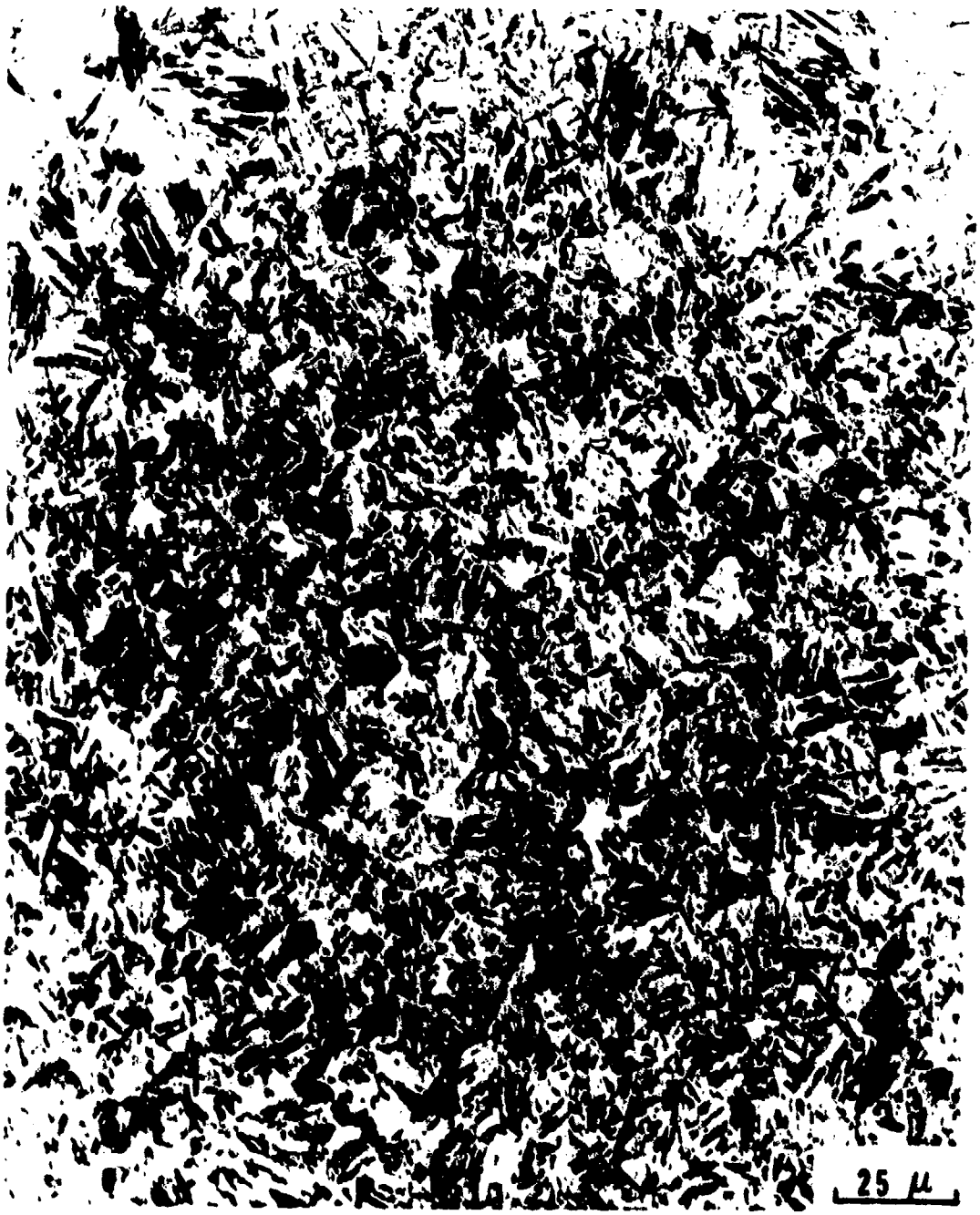

XBB 732-659

4130 (870, Oil) AQ

Fig. 49

XBB 732-658

4130 (870, Oil) AQ

Fig. 50

XBB 732-661

4330 (1200, IBQLN) AQ

Fig. 51

XBB 732-660

4330 (1200, Oil) AQ

Fig. 52

XBB 732-633

4330 (1200, Oil) AQ

Fig. 53

XBB 732-638

4330 (1200, Oil) AQ

Fig. 54

XBB 732-639

4330 (1200+870, 011) AQ

Fig. 55

XBB 732-640

4330 (870, Oil) AQ

Fig. 56

XBB 732-641

4140 (870, 011) AQ

Fig. 57

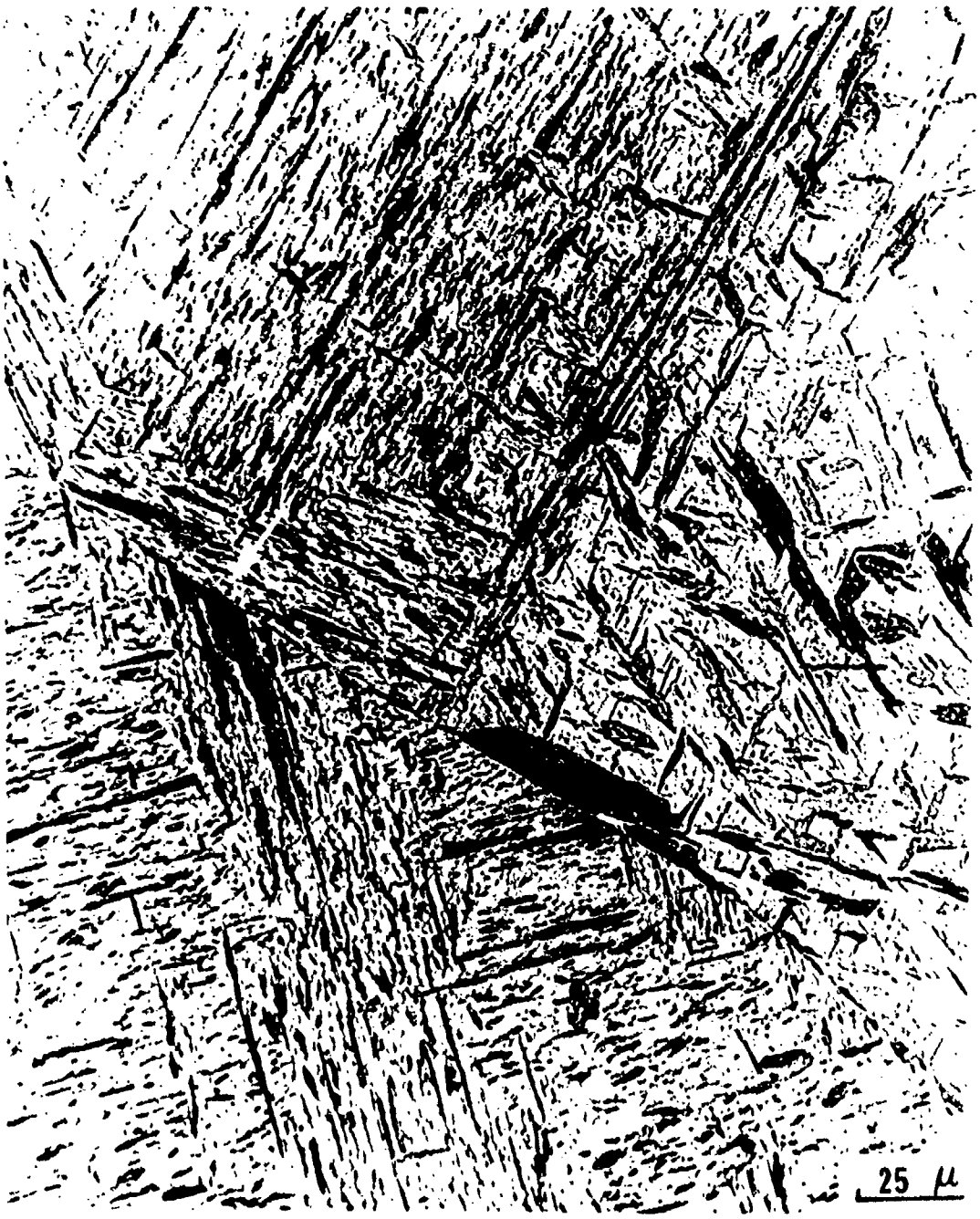

XBB 732-647

4140 (1200, Oil) AQ

Fig. 58

XBB 732-646

4140 (1200, Oil) AQ

Fig. 59

XBB 732-636

4140 (1200, Oil) AQ

Fig. 60

XBB 732-645

4140 (1200, Oil) AQ

Fig. 61

XBB 732-644

4140 (1200, Oil) AQ

Fig. 62

XBB 732-643

4340 (1200→870, Oil) AQ

Fig. 63

Reproduced from best available copy.

XBB 732-642

4340 (1200→870, Oil) AQ

Fig. 64

XBB 732-0629

4340 (1200→870, Oil) AQ

Fig. 65

XBB 732-633

4340 (1200→870, Oil) AQ

Fig. 66

XBB 732-0628

4340 (1200→870, Oil) AQ

Fig. 67

XBB 732-0631

4340 (1200→870, 011) AQ

Fig. 68

XBB 732-0630

4340 (870, 011) AQ

Fig. 69

Reproduced from best available copy.

XBB 732-649

300-N (1200, O11) AQ

Fig. 70

XBB 732-648

300M (1200, oil) AQ

Fig. 71

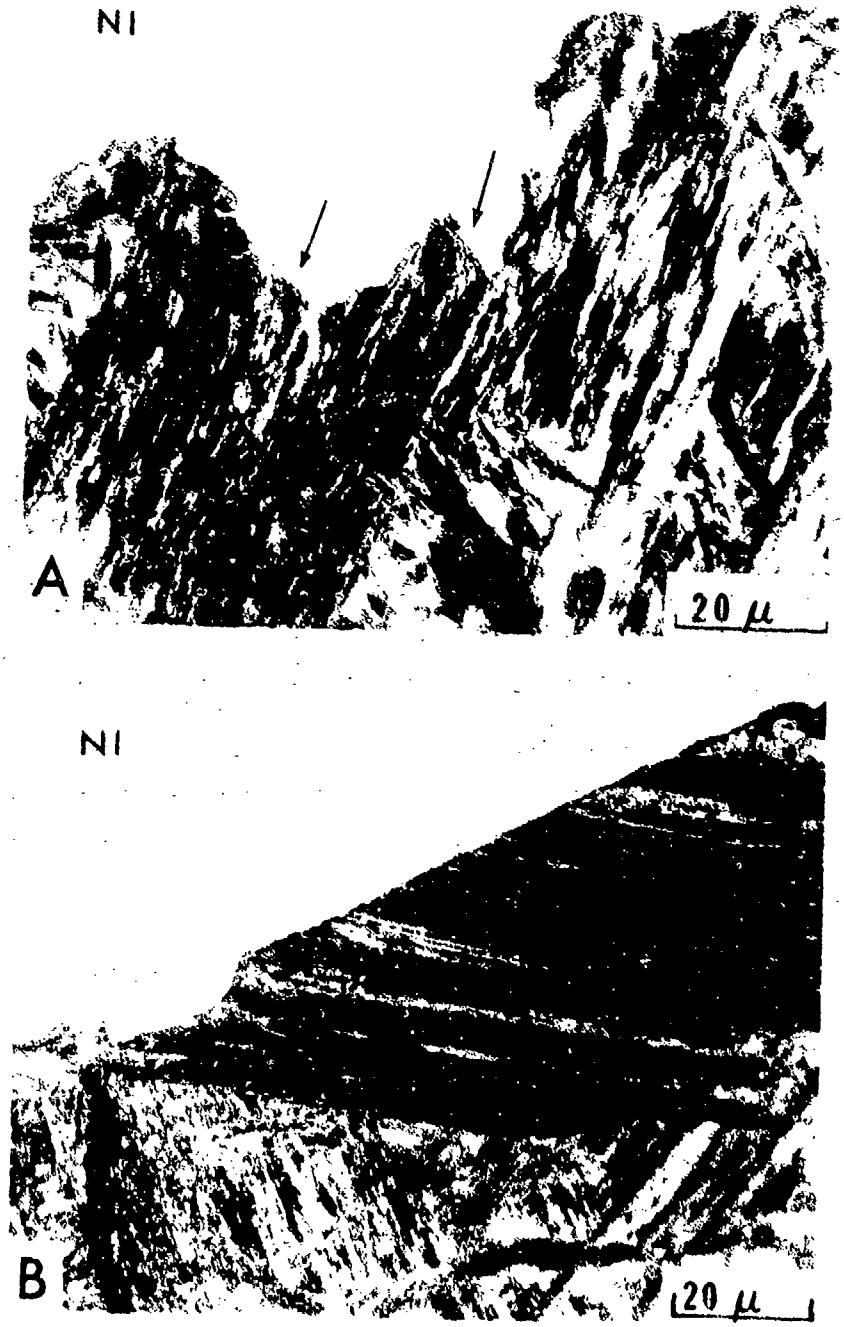

XBB 732-637

4130 (1200, Oil) AQ

Fig. 72

XBB 732-648

300M (1200, Oil) AQ

Fig. 71

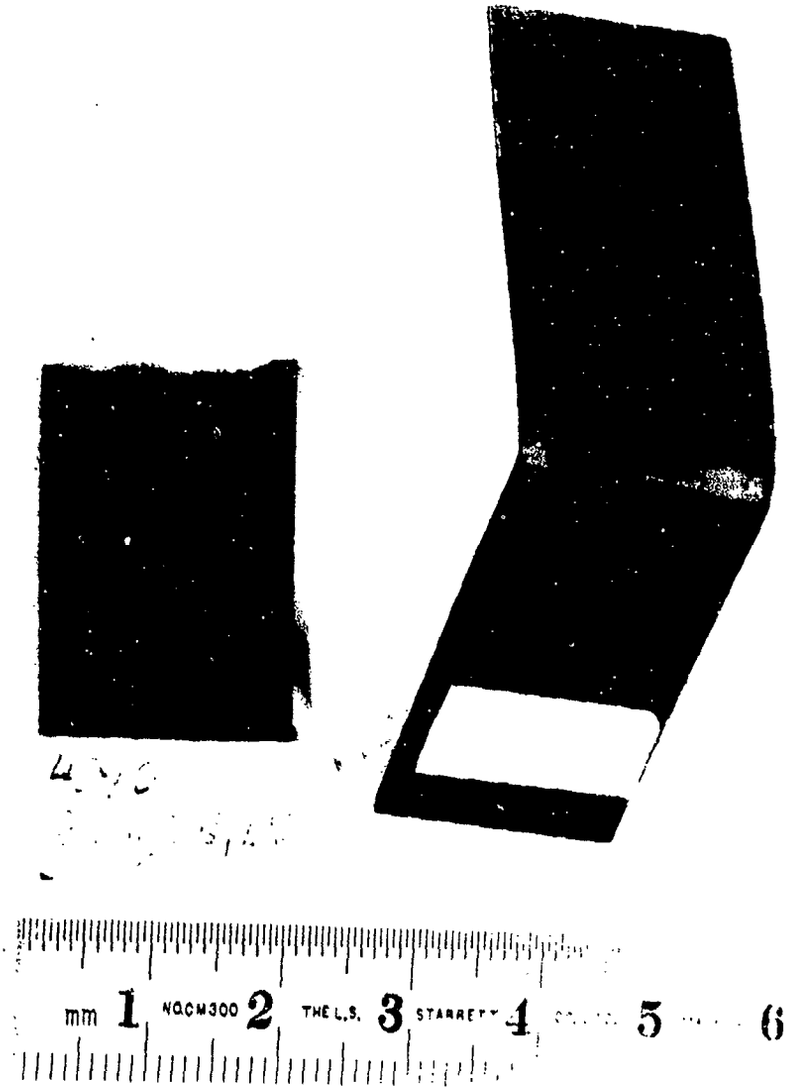

XBB 732-926

Fig. 73

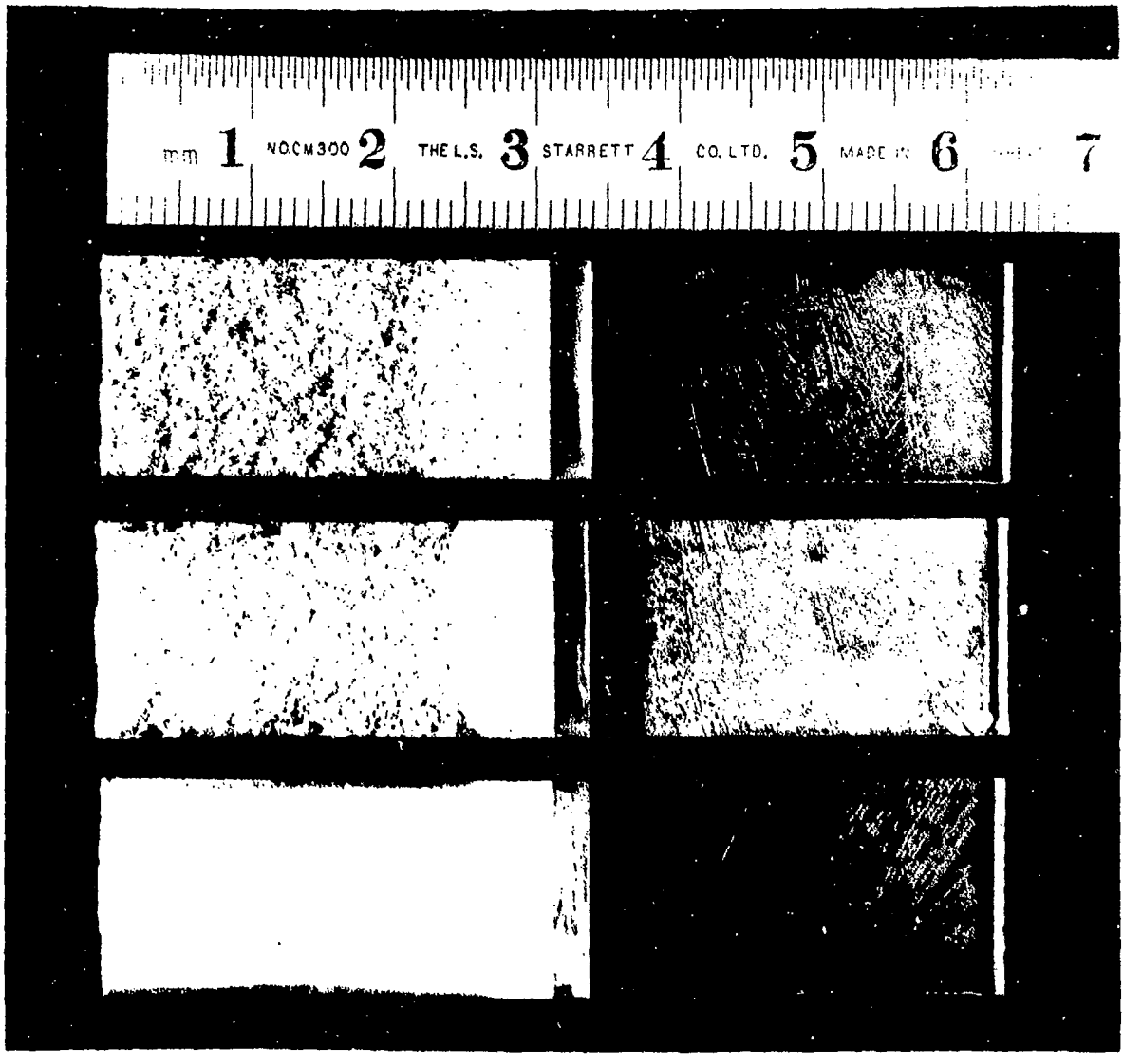

XBB 732-927

4130, Lower (870, Oil) AQ
Middle (1200, IBQLN) 200
Top (1200, IBQLN) 350

Fig. 74

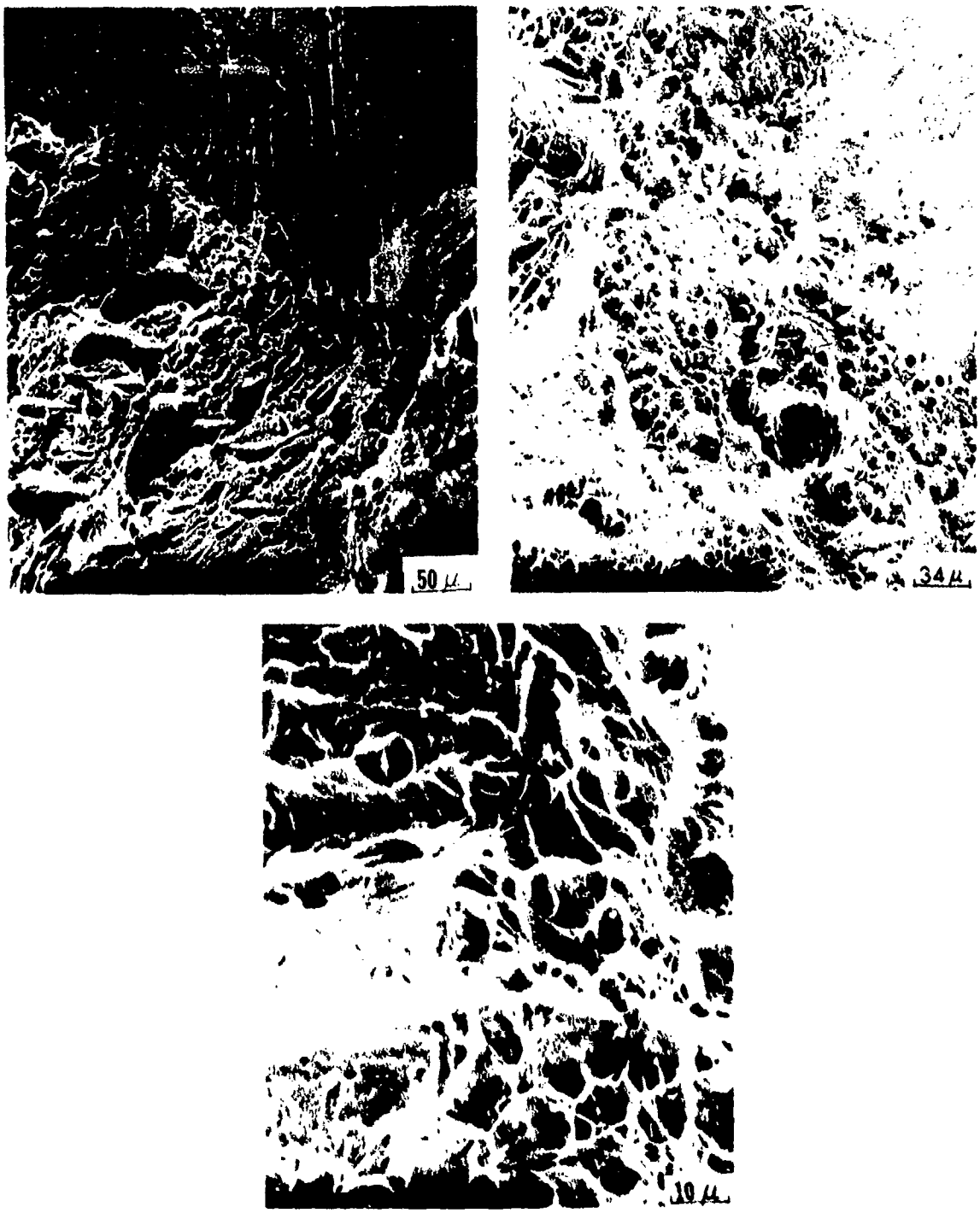

XBB 732-634

4130 (1200, IBQLN) AQ

Fig. 75

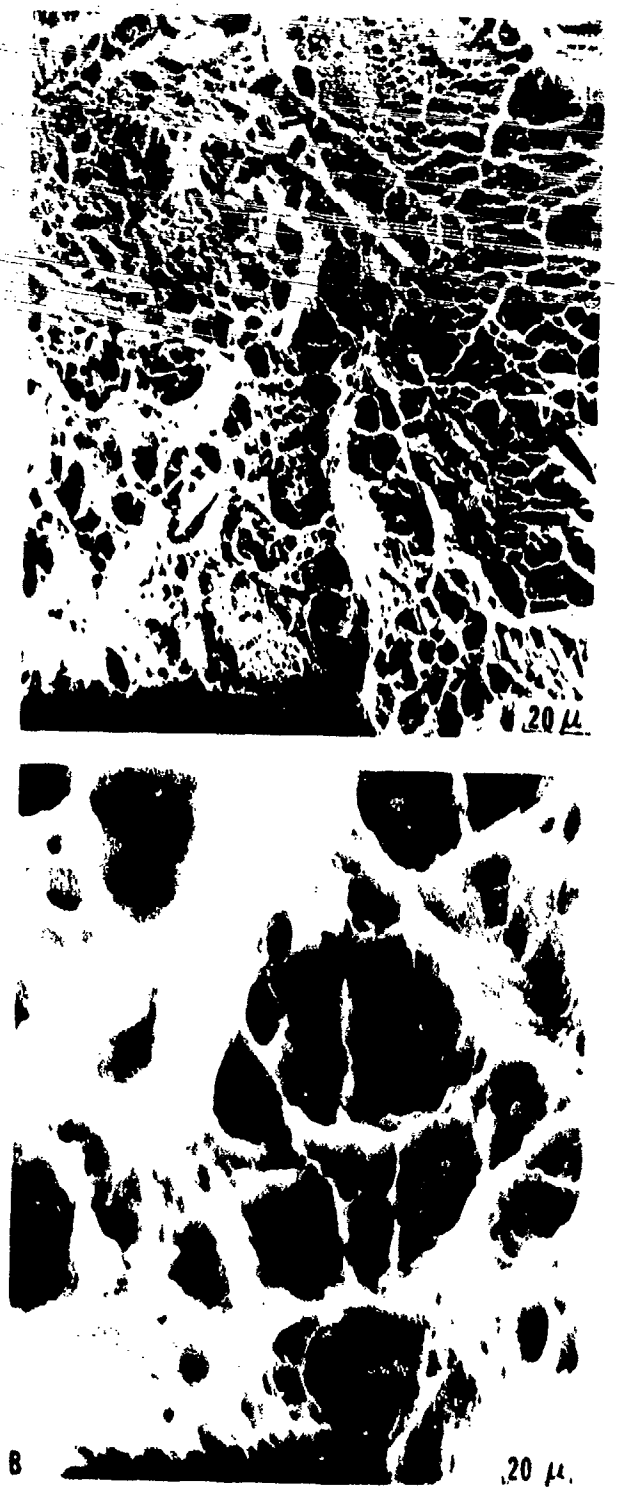

XBB 732-0618

4130 (1200, Oil) AQ

Fig. 76

XBB 732-607

4130 (1200, Oil) AQ

Fig. 76 continued

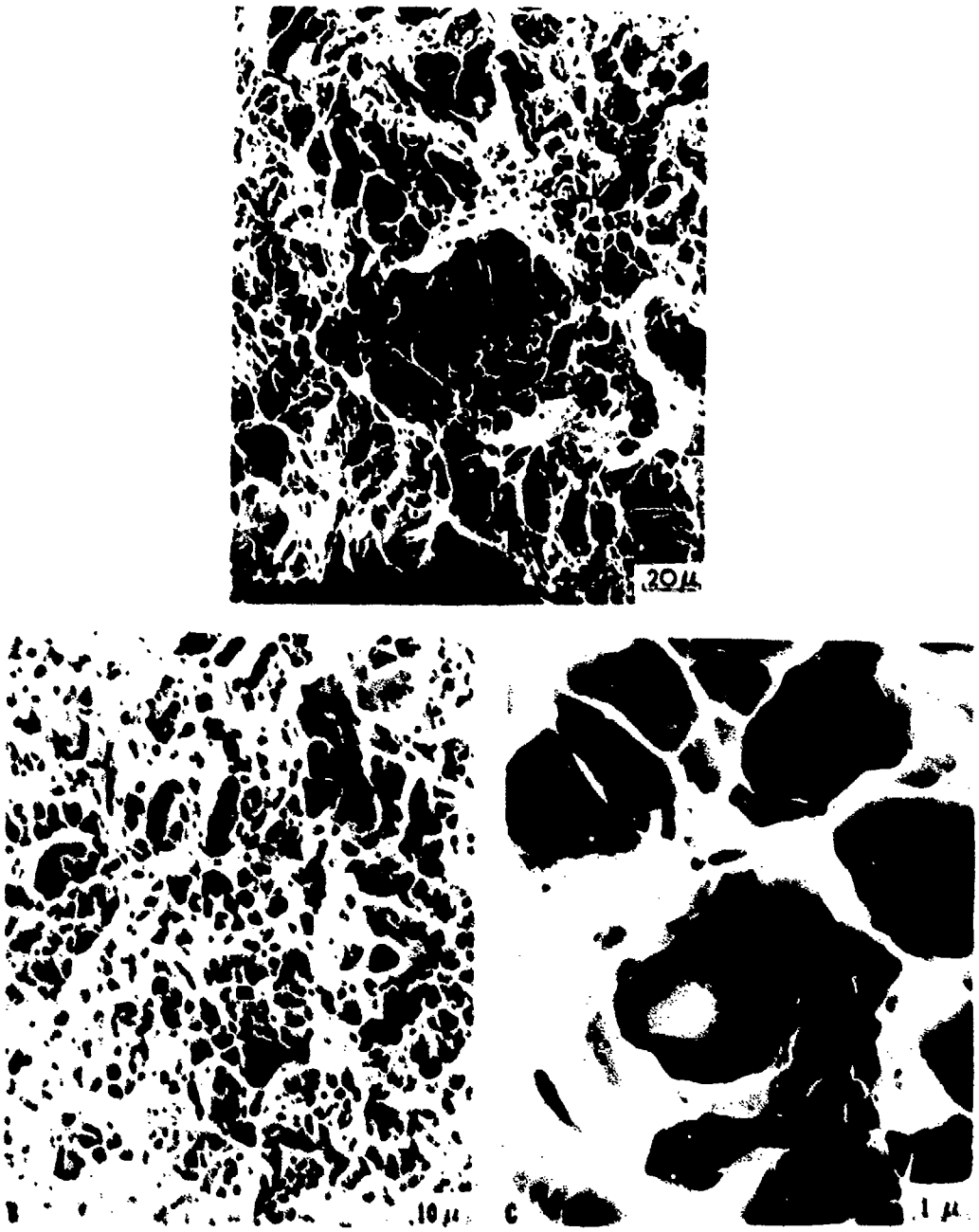

XBB 732-606

4130 (870, 011) AQ

Fig. 77

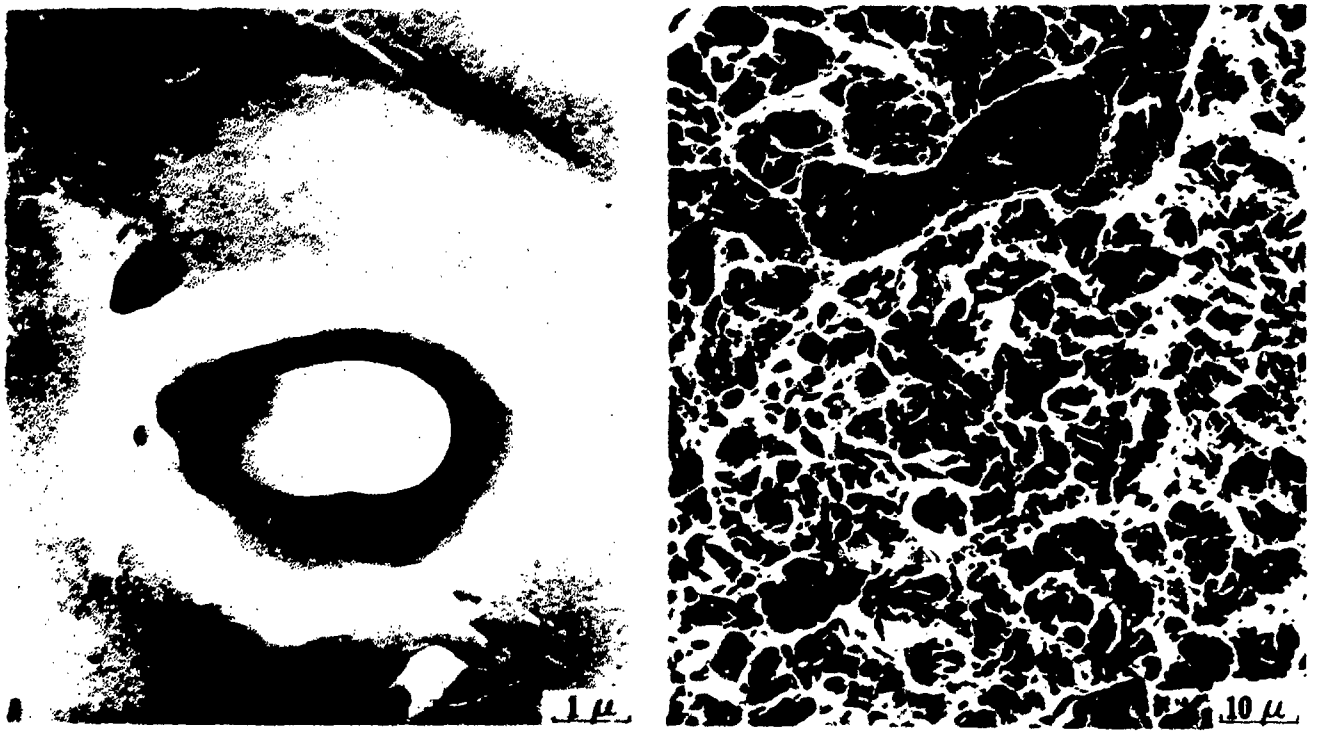

XBB 732-0621

4130 (870, Oil) 350

Fig. 78

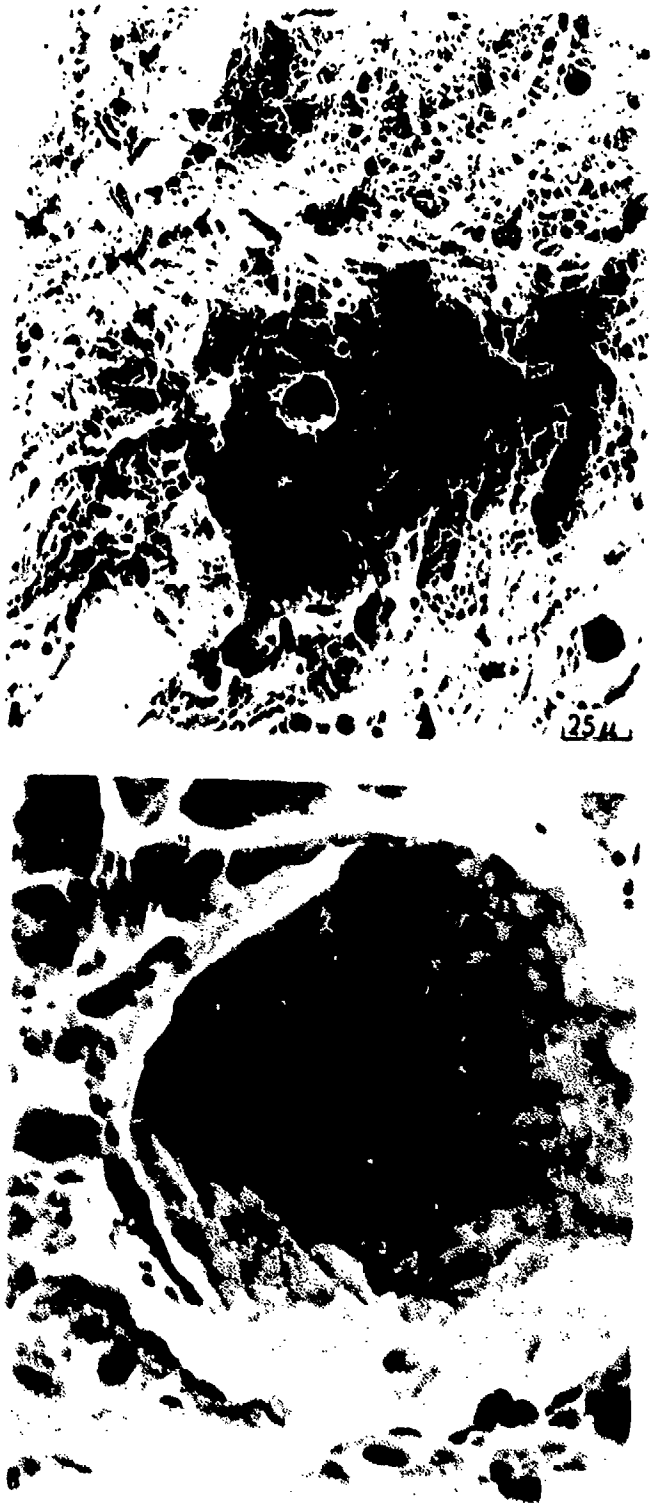

XBB 732-0617

4130 (1200, IBQLN) 200

Fig. 79

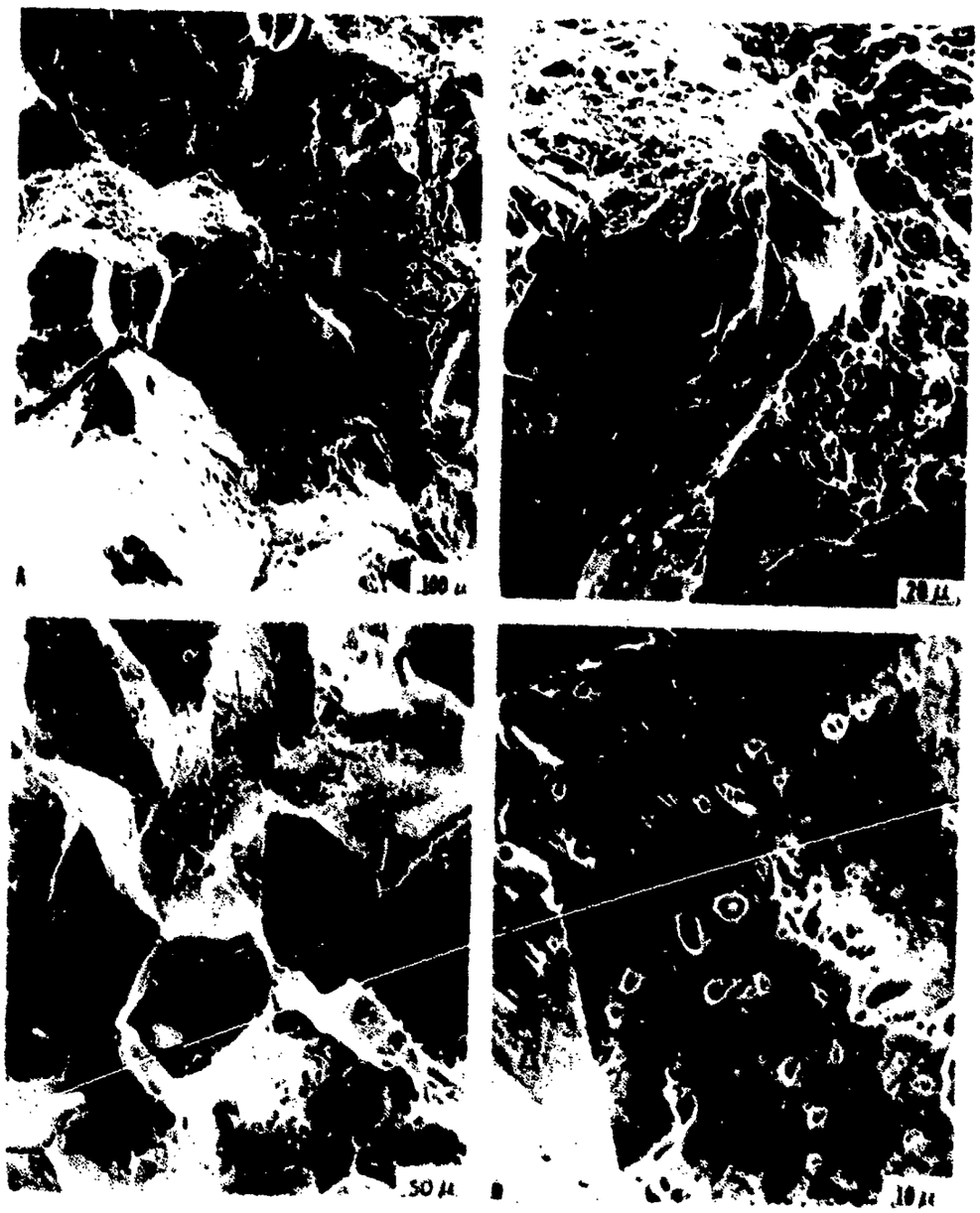

XBB 732-604

A & B. 4130 (1200, IBQLN) 280

C & D. 4130 (1200, IBQLN) 350

Fig. 80

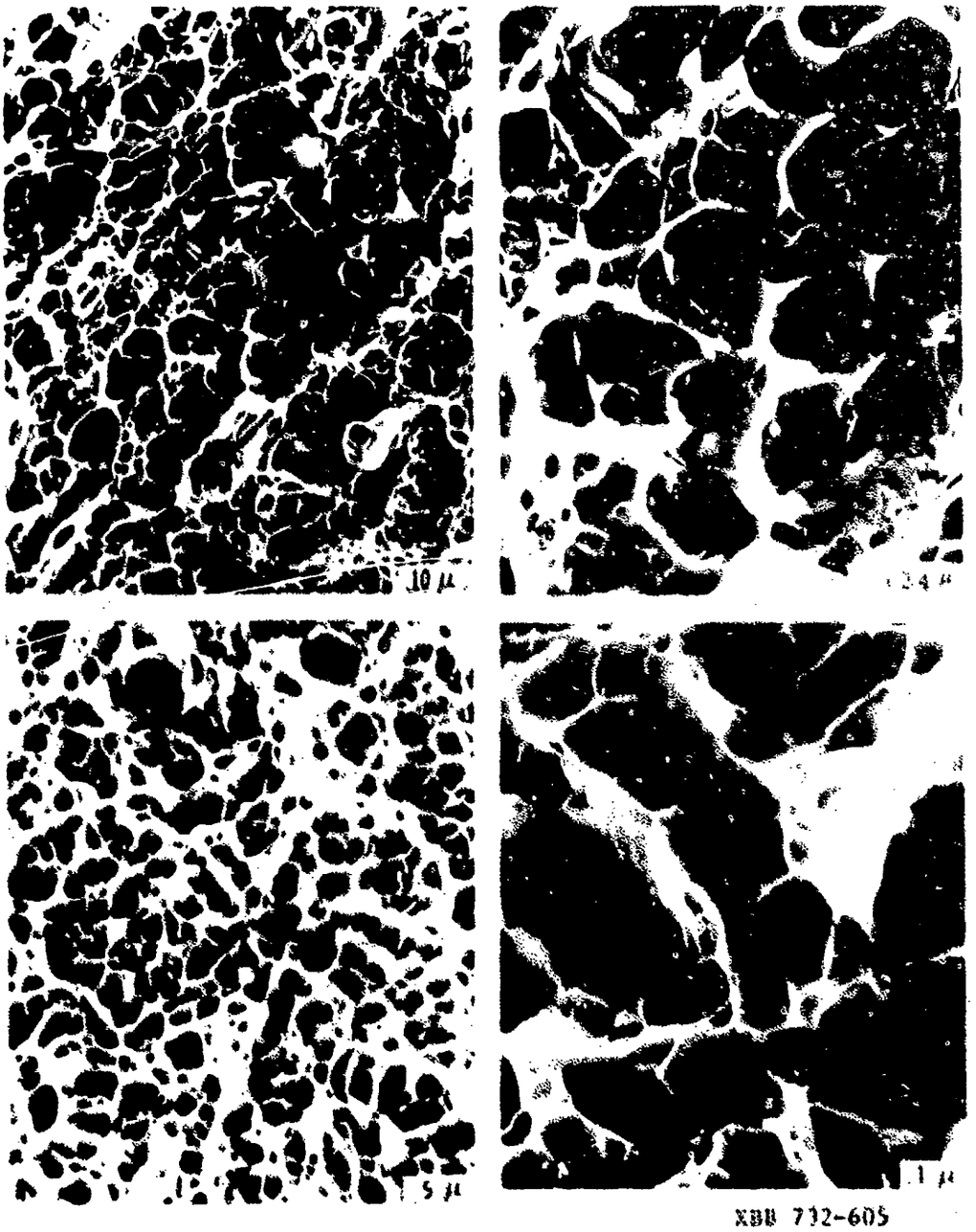

XBB 732-605

Fig. 81. Top 4330 (1200, IBQLN) AQ

Fig. 82. Bottom 4330 (870, Oil) AQ

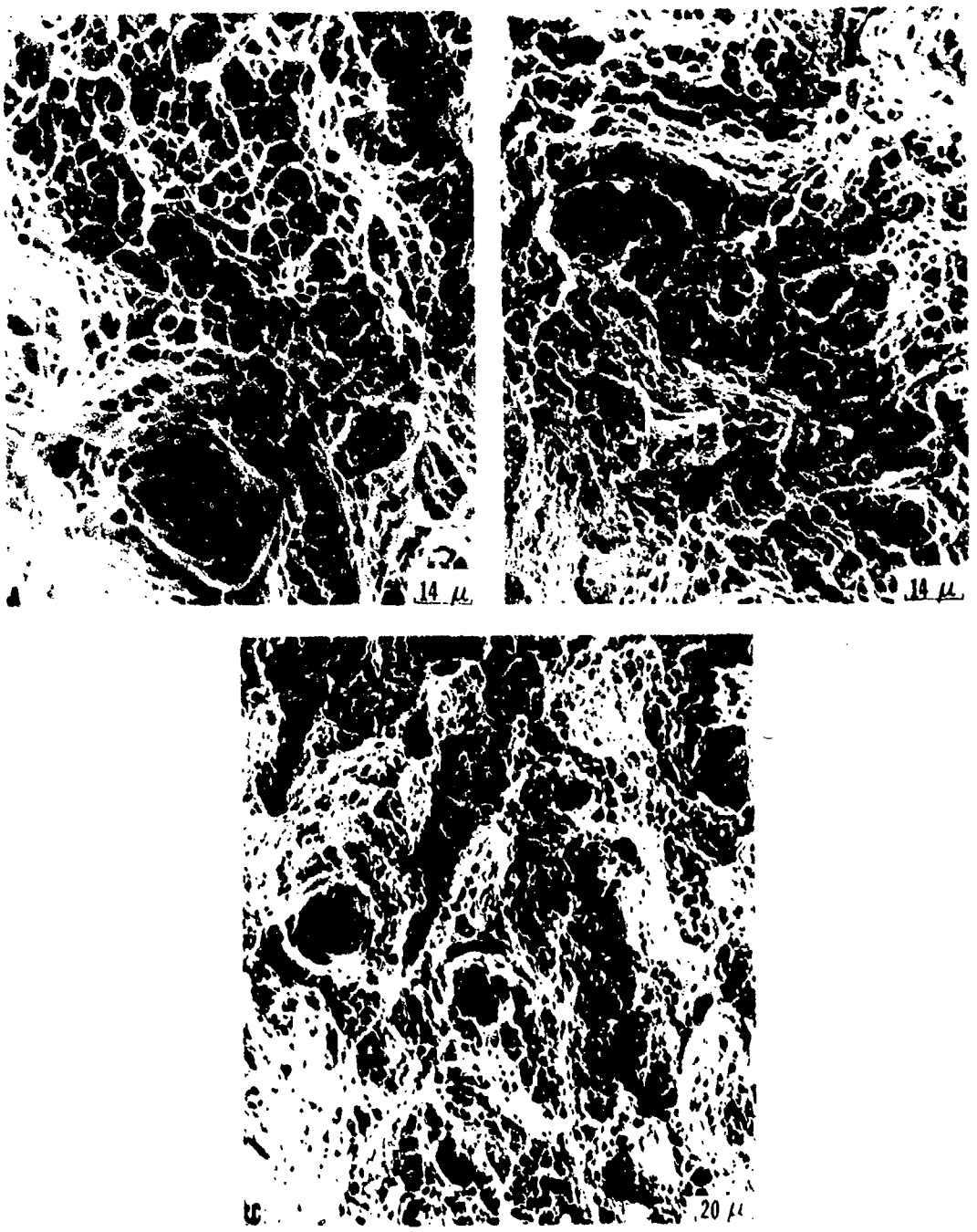

XBB 732-611

Fig. 83. A and B 4330 (1200, IBQLN) 350
C 4300 (870, Oil) 350

XBB 732-0623

4340 (1200, Oil) AQ

Fig. 84

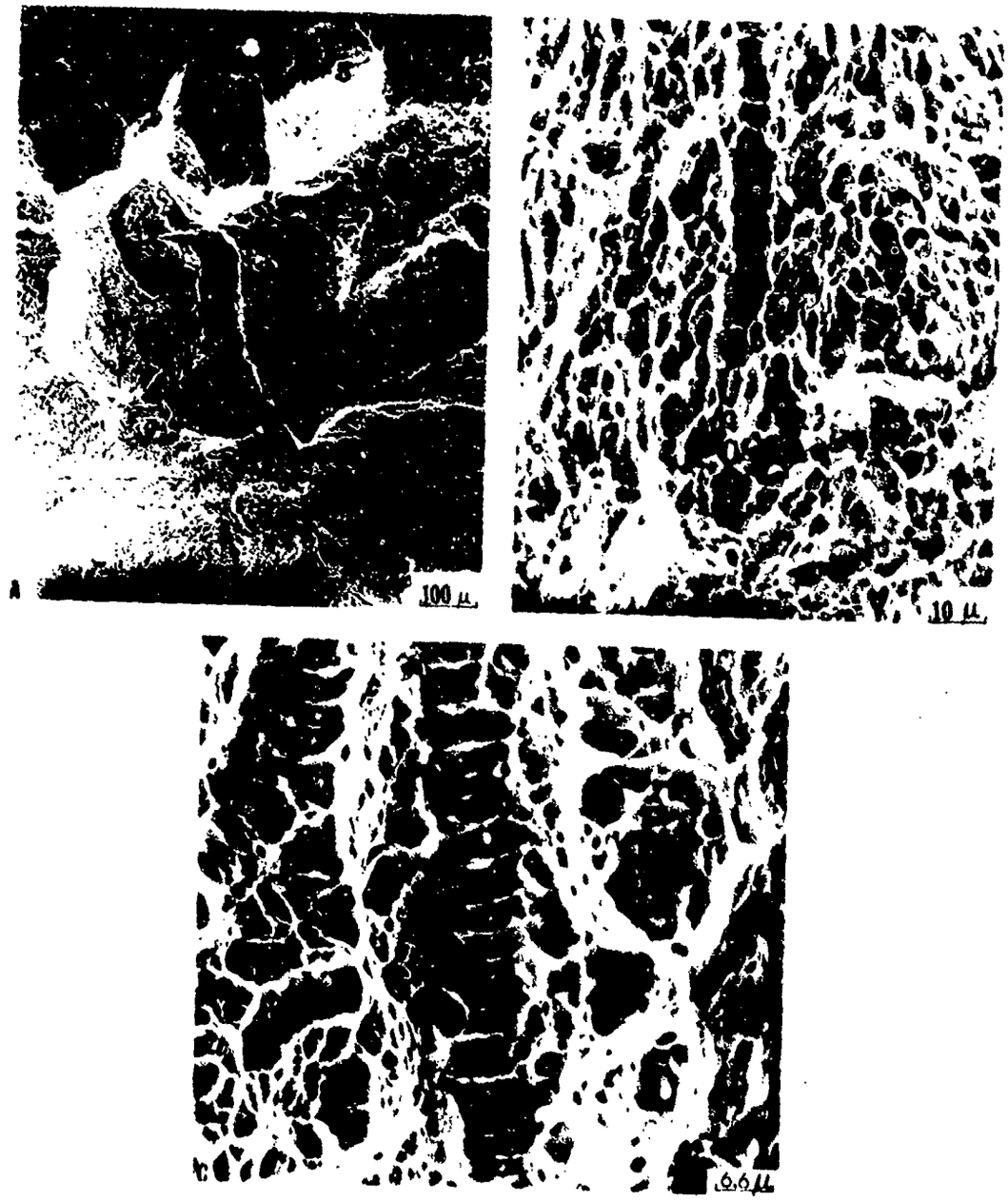

XBB 732-610

4340 (1200→870, Oil) AQ

Fig. 85

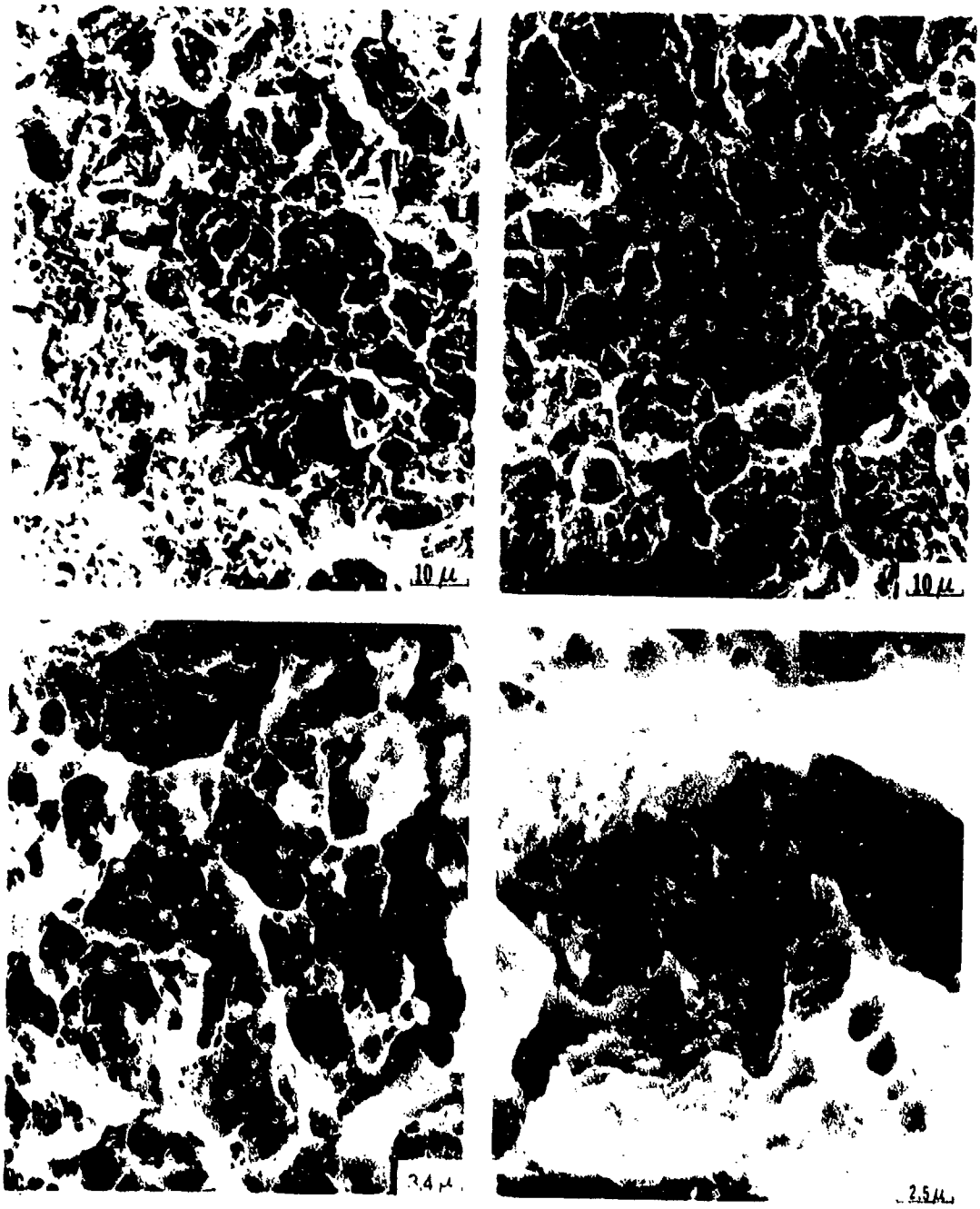

XBB 732-609

4340 (870, Oil) AQ

Fig. 86

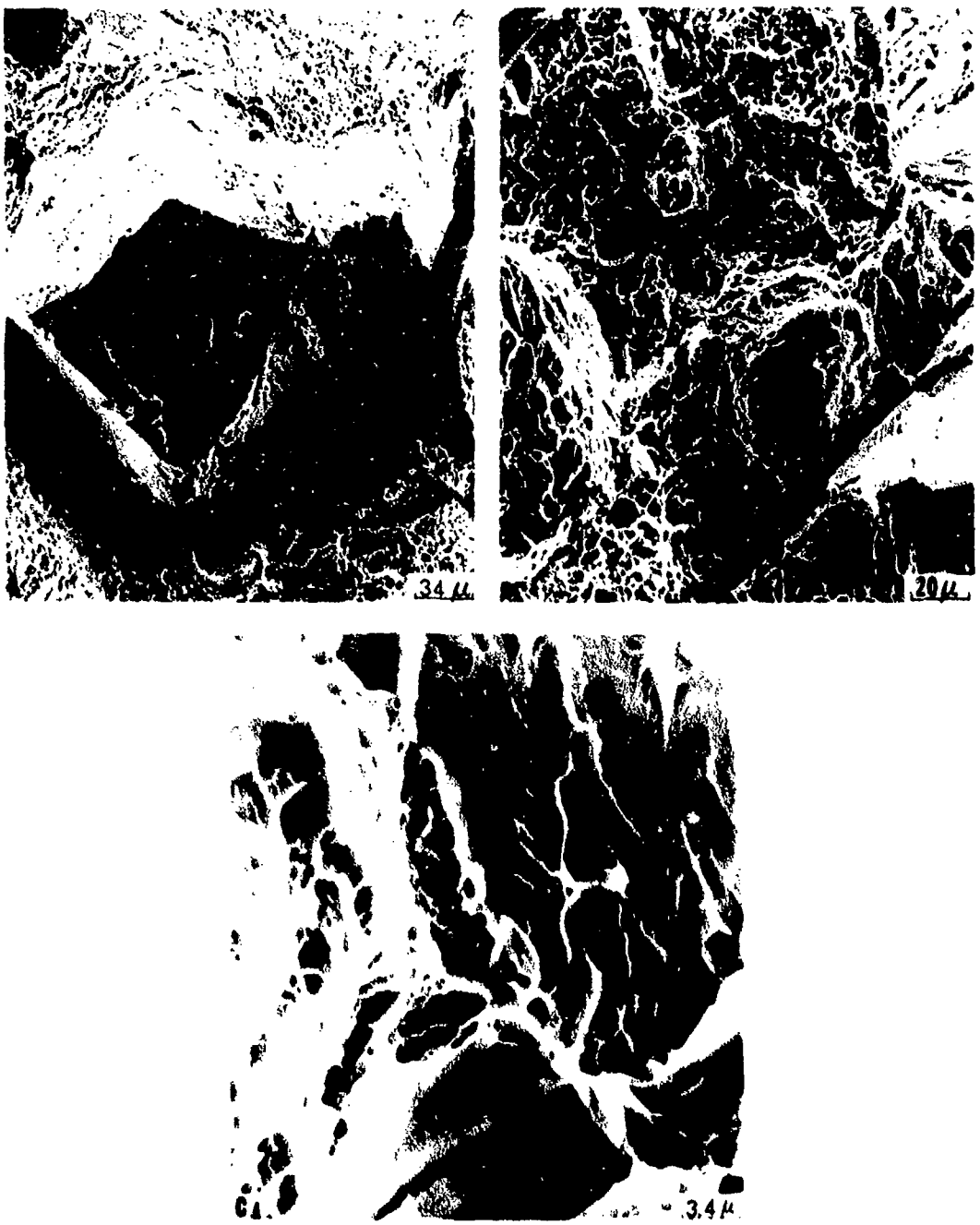

XBB 732-608

4340 (1200→870, Oil) 200

Fig. 87

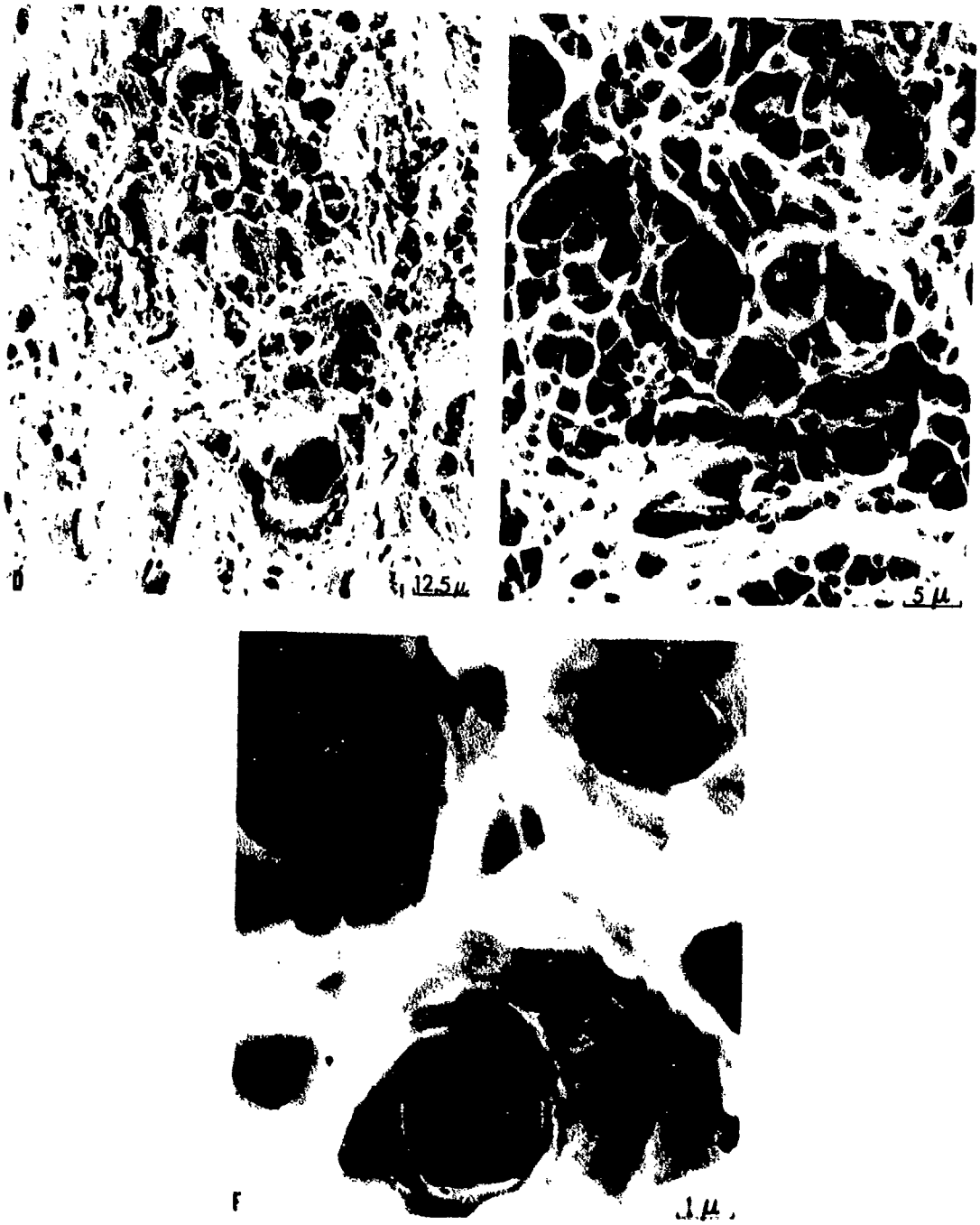

XBB 732-0615

4340 (1200→870, Oil) 200

Fig. 87 cont'd

XBB 732-0614

4340 (1200, 870, 011) 280

Fig. 88

XBB 732-0616

4340 (1200, 870, 011) 280

Fig. 88 cont'd

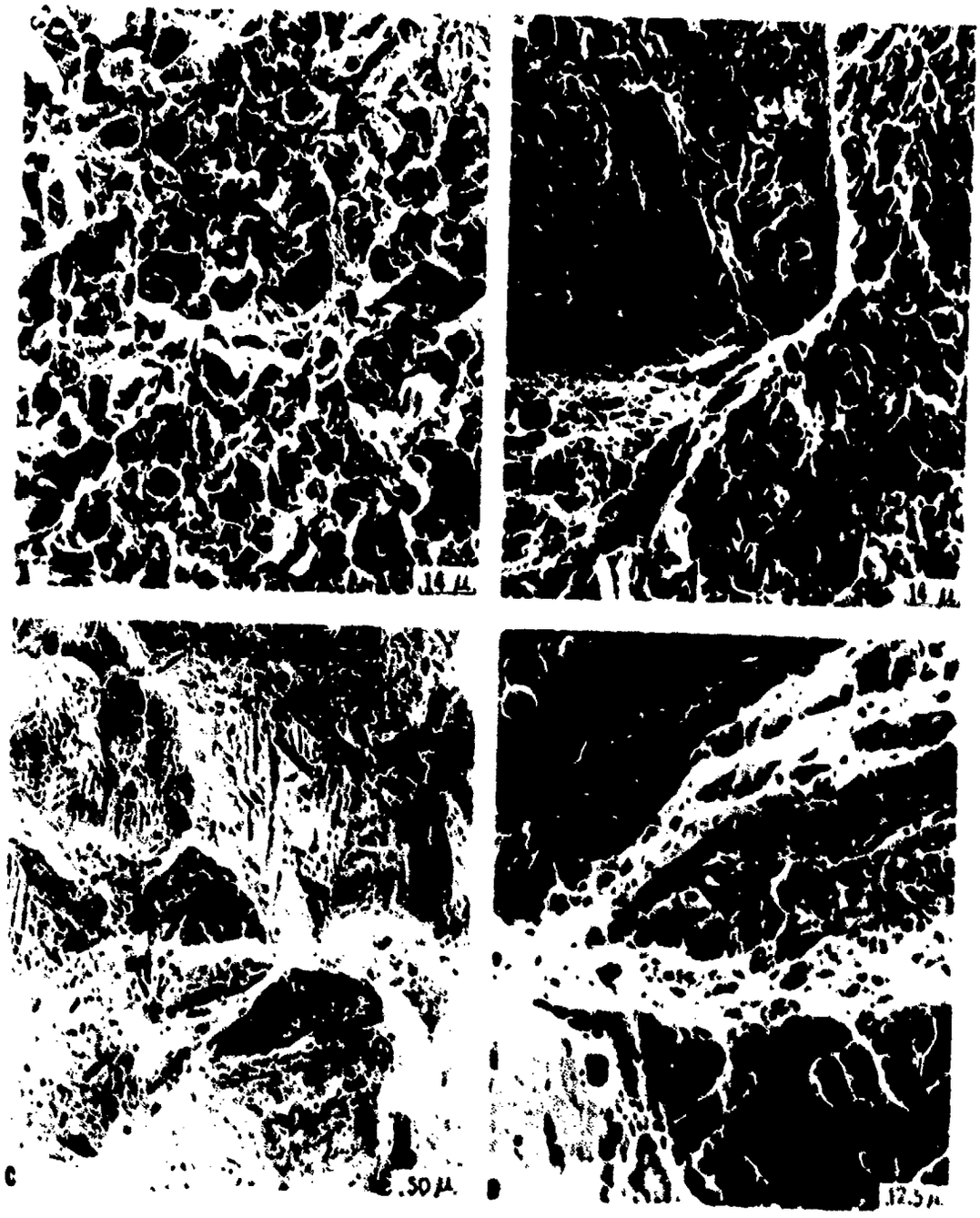

XJB 732-612

4140, A (870, 011) 280
B-D (1200, 011) AQ

Fig. 89

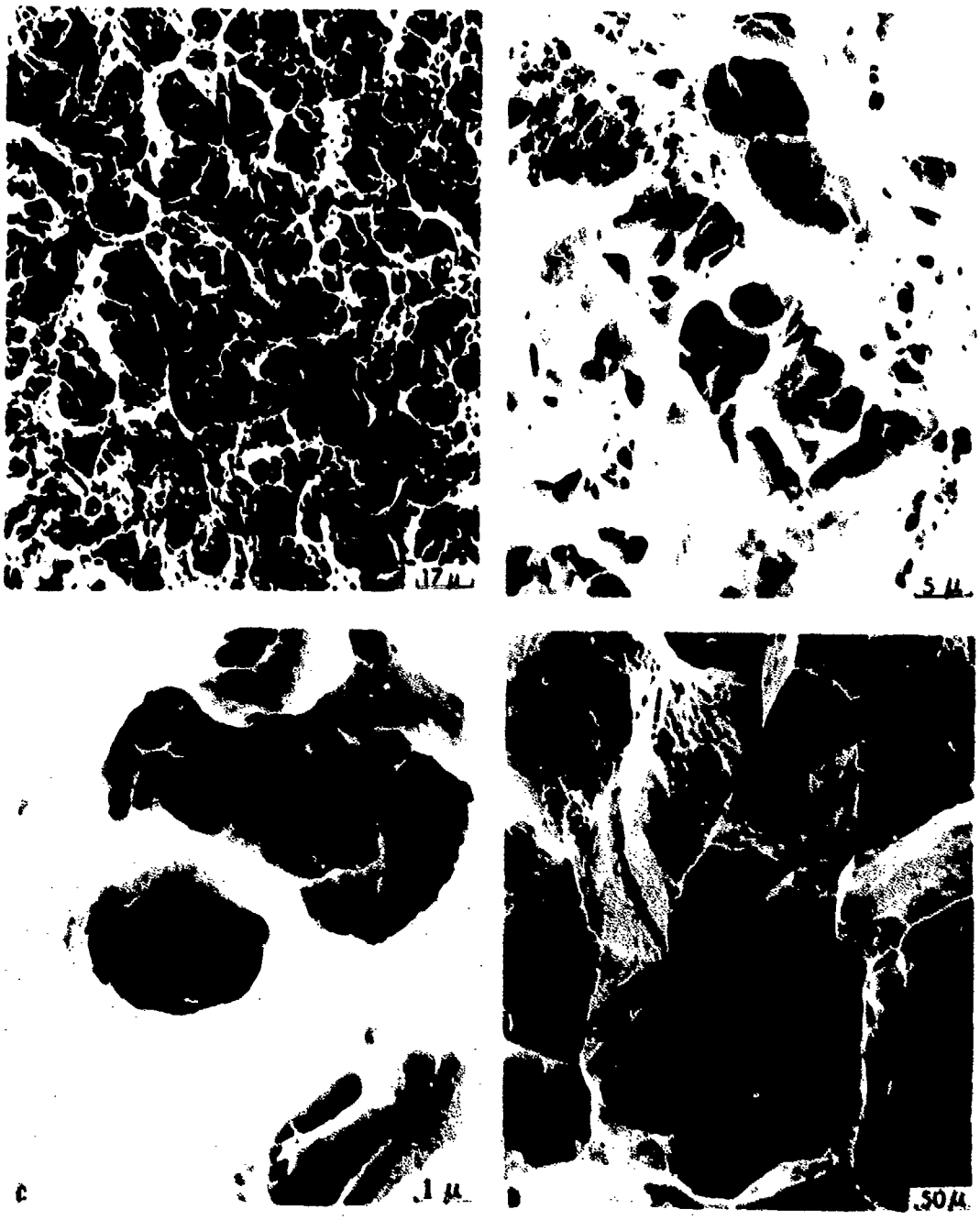

XBB 732-613

4140, A (870, 011) 280
B&C (870, 011) 390
D (1200, 011) 350

Fig. 90

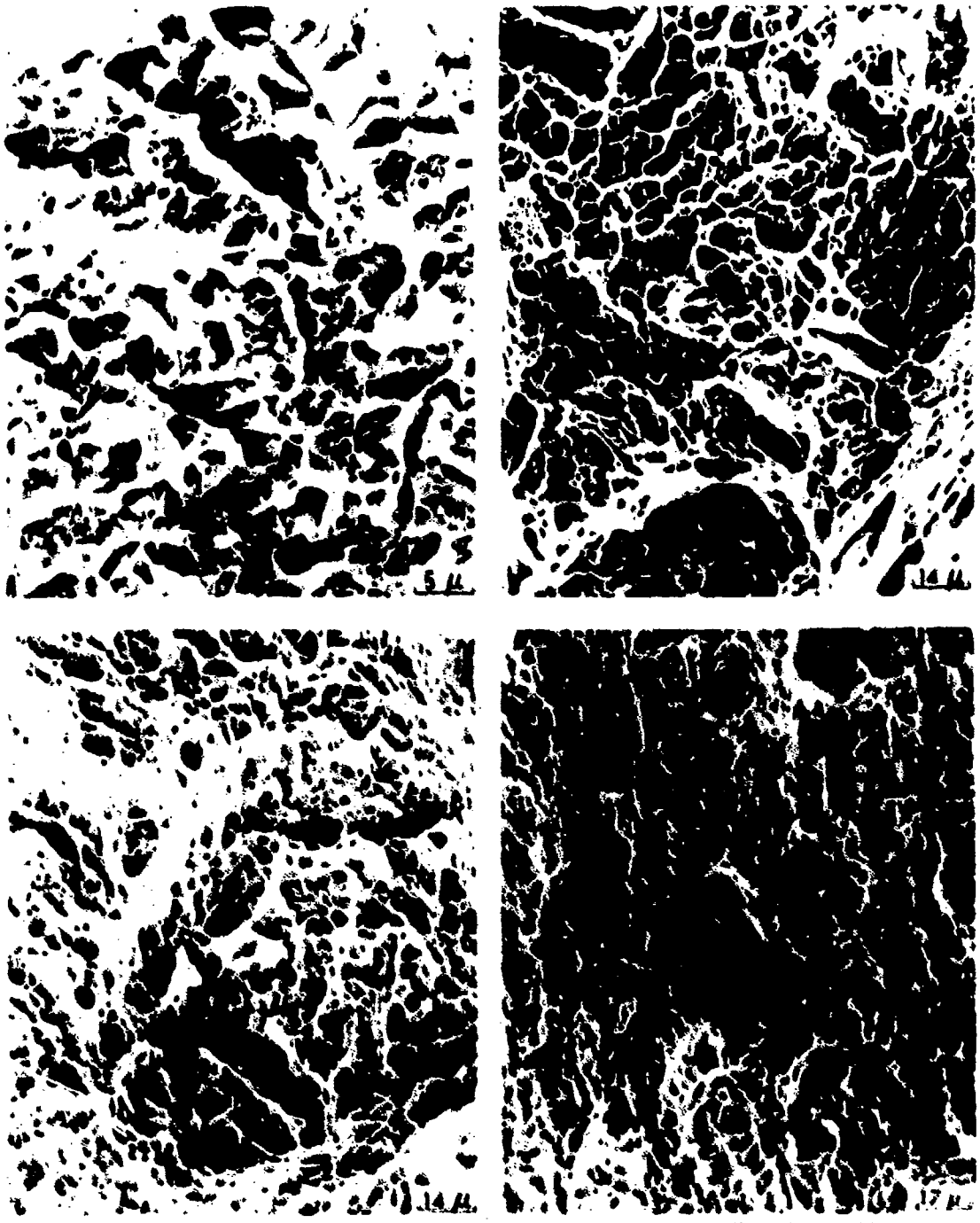

XBB 732-0619

300-M, A (870, 011) AQ
B (1200, 011) AQ
C&D (1200, 011) 325

Fig. 91